박 사 학 위 논 문

Analysis of Water Resources Variability in the Lake Chad Basin Based on Gravimetry, Altimetry and Multispectral Imageries

중력 및 고도 측정과 다분광 영상자료에 의한
Chad 호 유역의 수자원 변동성 분석

지도교수 이 상 일

동국대학교 대학원 건설환경공학과

BUMA WILLIBROAD GABILA

2019

박사학위 논문

Analysis of Water Resources Variability in the Lake Chad Basin Based on Gravimetry, Altimetry and Multispectral Imageries

중력 및 고도 측정과 다분광 영상자료에 의한
Chad 호 유역의 수자원 변동성 분석

BUMA WILLIBROAD GABILA

지도교수 이상일

이 논문을 박사학위 논문으로 제출함

2018년 12월

윌리브로드 부마의 공학 박사학위 논문을 인증함

2018년 12월

위원장 이 주 현 (인)

위 원 강 부 식 (인)

위 원 김 범 주 (인)

위 원 조 준 호 (인)

위 원 이 상 일 (인)

동국대학교 대학원

Table of Contents

LIST OF TABLES

LIST OF FIGURES

ACKNOWLEDGMENTS

My academic path has been full of challenges and uncertainties which I had to find a way to accommodate. This was not an easy task and for that, I am sincerely grateful to the Lord almighty and everyone for all their support and encouragement as I went through this journey.

First, I am heartily thankful to my primary supervisor, Professor Sang - Il Lee, whose encouragement, guidance and support from the very beginning enabled me to develop an understanding of the problems I was facing. During the past five years, working with Professor Lee has been a wonderful experience. His wide knowledge, strong research skill and hard-working attitude have inspired me and will have a profound effect on my academic career forever. He made available his support in a number of ways towards the realization of my PhD research. It would not have been possible without him at my disposal. My heartfelt gratitude also goes to Prof. Joo-Hyeon Lee, Prof. Boosik Kang, Prof. Bum Joo Kim, and Dr. Jun-Ho Cho for their insightful comments which helped to improve the quality of this PhD thesis. Thanks to all my lab mates who stood by my side and never gave up on me and my numerous questions.

Besides, I would also like to show my gratitude to Dongguk University and the Korean Government for offering me wonderful scholarships to undertake my graduate studies in this outstanding university and beautiful country. I will forever be grateful for this life changing experience.

My sincere gratitude goes to the professors and lecturers of the department of Water Resources and Environmental Engineering Systems for providing me with a suitable environment and great facilities to undertake my studies.

Special thanks go to all my friends for all the motivations and great times we spent together. Especially the active members of the St. Pats

Falcons Football Club. Playing with you guys was a great balance between school works. Thank you too Agbortoko B. for making life here more comfortable.

Many thanks to you, Kimberly Gongora, for all the calls, laughter, exquisite trips and great times we shared together. Thank you for always wanting to read through my work even though you barely understood anything. You are such a beautiful soul and cute darling, do not change.

An honorable mention goes to my family. I deeply owe my parents, Buma Doh John and Bih Buma Hasana for all their prayers, financial, moral support and unconditional love they have showed me all through my academic life. Thank you very much mom, I truly appreciate all the numerous calls even when I was not ready for one. They came in very handy and were a great means of motivation especially on the down days. Mummy Hadjia Ajuji Ali has always been there for me in so many ways and for that, I will forever remain grateful. Same goes to my brothers; Bertrand, Doh, Brain, Junior, and my sisters. Without the support of the above-mentioned people, I would not have made it this far.

Finally, I will like to thank the Lord almighty for his constant love and protection all through these years.

I love you all

Seoul, January 2019

Willibroad Buma

ACCRONYM

AWEI:	Automated Water Extraction Index
CLM:	Community Land Model
ETM+:	Enhanced Thematic Mapper Plus
GFZ:	Geoforschungszentrum Potsdam
GLDAS:	Global Land Data Assimilation System
GPCC:	Global Precipitation Climatology Centre
GPS:	Global Positioning System
GRACE:	Gravity Recovery and Climate Experiment
JPL:	Jet Propulsion Laboratory
LCB:	Lake Chad Basin
LSMs:	Land Surface Models
MNDWI:	Modified Normalized Difference Water Index
NASA:	National Aeronautics and Space Administration
NDVI:	Normalized Difference Vegetation Index
NDWI:	Normalized Difference Water Index
OLI:	Operational Land Imager
PO.DAAC:	Physical Oceanography Distributed Active Archive
SRTM:	Shuttle Radar Topography Mission
STL:	Seasonal and Trend decomposition using Loess
TRMM:	Tropical Rainfall Measuring Mission
TWS:	Terrestrial Water Storage
TWSA:	Total Water Storage Anomaly
VIC:	Variable Infiltration Capacity
WaterGAP:	Water - Global Assessment and Prognosis
WGHM:	WaterGAP Global Hydrology Model

ABSTRACT

Lakes and reservoirs make up most of the surface freshwater bodies. Majority of this natural resources are often exposed to unfavorable climatic conditions and human interactions. For it to keep serving the needs of humans and its immediate environment, proper management procedures are needed. A step towards achieving proper management will be to quantitatively and qualitatively understand their hydrological variability over time. This can only be achieved with consistent data availability over a given period. Consistent observations of lakes and reservoirs are often lacking in some parts of Africa. Sometimes in areas where these water bodies are crucial to the existence of their communities. Determining the quantitative and qualitative estimates of water balance entities in such areas are important to understand the variations of these waterbodies.

This study analyzes the hydrological behavior and properties of the Lake Chad Basin (LCB) in Africa. The size of Lake Chad alongside extreme climatic and environmental conditions hinders the continuous collection of field observation. A common problem faced in hard to reach areas with few poor infrastructures. This makes water management difficult and unreliable. The Study period is from Jan 2003 – Dec 2016. The study was divided into two phases for proper understanding; Lake Chad's Hydrological variability and Area Change Estimation. For the Hydrological variability, Total Water Storage (TWS) from Gravity Recovery and Climate

Experiment (GRACE), Lake Level from Satellite Altimetry and water fluxes from Global Land Data Assimilation System (GLDAS) were used to study the spatiotemporal variability of hydrological parameters of the LCB. For the lake area, Landsat 7 and 8 images were used to estimate area changes around Lake Chad. The Automated Water Extraction Index (AWEI), Normalized Difference Water Index (NDWI), Modified Normalized Difference Water Index (MNDWI) and Normalized Difference Vegetation Index (NDVI) were compared for the area extraction process.

Results show that estimates of TWS has similar variation patterns to Lake water level estimates. Estimates of groundwater volume changes derived by combining altimetric lake volume with TWS over the drainage basin showed a similar pattern to the groundwater estimates from WaterGAP Global Hydrology Model (WGHM) outputs. For the lake area extraction, the MNDWI was a better indicator and was used to estimate the lake's area changes from 2003-2016. Monthly area estimates showed an increasing trend and ranged between ~1242 km^2 and 2231 km^2. For validation, trend analysis between the Landsat area estimates and the Total Water Storage Anomaly (TWSA) GRACE showed a good match. This work shows the importance of remote sensing in a developing area. The results also suggest the use of freely available high-quality imagery data to address existing lake crisis. This could be of use to the management of the LCB for current and future management.

CHAPTER I: INTRODUCTION

A wide variety of species depend on inland water bodies for their survival. These waterbodies aid enormously in human well-being and terrestrial ecosystems (Charles V., 2005). Their uses range from serving as a form of habitat, to being an important component in the carbon cycle (Moss B., 2012). They are heavily used for energy production, fishery, transportation and irrigation (Stendera et al., 2012; Carvalho et al., 2013a). It is of essence to properly manage and sustain these resources to keep up with our needs. Such an ambition can only be achieved in areas where consistent and high-quality in situ large scale data are available. This is often lacking in most developing parts of the world (Swenson and Wahr, 2009). Also, the size and distribution of most freshwater bodies present a challenge for traditional onsite watershed assessment due to time, cost, and logistic constraints. Under these circumstances, researchers have used remotely sensed data sets as an effective tool to access water quantity and quality indicators over time. Spatial water distribution data has been used for a wide array of water-related research and planning activities. Mapping these inland waterbodies distribution in space and time has proven to be cost effective and sustainable method of management (Cole et al., 2007; Haas et al., 2009; Craglia et al., 2012; Novoa et al., 2012; Julia et al., 2016).

Most of the data availability and managerial challenges mentioned above are associated with most waterbodies within the African continent. Africa's lakes are the most exploited amongst the freshwater resources on the continent. Extreme climatic conditions threaten the ecological functioning of these waterbody. Coupled with

a growing population, exploitation of this water resource shows no sign of abating (Adrian et al., 2009; Jean-François et al., 2016). Monitoring of inland surface water status is increasingly seen as an important issue worldwide, because of the crucial role they play within their ecosystems, importance in human health, and in carbon sequestration.

Fortunately, remote sensing has made the large-scale study of this natural resource feasible and less costly. Remote sensing could be defined as the collection of data about an area by sensors that are not in direct contact with the area (Jensen, 1996; Lillesand et al., 2008). Remote sensing satellite data have been applied to identify and study various waterbody features like lakes, marshy vegetation and even the ocean. This data has helped in understanding the spatial pattern, significance and extent, of most waterbodies to their local community. It has also helped with identifying and monitoring these natural resources (Bhuvaneswari et al. 2011; Rani et al. 2011). Many types of remote sensing data have been used in numerous studies around the world: On a global scale, (Pete et al., 2018) used satellite observations to automate a method of mapping mangroves where they concluded that Asia has the highest proportion of mangroves with ~38% of the global total. Find submerged wetlands; A harmful algal bloom detection warning system was developed by (Sita et al., 2018) using data-driven models that rely on spatiotemporal remote sensing and some field data to identify factors controlling harmful algal blooms propagation, provide a same-day distribution (nowcasting), and forecast their occurrences up to three days in advance; Using Multi-angle Imaging SpectroRadiometer (MISR), the analysis of over 23,000 globally distributed wildfire smoke plume injections were presented in

a study carried out by (Maria et al., 2018). Their results showed heavily forested regions of North and South America and Africa produced the most frequent elevated smoke plumes with some being injected at an altitude >2 km for all those regions. From these few examples, we see that remote sensing datasets can be applied in a wide variety of field. This is mainly due to its wide areal coverage, repeatable observations and multiple sensors that are often updated over time. The interpretation of all these different data products is enhanced when integrated with other geospatial information, this integration being particularly enabled through GIS technologies and software.

Historically, Lake Chad was ranked among the largest lakes in the world. Weather changes, precipitation frequencies, poor irrigation and other mismanagements have caused the water level to drop to approximately 90% of its value in 1963 (Coe et al., 2001; Campbell et al., 2008; Luxereau et al., 2011; Gao et al., 2011; LACBO, 2013). The lake is shared by Cameroon, Chad, Nigeria and Niger (Figure 1). It is a closed lake whose basin extends as far as Libya, Sudan and Algeria.

The LCB is in a semi-arid region within the Sahel. The basin spans more than 2.4 million square kilometers and at its center lies the Lake Chad. Precipitation, river discharges, climatic indices and anthropogenic activities highly influences the hydro-climatic system of the basin this intend, has a direct influence on Lake Chad (Leblanc et al., 2011; Lauwaet et al., 2012). Water level within the lake is largely controlled by the inflow from two perennial rivers, the Chari-Logone River from the south and the Komadugu-Yobe River from the northwest which is highly seasonal. Shifting patterns of rainfall associated with the West African Monsoon highly fluctuates the inflow from these rivers, making the lake sensitive to drought.

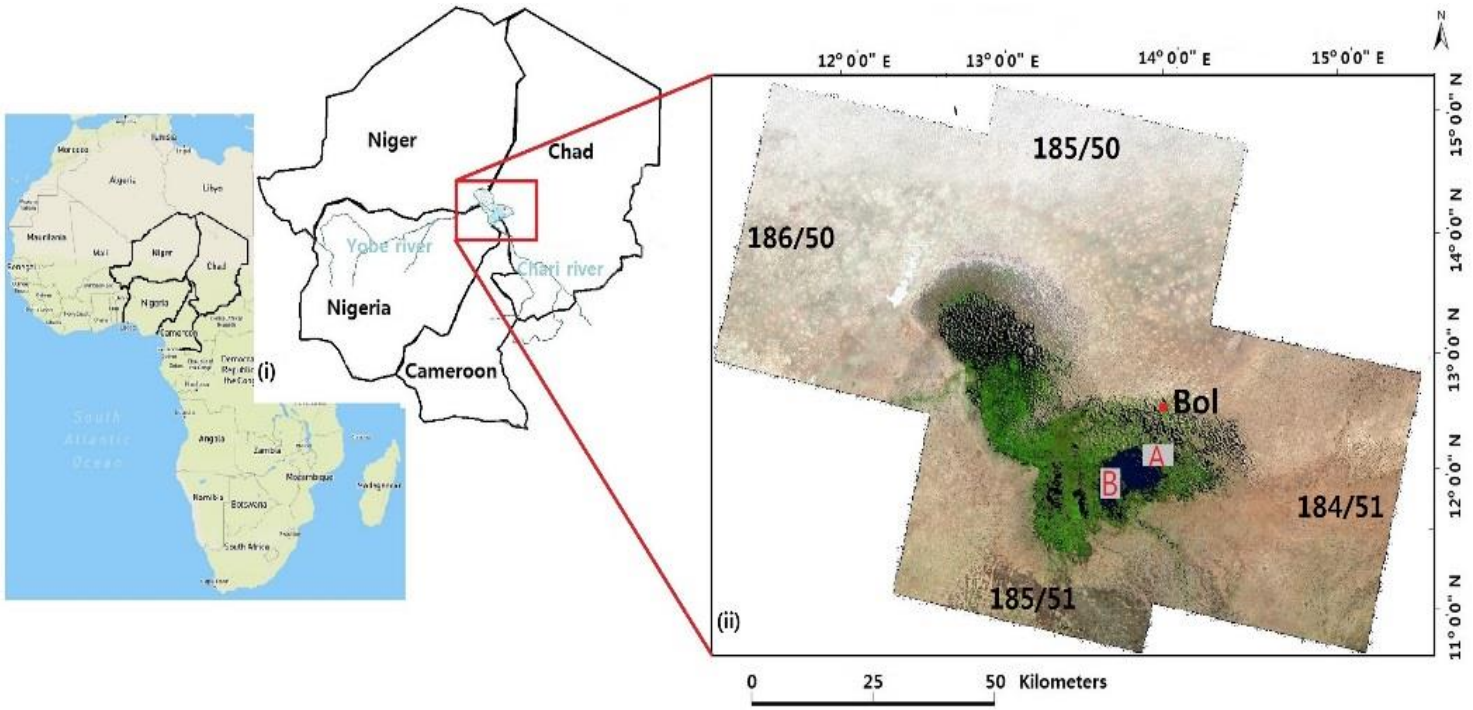

Figure 1. Location of Lake Chad Basin with area of permanent water. (ii) Four Landsat images with their respective Path/Row mosaicked to form a complete study site. Point A and B represents the locations of the high-resolution reference data. Bol is the closest village to the lake where most ground hydrological measurements collected by the LCB.

As a result of these extreme climatic conditions, high population growth rate, the construction of dams, and the development of irrigation agricultural facilities in the last four decades, the surface area of Lake Chad has decreased by ~80 per cent. The lake's surface area has plummeted from $\sim 25000\ km^2$ in the 1960s to $\sim 3000\ km^2$ today. In the 1960s, fishermen captured ~200,000 metric tons of fish every year, this served as a source of income and food for the lake inhabitants and beyond. Animal grazing during that period was very feasible and conflicts between herders and farmers were unheard of. However, with the recent reduction of the lake, most villagers lost their pastures. This has triggered food insecurity, social conflicts and poverty within the area. Some people have fled the area while others stayed and moved towards the available water resource to fend for themselves (Figure 2).

This reduction in lake size has proven to be a huge ecological disaster which has destroyed both livelihoods and biodiversity. Cadre Harmonisé, a food security analysis tool unique to West Africa, demonstrated that this crisis has contributed to soaring food insecurity, with more than 6.9 million affected in the regions of the four countries surrounding the lake (FAO, 2017). In the FAO's response strategy for 2017-2019, aimed at addressing the Lake Chad Basin crisis, part of the strategic framework is to manage the natural resources as well as resource-based conflict reduction by promoting sustainable management of land use, pasture and water resources at community level (FAO, 2017). This involves monitoring these resources at cross-border levels. A step towards achieving cross-border level results would be to understand the changes experienced by the lake over space and time.

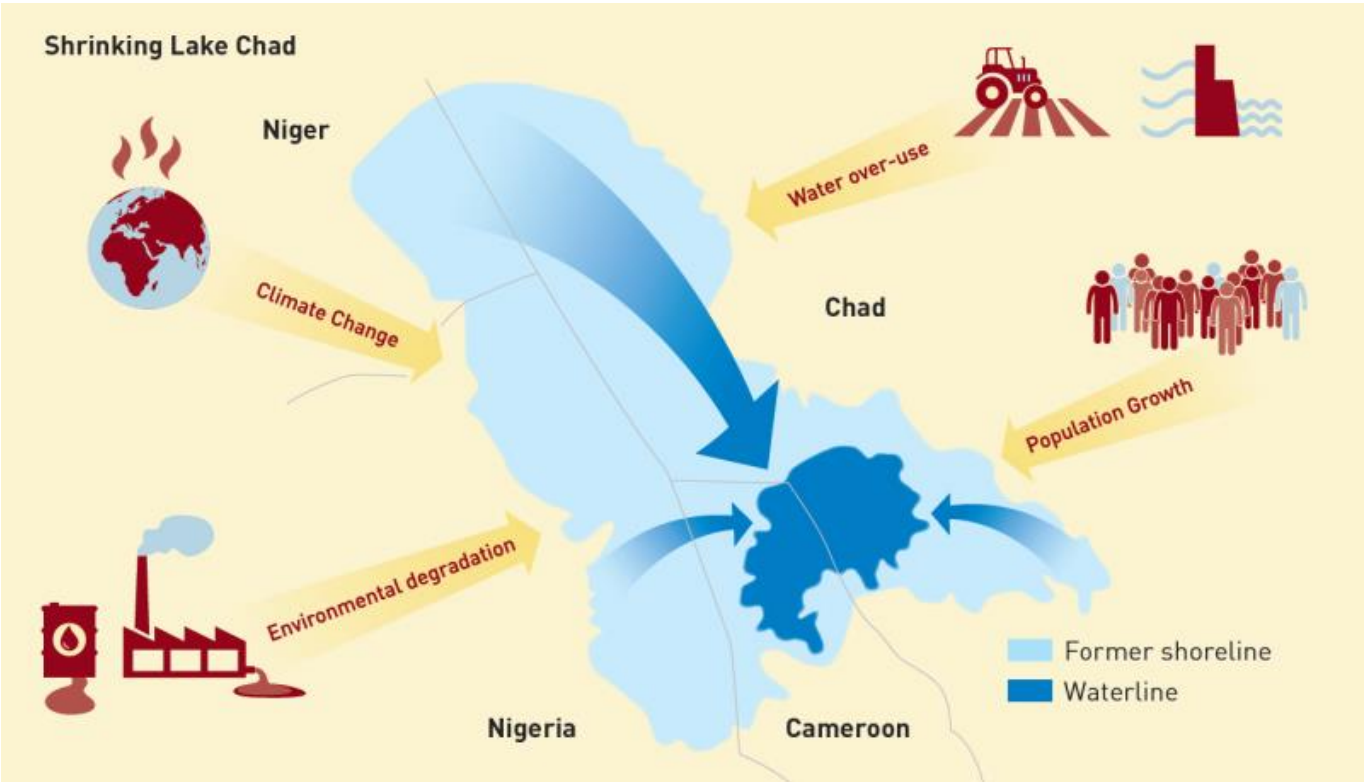

Figure 2. Causes and effects of a shrinking Lake Chad (Climate Diplomacy, 2016).

This can be investigated by carrying out an in-depth study of the lake's hydrological variations using remotely sensed and hydrological model data sets which are free to the public and regularly updated. Most waterbodies in this part of the world suffer from spatially and temporally inconsistent ground data. This makes the use of remote sensing data the best place to start in terms of water management studies (Swenson and Wahr, 2009). Satellite Gravimetric, altimetric and hydrological model data has proven useful to study temporal variability of water bodies. Likewise, Landsat images have been widely used for water body extraction or mapping using either a hard or a soft classification method. Increase in availability of their respective products provides opportunities to study and estimate water budgets as well as different components of water balance within the basin.

From 2003-2016, available data from the Gravity Recovery and Climate Experiment (GRACE) which measures the monthly temporal variations in the gravity field at a distance of about 220 km and above 500 km of the land surface was used for this study. Coupled to that, data products from satellite altimetry, Global Land Data Assimilation System (GLDAS), rainfall data from Tropical Rainfall Measuring Mission (TRMM), and WaterGAP Global Hydrology Model (WGHM) were also used to inquire the hydrological variability within this region. After which, a series of 416 Landsat images were used to investigate the area changes in Lake Chad over the same period. Finally, comparison between generated estimates were carried out against some observed data. In areas where ground-based hydrological measurements are lacking, satellite and hydrological model products has been used to make up for this in situ data shortage.

They have also served as inputs to land surface and atmospheric models and verification of these models. (Rodell et al., 2004; Boronina & Ramillien, 2008; Leblanc et al., 2011).

Total Water Storage Anomaly (TWSA) from the GRACE Satellites, lake levels from altimetry and hydrological model products over the Lake Chad basin were used to study the variability in its hydrological cycle. The effects of varying climatic parameters in this region and the estimation of total discharge using the water balance equation was carried out.

This was followed by estimating the area changes of available surface water within the Lake Chad basin using Landsat Thematic Mapper (TM), 7 Enhanced Thematic Mapper Plus (ETM+) and 8 Operational Land Imager (OLI) imagery. Four reflectance indices: AWEI, NDWI, MNDWI and NDVI were tested for extraction of the lake surface area from our Landsat data. MNDWI gave us the best results and was therefore used to calculate the areal extent during our study period. GRACE-derived TWSA changes and some meteorological data from the LCBC were used to complement our area estimates

1.1. Problem statement

The Lake Chad Basin whose interconnected water system, the Lake Chad (Figure 1), spans through several African countries, providing natural resources for over 30 million people in the region (Leblanc et al., 2007). The basin is situated in the middle of the Sahel, lies at an altitude greater than 300 m above the mean sea level in a region where the Sahara Desert meets the Savannah lands (Figure 3).

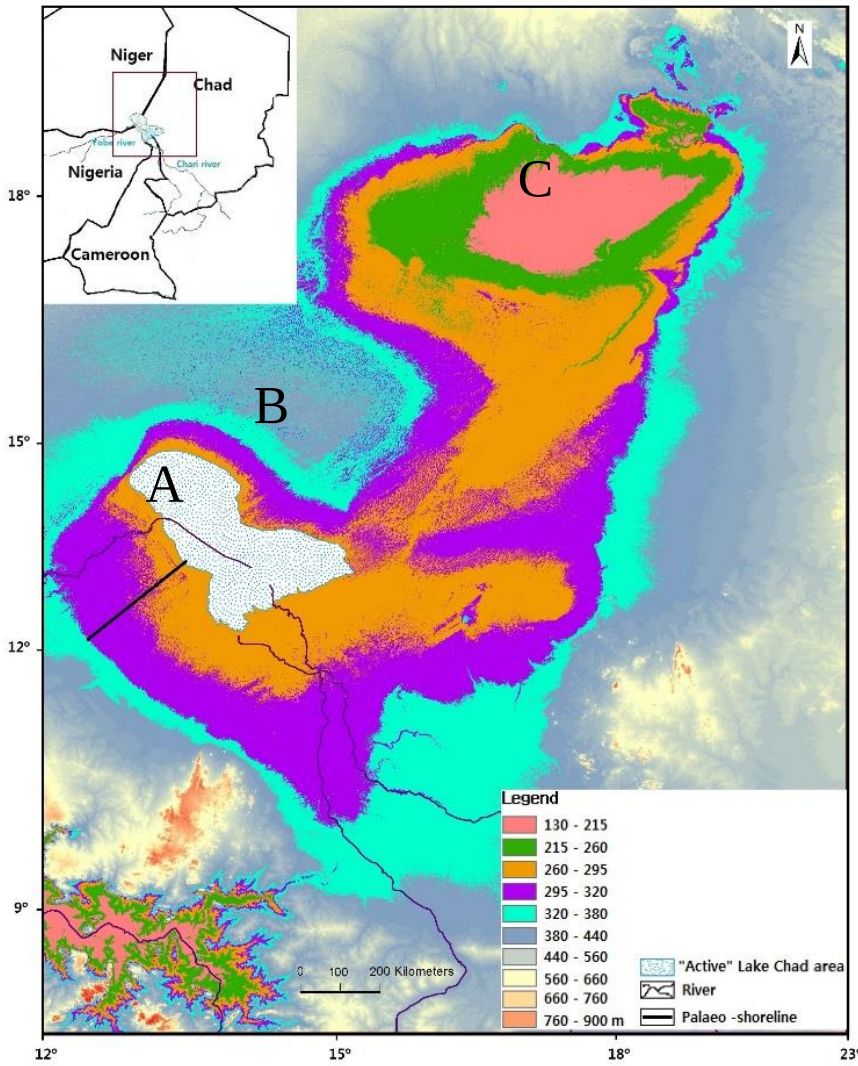

Figure 3. SRTM30 DEM of the Lake Chad Basin. A and B represents the shoreline of the "mega" and "active" Lake Chad respectively. The active Lake Chad shoreline have an elevation of about 290m asl. C is the lowest point within the basin.

The lake's surface area and water levels have fluctuated greatly after 1960s. Between 1963 and 2013, Lake Chad, has lost about 90% of its water mass (Crétaux & Birkett, 2006; Bader et al., 2011). This significant loss of water within the basin is evident in the Shuttle Radar Topography Mission (SRTM) Digital Elevation Model (DEM) in Figure 3. The lake shoreline receded from point A to point B. On an

average, about 55% of the lake area is covered by vegetation and marshes. Open water occupies about 10% of the lake area (Figure 4).

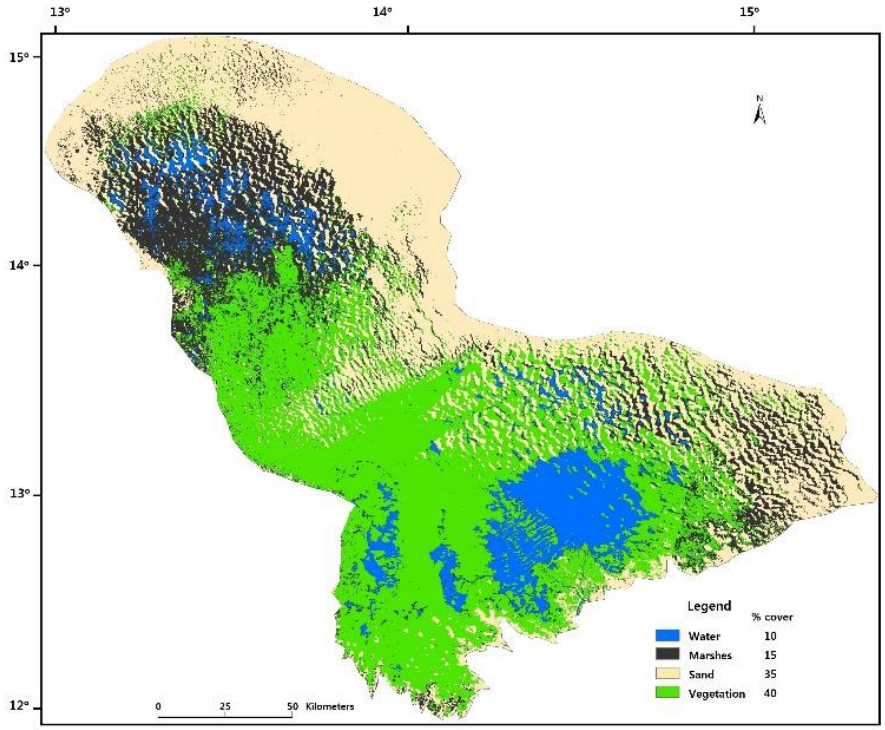

Figure 4. Averaged land cover types for Jul-Dec 2016

The resulting reduction in Lake Chad is visible in this false-color images from Landsat which better differentiates between vegetation (red) and water (gray) (Figure 5). Transition over time is visible, however, drought does not affect the entire lake equally. Additionally, there is a barrier of land described by Gao et al., 2011 is still somewhat present in recent times.

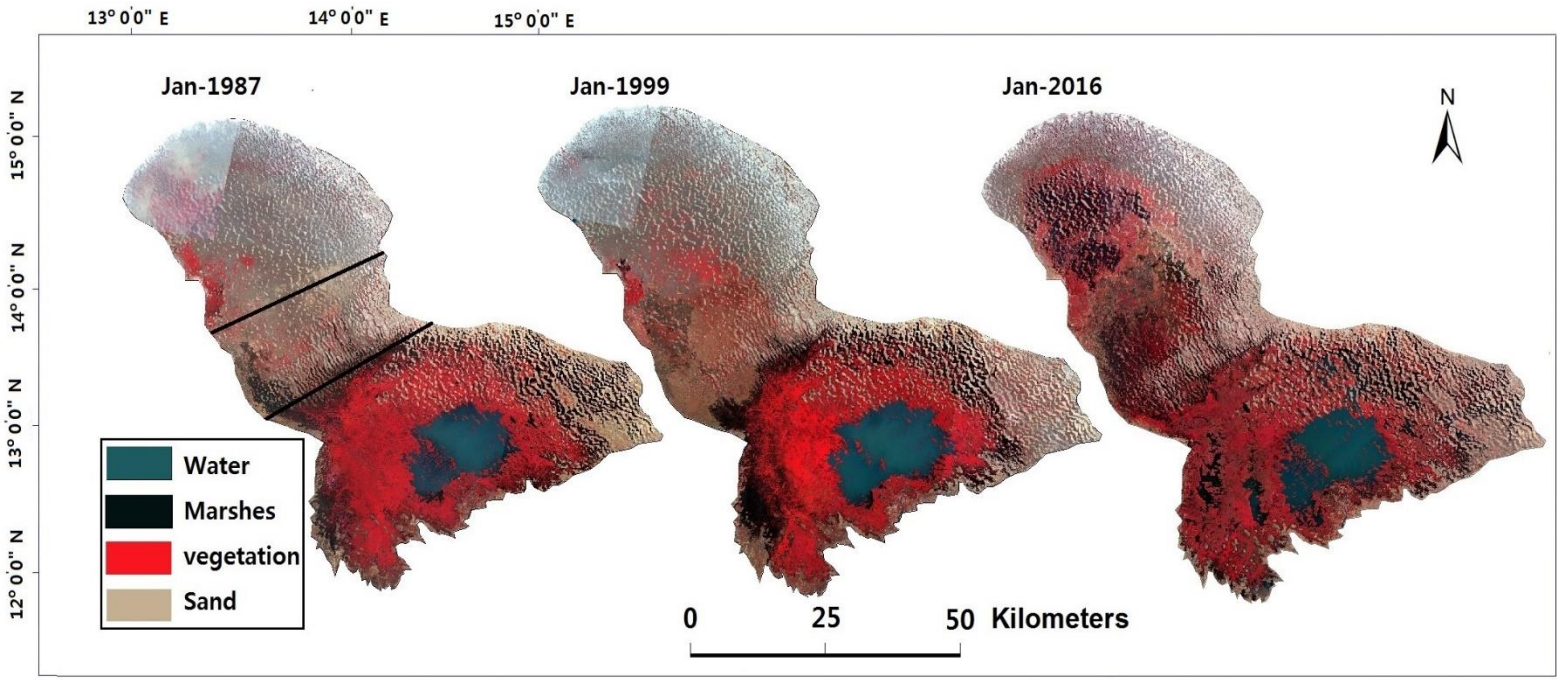

Figure 5. False color composite image produced using a combination of Landsat TM (4, 3, 2) and OLI (5, 4, 3) bands. The bars in the Jan-1987 image represent the split described by (Gao et al., 2011).

This reduction, mainly caused by climate change and human forces, threatens the resources and livelihood of the more than 30 million people in the region. Thus, there is an urgent need to understand the hydrological variability and quantification of available surface water within the basin. Lack of ground-based observation data is a major problem associated with this type of work. Globally, studies in areas with low data availability have used a combination of remotely sensed data from varying sources for their individual research interest.

1.2. Aim, objectives and limitations

In this study, I used Satellite Gravimetric, altimetric, hydrological model products and Landsat images over the Lake Chad basin to;

(1) Study the variability in its hydrological cycle.

(2) To infer the effect of rainfall water storage in this region

(3) To analyze the changes in areal surface water coverage in Lake Chad using the appropriate water index derived from Landsat imagery.

(4) Comment on the link between climatic parameters and surface water extent.

The LCB is situated in one of the least developed regions in Africa. Up to date datasets were unavailable and the few available required higher costs for purchase. The datasets also had missing values which were filled using standard statistical methods. This was one of the major limitations encountered during this study. As such, some analyses were dependent on documented data and information in scholarly articles, journals, consultations with the supervisor and the web.

1.3. Thesis structure

In order to achieve the above objectives, this thesis is organized in 6 chapters (including the current one). The thesis is based on various articles. For clarity purpose, Chapter 4 and 5 will be explained under these main headings; Lake Chad's Hydrological variability and Area Change Estimation. This is the order in which their results were published.

Chapter 2 presents a concise review of water availability and management assessment in the continent. Furthermore, a review of previous works where a remotely sensed data from various sources has been used in a new and innovative way to will be introduced.

Chapter 3 presents an introduction of the data sets used in this thesis. In this section, the basic concepts associated with each data creation is presented. The most important scientific instruments of the satellites or models used for data creation are presented. The data acquisition methods are also introduced and problems associated with most of the data are addressed.

The Fourth Chapter presents an approach for inquiring and viewing what the hydrological variations has been like over the last decade. In the section, the time series of the GRACE monthly estimates were decomposed into their trends, seasonal and noise components. Followed by an investigation of the subsurface water volume changes in the area. This was achieved by using data from GLDAS and groundwater estimates from WGHM to investigate the performance of the derived subsurface water levels. A detailed discussion of the result is also presented

The Fifth Chapter demonstrates the usefulness of moderate resolution images from Landsat in delineating surface water area of inland water bodies. This case study illustrates advantages and drawbacks of four water indices (AWEI, MNDWI, NDVI, and NDWI) used for area extraction and proposes some improvements. A very high resolution image was used to verify how accurate were derived area from the Landsat images were. The chapter also includes a discussion on the values obtained.

The thesis ends with a general conclusion that summarizes its findings and brings together and synthesizes the previous chapters. This chapter (Chapter 6) also provides some perspectives for future research.

CHAPTER II: LITERATURE REVIEW

Lake Chad is geographically significant in west-central Africa because of its socio-economic and cultural prominence within the area. It was the 6th largest lake in the world but recently has dried up into fragmented collections of water bodies in the northern and southern pools (LCBC, 2014). Precipitation rates here could vary between ~1,400 mm/year in the south to ~10mm/year in the north. Four main climatic zones can be identified in the LCB

- The Humid zone in the Southern part
- The dry humid zone between the CAR and Chad
- Semiarid zone at the center between Chad, Niger and Nigeria
- The Northern arid zone in Niger and Chad.

The LCB is a sedimentary groundwater basin composed of three main aquifers: the upper Quaternary with the Lower Pliocene, the Continental Terminal and the Cretaceous lower aquifer. The main source of aquifer recharge here is the Lake Chad. This makes the aquifer system very sensitive to climatic changes (GWP, 2013). Isotopic studies identified recharge zones higher areas and in exposed sand dunes around the basin. Leakages from the surrounding rivers, Lake Chad and wetlands also contribute to aquifer recharge. Groundwater recharge has decreased in recent years mainly due to drought and excessive human exploitation in the upstream regions. With over 60% of the basin population being farmers, irrigated agriculture is the first water user in this area. Groundwater is heavily used for irrigation during the dry seasons.

2.1. The surface waters

The LCB could be subdivided into two river subsystems: The Chari-Logone River subsystem, which covers ~650,000 km^2 contributing over 80% of water into the Lake Chad, and the Komadugu-Yobe River subsystem covering ~148,000 km^2 but contributes ~3% of inflow into the Lake Chad. Water from the Chari-Logone River flows into the Lake from the South and sometimes flows to the North during peak seasons owing to the lake's gradient and prevailing winds. During the nineteenth and twentieth century, five major water recession phases were recorded within the basin. Leblanc et al 2011 described these phases as Mega, Large or Normal, Average, Small and Dry Small Lake Chad depending on the water levels or depth.

The existing permanently open water bodies and seasonal ponds around the basin provide livelihood options in farming, fishing and livestock herding for the population. Soils close to the Lake are prone to droughts and can easily be flooded during extreme flood years (Luxereau et al., 2012). Farming and fishing systems here are developed to exploit the seasonal flooding of the lake shore with most farmers usually relying on new land to maintain fertility levels (Sarch & Birkett, 2000). Most communities around the lake carry out small-scale Agropastoral and fishing livelihoods. This makes them highly dependent on water availability from the lake and local rainfall. Cotton, maize, potatoes, soybeans, millet, wheat, sugarcane and vegetables are the common crop types cultivated in the area (Fortnam & Oguntola, 2009; FEWS, 2010). Mixed crop farming is widely covered in this area with most of it carried out without the use of fertilizers and harvest

done by hand (Odada et al., 2009). Previous study shows that from 1983 to 1994, water used for irrigation in this area increased fourfold compared to the levels during 1953–1979 (Coe & Foley, 2001). Current and potential water used for irrigation by the four countries surrounding the lake was estimated by the FAO. Nigeria recorded the highest usage of water for irrigation purposes.

Table 1. FAO current and potential volume used for irrigation.

Country	Area under irrigation (ha)	Irrigation potential within the whole basin (ha)	Gross irrigation water requirement (km^3/year)	
			Per ha (m^3/ha.year)	*Total* (km^3/year)
Nigeria	82,821	304,000	1,000	3,040
Chad	14020	277500	15500	4.163
Cameroon	13820	66700	12500	0.834
Niger	2000	11000	0.215	2000
Sudan	500	4000	7500	0.03
Central Africa	135	16500	16500	8.250
Algeria	0	18000	0	0

The fishing sector consist of thousands of artisanal fishers. They mostly fish in the open water, along pools, water channels around villages and islands surrounding the lake. Most of their catch are smoked and dried.

2.2. Water resource conflicts and their causes

When access to and allocation of water becomes difficult, it is very common for water conflict to arise. Even in cases where there is an abundance of water, making this resource available to different users and uses has emerged to be a cause of dispute. Similarly, a decline in water quantity or quality can trigger mass migration which could socially and politically destabilize destination states (Carius et al., 2004). It is projected that the population of people living around the lake may reach 80 million by 2030 (Okonkwo & Demoz, 2014). Population increase implies an increase in demand for water resources and all its benefits (Fokou, 2010; Haller et al., 2013). In areas where this resource becomes scarce, conflicts are bound to happen. The prevalence of poverty and poor living conditions in the Lake Chad region has been well documented. Most of the lake's problems were never addressed by all its surrounding countries (Okpara et al.,2015; Angerbrandt, 2017). Farming is the main income generating activity in this region. The Lake Chad Basin provides water for irrigation. The four countries surrounding the basin have built dams around the lake, changing the flow of water.This has affected farming activities in the region. Consequently, fertile land has become scarce, leading to ethnic clashes and tensions between communities (Ngatcha, 2009; Angerbrandt, 2017) The UN already reported numerous conflicts over control of the lake's remaining water among nationals of its surrounding countries (UN, 2012). With some 7 million people suffering the risk of severe hunger, some 50,000 of them are already facing famine (FAO, 2017). Any recent drought may worsen the situation if the authorities are not fully prepared.

2.3. Previous studies on the basin

As previously mentioned, the lake's surface area was estimated to be ~25,000 square kilometers equivalent to one tenth of its area in 1960 (Grove, 1996). In 1991, Lemoalle, described the Lake as a "Small Chad" after they compared their observations to that of the "normal lake" described by Tilho et al., in 1928. Water levels exceeded 280m above sea level (asl) during that period. Studies from Coe et al., 2001 and Luxereau et al., 2011, reported that this lake levels have fluctuated considerably over the past decades. Extreme drought brought about a sandy barrier which divides into a Northern and Southern section. Some researchers used a hydrological model to simulate the effects of bathymetry, human interactions, and climate variability on the lake level, surface area, and water storage. They concluded that siltation and severe drought caused the lake to split in 1972 forming the sandy barrier. Over the years, the lake has failed to merge back into a single lake even during the peak of the raining season. Most river channels along the Komadugu-Yobe River which serves as a passage way for water into the Northern section of the lake have been clogged by invasive species and sedimentation. Strips of land occupied by invasive species contributed to the diversion of flow away from the Lake (Bdliya & Bloxom, 2007). Main ecological zones within the lake includes;

1. Permanent open water in the Southern portion of the lake
2. An archipelago zone in the South-East of the lake.
3. Seasonally inundated swamps in the West and Northern section

(Isiorho, 1987; Lemoalle, 1991).

The hydrological or ecological properties of the lake are not restricted by those three points above. Over the years, some researchers have studied diverse but specific aspects of the lake's hydrology (Isiorho, 1990; Isiorho et al., 1996; Birkett, 2000; Leduc et al., 2000; Massuel, 2001; Leblanc et al., 2007; Goni, 2006; Boronina and Ramillien, 2008; Ngounou Ngatcha et al., 2008). Researchers found that water balance in this area reflects the interactions between rainfall, evaporation, lateral inflow, and groundwater. Inundated areas varied substantially depending on the amount of annual rainfall and run-off during a given season. Extreme swings in Lake Chad's water levels are not new to researchers. The lake has experienced wet and dry periods for thousands of years, according to paleoclimate research (Schneider 1989; Birkett, 2000). Coe & Foley, 2001 pointed out that persistent drought in this area was the driving force behind the lake's continuous decrease. Another study tied the lake's decreasing trend to an increase in irrigation activities around the lake (Campbell, 2008). Altimetric measurements of water height were used to estimate river discharge around the Chari-Logone River confluence using imperial regression techniques (Coe & Birkett, 2004). The authors successfully estimated the height of the permanent waters 600 km downstream of the lake 39 days in advance. The consequent effects of the lake's decrease on surface and groundwater recharge have not been adequately addressed by the appropriate water authorities.

This is not the first time remote sensing data sets or hydrological models have been used in the studies of the lake. They have been heavily used in the past. For instance, to compensate for the lack of hydrological data within the basin, past water levels and inundated areas were reconstructed from 1973-2011 using

hydrological models (Lemoalle et al., 2012). The authors also simulated the effects of abstraction for irrigation purposes, inflow from inter basins and climate change impacts on the lake. Other studies focused on the changes in stream flow patterns connected to the lake (Li et al., 2007; Campbell, 2008; Le-Coz et al., 2009). (Leblanc et al., 2006) reported on the existence of a mega-lake Chad. They used satellite images from Landsat and Moderate Resolution Imaging Spectrometer (MODIS) for its reconstruction. Landsat Multispectral Scanner (MSS) band 7 (0.8–1.1 μm) data from 1973 to 1976 and Meteosat data in the visible channel from 1977 to 1990, were used to investigate the maximum inundation in the Northern side of the lake (Lemoalle, 1991).

Thermal remote sensing techniques, such as the Meteosat thermal maximum composite data, was used to account for the variability of inundated areas within the lake under flooded vegetation. Researchers found that the variability of the inundated areas observed in the Northern pool to be about 60% greater than that of the Southern pool (Leblanc et al., 2003). Estimates of actual evapotranspiration over the Lake Chad Basin were computed using the S-SEBI algorithm and then compared with ET estimates derived from GRACE. Both solutions showed a similar pattern in ET over the basin (Boronina & Ramillien, 2008). Using multivariate regression analysis of time series from 1988–2012 on a sub-regional level, two hydrological systems, lake levels and rainfall data, were incorporated to investigate the correlations and predictive capacities of lake water levels, rainfall and temperature variability to inter-annual variations of harvested maize and millet (Erik et al., 2016).

The over 30 million people settled in the Lake Chad Basin belong to some of the poorest countries in the world. Agriculture being their main go to activity for survival is at risk with recent droughts. It has been a daunting task to meet the managerial needs of the Lake Chad. Limited and low-quality ground data hinders feasibility studies of the lake (Swenson & Wahr, 2009; Allen et al., 2011). This could be the reason of the slow pace in the management processes. In their recent response strategy to the Lake Chad Basin crisis, the FAO is seeking to promote sustainable peace, resource-based conflict reduction and natural resource management at cross-border level. Their general approach will be to create conditions for recovery that are socially, economically and environmentally sustainable. To achieve this task, they laid down several points which if followed, could lead to a possible recovery of the lake and enhance the lives of its inhabitants. One of those points is to promote informed programming and policy processes through analysis of natural resource management. They encouraged the mapping and analysis of existing resources within the basin. Given the shortage of in situ data, remote sensing data sets can serve as a gateway towards realizing these outcomes.

CHAPTER III: MATERIALS

3.1. Terrestrial Water Storage from GRACE

Satellite gravimetry could be defined as the art of mapping the Earth's gravity field using satellites. Redistribution within the Earth's system brings about changes in its gravity field (Rummel, 2005). Gravity potential, used to express the Earth's gravity field, is the sum of the normal gravity potential and disturbing potential (Xu et al., 2007). Given that normal gravity potential can be derived analytically, satellite gravimetric missions focus on providing information on the disturbing potential (T). Disturbing potentials are most commonly represented by a series of spherical harmonic coefficients (Rummel et al., 2002). It can be calculated using equation (1)

$$\mathrm{T}(\mathrm{r},\varphi,\lambda) = \frac{GM}{R}\sum_{l=2}^{L}\left(\frac{R}{r}\right)^{l+1}\sum_{m=0}^{L}\left(\overline{C}_{lm}\cos m\lambda + \overline{S}_{lm}\sin m\lambda\right)\overline{P}_{lm}(\sin\varphi)$$

$$= \frac{GM}{R}\sum_{l=2}^{L}\left(\frac{R}{r}\right)^{l+1}\sum_{m=-l}^{L}K_{lm}Y_{lm}(\varphi,\lambda), \qquad (1)$$

Where:

$\overline{\boldsymbol{P}}_{\boldsymbol{lm}}, \overline{\boldsymbol{Y}}_{\boldsymbol{lm}}$: Real and complex valued Legendre functions of degree l and order m respecctively

$\overline{\boldsymbol{C}}_{\boldsymbol{lm}}, \overline{\boldsymbol{S}}_{\boldsymbol{lm}}, \boldsymbol{K}_{\boldsymbol{lm}}$: spherical harmonic coefficients, K_{lm} is the complex of $\overline{C}_{lm}, \overline{S}_{lm}$

$\boldsymbol{G}, \boldsymbol{M}$: gravitational constant and mass of the Earth; $\boldsymbol{R}$: Earth's mean radius

$\left(\frac{\boldsymbol{R}}{\boldsymbol{r}}\right)^{\boldsymbol{l+1}}$: Field attenuation of altitude

$\mathbf{r}, \boldsymbol{\varphi}, \boldsymbol{\lambda}$: spherical coordinates at the point of interest

$\boldsymbol{l}, \boldsymbol{m}$: spherical harmonic fegree and order

C and ***S*** are the gravity field unknowns which are to be determined from the gravity field observations. Satellite gravimetry TWS are derived from a monthly to decadal scale based on the assumption that mass changes over the continents mainly arises from the redistribution

of water masses (Ramillien et al., 2008). For this assumption to be valid, the short-term non-hydrological mass changes like those arising from post-glacial rebound (Purcell et al., 2011; Wahr & Zhong, 2012), earthquakes (Fuchs et al., 2013) and erosion(Schnitzer et al., 2013) need to be insignificant. Also, the signals must be corrected for well-known and modeled signals from the Earth and ocean tides, and atmospheric and ocean dynamics (Sakumura et al., 2014).

Some limitations are associated with satellite gravimetry. Like for instance, obtaining absolute amount of water storage using this method is impossible as the absolute gravity signals are usually impacted by all kinds of masses on the Earth's surface and its interior. However, relative water mass changes with respect to some reference value can be derived.Another limitation is that the origin of the mass change cannot be pin pointed to a specific hydrological change component. Additional information is usually required to define whether the mass change was caused by surface water or groundwater or a non-hydrological process (Wahr et al., 2006).

Over the years, several missions have been executed to reveal some information about the Earth's gravity field. Among which is the GRACE mission which is based on a low-low satellite to satellite tracking (ll-SST). GRACE is a collaboration of the National Aeronautics and Space Administration and German space agencies (NASA and DLR). This mission was launched on March 17th, 2002. The mission has several partners for design, construction, launch and data assimilation, such as the Jet Propulsion Laboratory (JPL), the University of Texas Center for Space Research (CSR), the German Research Centre for Geosciences (GFZ), as well as Astrium GmBH, Space System Loral (SS/L), Onera and Eurocke GmBH. It was

developed to make detailed measurements of the Earth's gravity field and investigate the Earth's water reservoirs. It is determined by mass and shows how this mass is distributed around the planet and how it varies over time. Usage of GRACE to accurately determine the time variations in the Earth's gravity field is beneficial to many areas of scientific research such as oceanography, hydrology, glaciology or solid Earth sciences.

- ***GRACE instrumentation and measurement principles***

The concept of GRACE is based on the proportional relationship between gravity and earth density. The Earth surface has different objects of varying density. This variations in density makes a slight variation in the gravitational field. GRACE only mission is to detect these slight changes from space. GRACE has no sensor to observe the earth. Unlike most remote sensing satellite that uses radar or radiometers, the GRACE satellites act as the measurement devices (Rodell et al., 2009). Instead, it measures the distance between two identical satellites orbiting the Earth using a precise K-band (~10 μm) microwave system. This measurement range is the key scientific element of the GRACE mission. This distance is later on used to determine temporal variations of the Earth's gravitational field (Tapley et al., 2004).

The GRACE system consist of two chasing satellites flying at an altitude of 450-500 km in a near polar orbit with an inclination of about 89.5^0. The satellites orbit one behind the other in the same orbital plane at an approximate distance of 220 kilometers (137 miles). When gravity increases, the leading satellite accelerates before the second accelerates and catches up. As the pair circles the Earth 15 times a day, areas of slightly stronger gravity (greater mass concentration) affect

the lead satellite first, pulling it away from the trailing satellite. As the satellites continue along their orbital path, the trailing satellite is pulled toward the lead satellite as it passes over the gravity anomaly. These minute differences in distance between the satellites are measured using the K-band microwave system. Making it possible to map the gravitational field of the path observed. Changes in the inter-satellite distance are the mission data.

In addition to the K-band, each satellite carries an accelerometer, located at each satellite's center of mass. With a precision of ~0.1 nanometer per second squared, the accelerometer measures the non-gravitational accelerations (such as those due to atmospheric drag) so that only accelerations caused by gravity are considered. With the help of the Satellite's Global Positioning System (GPS), the exact position of the satellite over the Earth can be determined within a centimeter or less (Figure 6). The resolution of the gravity field depends on the orbital height. The lower the orbit, the better the resolution, but also the more drag on the satellites which decreases the satellite's lifetime.

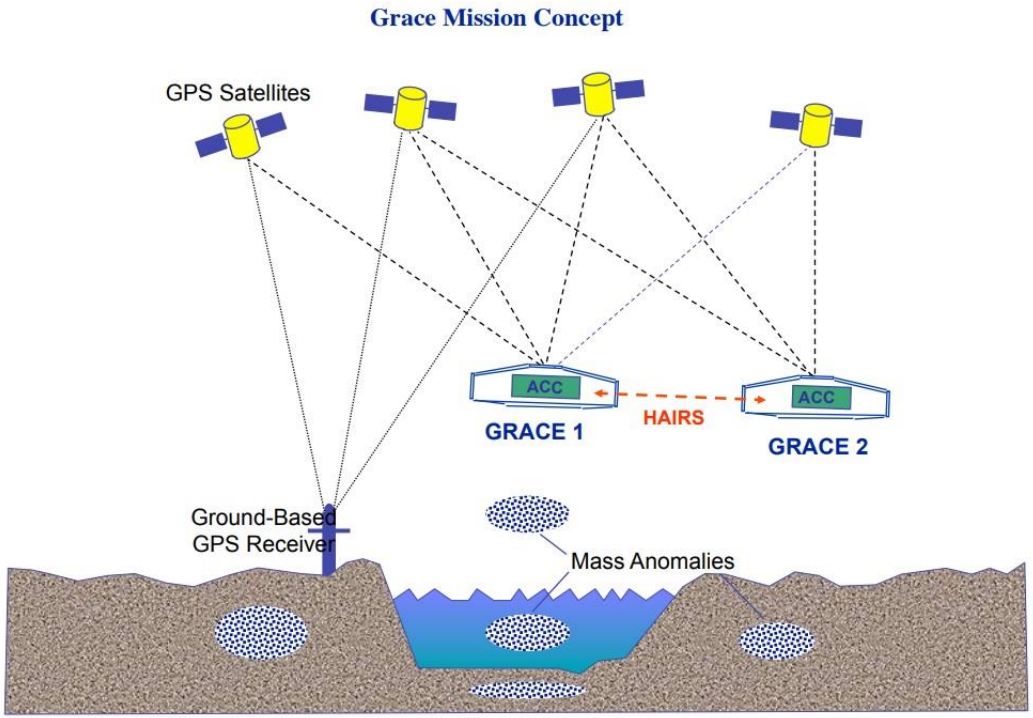

Figure 6. GRACE twin satellites passing over different gravity field of the earth surface. When the gravity increases below, leading satellite (GRACE 1) accelerates, creating a distance between the two satellites (GRACE 2) (Lee et al., 2012).

- ***GRACE data structure***

Extraction of Earth gravity models is being handled by the three processing centers within the GRACE project Science Data System (SDS): The Center for Space Research at the University of Texas, Austin (UTCSR), Jet Propulsion Laboratory (JPL) at Pasadena, USA and the Geoforschungszentrum in Potsdam, Germany (GFZ). After validation, the SDS distributes monthly models of Earth gravity field, to the public via the Physical Oceanography, Distributed Active Archive Center (PO.DAAC) at JPL and Information Systems and Data Center (ISDC) at GFZ.

The raw stream data, also known as the level-0 data from each GRACE satellite is received at the raw data center of the Mission Operation System (MOS) twice per day and stored in appropriate files (Bettadpur, 2003). The SDS centers later retrieves some files and instrument and ancillary housekeeping data like GPS navigation solutions and space segment temperatures (Bettadpur, 2007). During this second stage of data collection, the inter satellite range-rate measurements (m/s), accelerometer data, attitude and positioning data are also archived and forms what is known as the level-1 data.

Level-1 data generally includes the preprocessed, time-tagged and normal-pointed instrument data including the K-band ranging, accelerometer, star camera and GPS data of both satellites. Level-1 products are done primarily at JPL with support from the GFZ which is equipped with backup systems. The level-1 data are divided into level-1A and level-1B. Level-1A data are the raw data which have been calibrated and time-tagged in a non-destructive sense as the data can be reversed to obtain the original level-0 data if desired, except for bad data packets. Level-1A data products are not distributed to public.

Level-1B data products include among others, the intersatellite range, range-rate, range-acceleration, and the non-gravitational accelerations from each satellite. After validation, they are released to the public through PO.DAAC at JPL and ISDC at GFZ. These products are processed to produce the monthly gravity field estimates in form of spherical harmonic coefficients. The leve-1B data is possibly irreversible (Bettadpur, 2007).

The Earth's gravity field can be expressed as the sum of spherical harmonics. The gravity fields produced by GRACE represents a set of spherical harmonic coefficients, complete to a degree and order 120 (Crowley et al., 2006). These coefficients are provided as level 2 products after the removal of non-hydrological gravitational contributions. Level-2 data are the monthly and mean gravity field derived from calibrated and validated GRACE level-1 data products. The GRACE level-2 data are provided as sets of fully normalized spherical harmonic coefficients, C_{lm}, S_{lm}, also called Stokes coefficients. The degree and order of the coefficients are up to 60, 120, and 120 for CSR, GFZ, and JPL respectively.

Generated gravity fields requires spatial smoothing to reduce the effect of errors present in shortwavelength components. This is done during post-processing (Swenson & Wahr, 2006). To generate spatial maps of TWS anomalies in cm of equivalent water height, the sperical harmonic coefficients are smoothed with a Gaussian averaging kernel width (250 – 1000 km radius) and then expanded to regular grid (Wahr et al., 1998). After proper processing, GRACE uncertainty is about 2.1 cm. At a resolution >200,000 km^2, the uncertainty in the estimates begins increasing (Rodell & Famiglietti, 1999; Yeh et al., 2006b). On a time-scale ranging from months to decades, GRACE

estimates have been extensively used in the studies of Lakes around the World. Mapping variations within their temporal gravity fields with a high degree of accuracy (Tapley et al., 2004; Wahr et al., 2004; Joseph et al., 2008; Song et al., 2013; Longuevergne et al., 2013; Cai et al., 2015; Longuevergne et al., 2015; Yang etal., 2017; Shengnan et al., 2017; Mohamed & Karem, 2018).

Monthly sets of spherical harmonics from GRACE Release 05 (RL05) gravity field solutions from the Centre of Space Research (CSR) of the University of Texas at Austin from January 2003 to December 2016 were used for this study. With each monthly GRACE field consisting of a set of Stokes coefficients up to degree and order of 60. The C_{20} (degree 2, order 0) obtained from GRACE was changed to C_{20} from the Satellite Laser Ranging. Since the GRACE-C_{20} estimates has a larger uncertainty than those from SLR C_{20} (Chen et al., 2004; Cheng & Tapley, 2005).

Monthly variations in land gravity fields are mainly caused by monthly TWS changes which encompasses Surface water, soil moisture, groundwater and snow. A monthly equivalent water height represents a monthly anomaly in TWS, herein named TWSA. The data are available as monthly 1*1 grids TWS over our study area. Snow and ice are ignored since this part of Africa is humid.

3.2. Landsat imagery

Remote sensing systems make use of the electromagnetic spectrum (EM) which is a continuum of all electromagnetic waves (radiations) arranged according to frequencies and wavelength. EM comprises the span of all electromagnetic radiation and consists of many subranges, commonly referred to as portions, such as visible

light or ultraviolet radiation. Energy ranges from the high frequency, short wavelength (gamma rays) to the low frequency, long wavelength radio waves (Figure 7). Radiation used most frequently by current sensors is clustered in the visible to thermal infrared regions and portions of the microwave region due to atmospheric absorption and scattering, also referred to as attenuation.

Satellite imageries are usually generated from passive remote sensing systems. They are formed when sensor collects reflected radiation (wavelength, or $\lambda < 3\mu m$), usually generated by the sun, or emitted ($\lambda > 3\mu m$) radiation from an object (Campbell 2002; Rott 2000). When reflected values are collected digitally, each is assigned to a pixel with a unique column and row address. The area of ground represented by each pixel is equal to the instantaneous field of view and spatial resolution attainable by that specific sensor. For a sensor to be able to resolve a specific object, the feature's minimum dimension should be equal to or greater than the width of two pixels (Sabins & Floyd, 2007).

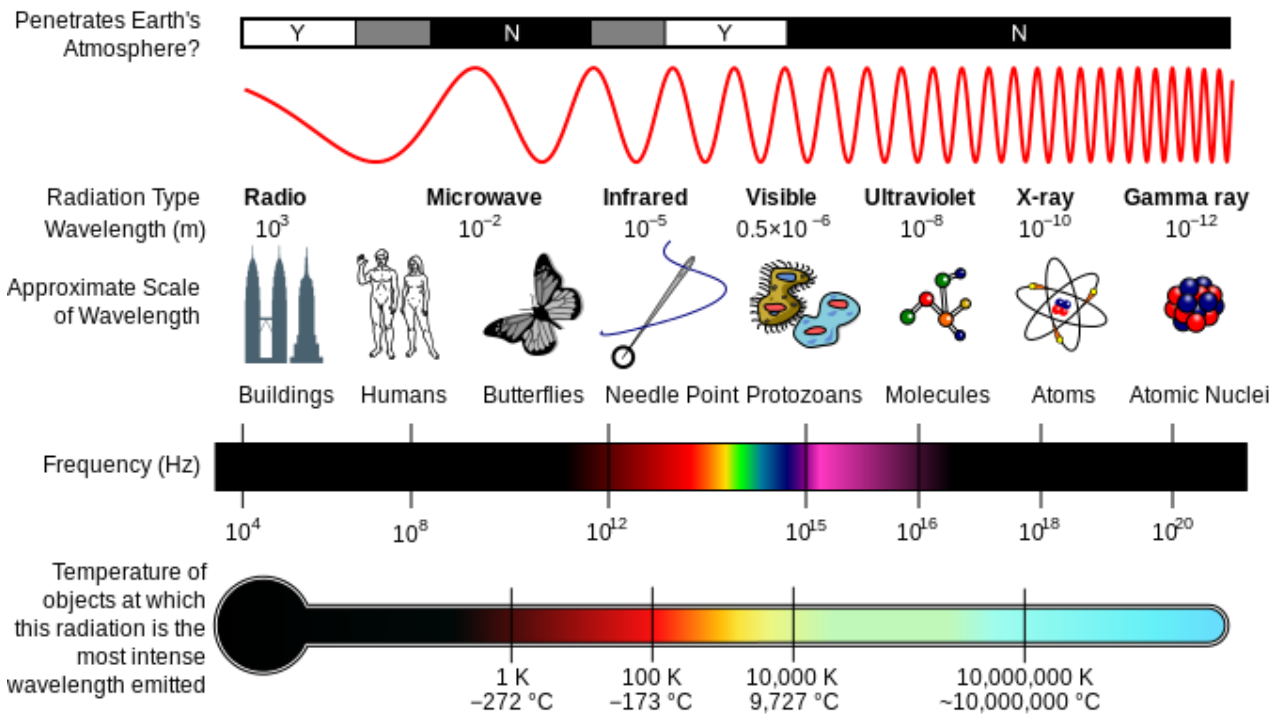

Figure 7. The Electromagnetic spectrum (NASA, 2016).

Satellite images used in this study were multispectral images from the Landsat 7 Enhanced Thematic Mapper Plus (ETM+) and Landsat 8 Operational Land Imager (OLI) sensors. Landsat 7 was launched in 1999. It uses a single detector and mirror to acquire data one pixel at a time by scanning back and forth. An approach known as the whisk broom scanning approach. With numerous moving parts, the scanners were more susceptible to failure. In 2003, the Scan Line Corrector failed, creating data gaps which creates issue for time-series data analysis. This resulted in it transmitting 22% less data than before. The ETM+ sensor collects bands ranging from blue-green (0.45-0.52 μm) to shortwave infrared (2.08-2.35 μm) with 30 m spatial resolution. It also collects a thermal band (10.4-12.5 μm) with 60 m resolution, and a panchromatic band (0.52-0.9 μm) with 15 m resolution for a total of eight bands. The Landsat 8 has been operating without error since 2013. It uses a push broom scanner with multiple selectors to scan a line of pixels all at once. This made it less susceptible to the wear and tear of having more moving parts (U.S.Geological Survey, 2017).

Just as the pictures on our television screens, satellite imagery is made up of tiny squares called picture elements (pixels), each having a different shade of gray. Pixels represent the relative reflected light energy recorded for that part of the image. Sensors that record electromagnetic energy, electronically record the energy as an array of numbers in digital format. This information is recorded as a single numeric value corresponding to the intensity of the energy detected from a given area (Figure 8).

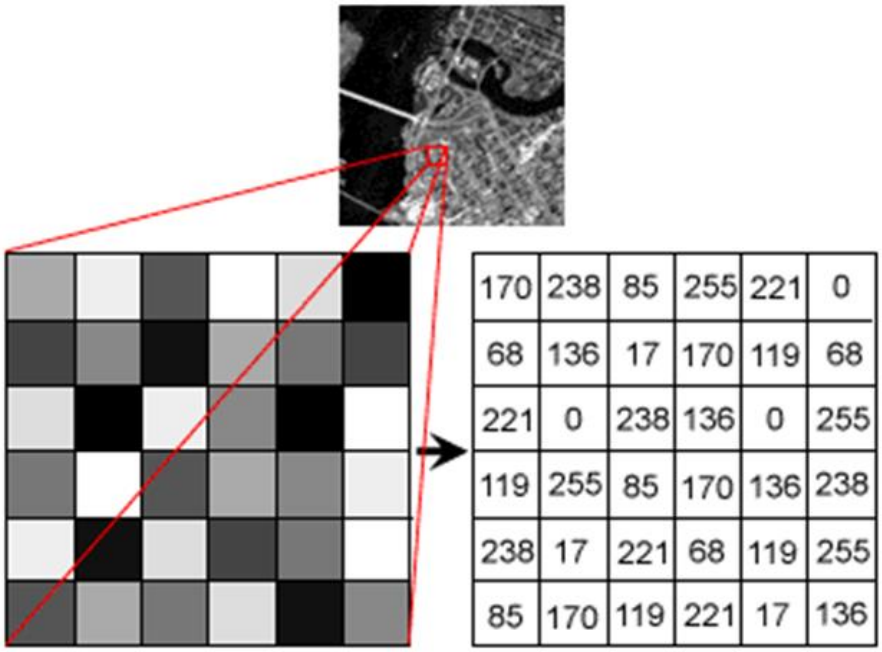

Figure 8. Illustration of a section of an image showing different intensities of reflected energy (CCRS, 2015).

Landsat sensors measures the amount of reflected energy for each 30m x 30m area. This is done for each segment of the electromagnetic spectrum separately storing their reflected energy values (numbers). These numbers can be converted to a grey-scale to produce a black and white image in pixel form. For Landsat, there are 7 bands of data. Each band of data provides records of how much energy was reflected within a given portion of the EM spectrum. For instance, band 4 measures the amount of Near Infrared energy reflected, and Band 3 measures how much green light was reflected.

Each pixel with an area of 30 x 30-meter square is assigned a numerical value corresponding to the amount of energy reflected from the Earth's surface. This data is stored in each band.

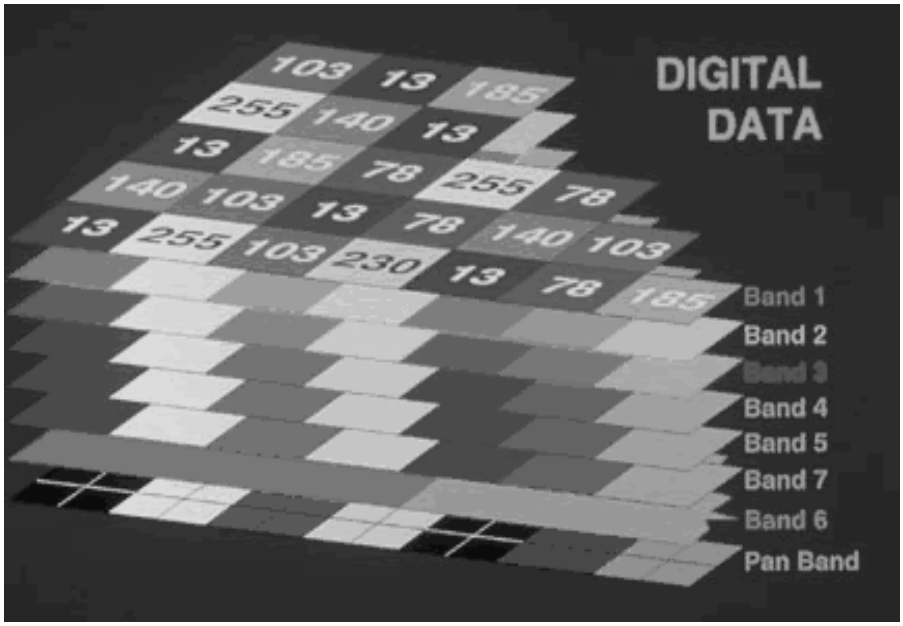

Figure 9. Amount of reflected energy is recorded for each pixel, in each band or wavelength on a scale of 0-255 (CCRS, 2015).

Separating the electromagnetic spectrum in different spectral bands has the advantage of combining these bands in various ways enabling scientist to gain more information from the images. In order to work with Landsat Band combination, we must understand the specification of each band;

Band 1: 0.45 - 0.52 µm (Blue). Is useful for mapping water near coasts, differentiating between soil and plants, and identifying manmade objects such as roads and buildings.

Band 2: 0.52 - 0.60 µm (Green). Spanning the region between the blue and red chlorophyll absorption bands, this band shows the green reflectance of healthy vegetation. Could be used to examine plant health and the amount of construction work carried out in a specific area.

Band 3: 0.63 - 0.69 µm (Red). The visible red band is one of the most important bands when it comes to distinguishing between vegetation

types. It could also be used for mapping soil type boundaries and geological formation boundaries.

Band 4: 0.76 - 0.90 µm (Near infrared). This band is especially responsive to the amount of vegetation biomass present in a scene. It is useful for crop identification, for distinguishing between crops and soil, and for seeing the boundaries of bodies of water.

Band 5: 1.55 - 1.75 µm (Mid-Infrared). This reflective-IR band is sensitive to turgidity -- the amount of water in plants. Turgidity is useful in drought studies and plant vigor studies. In addition, this band can be used to discriminate between clouds, snow, and ice.

Band 6: 10.4 - 12.5 µm (Thermal infrared). This band measures the amount of infrared radiant flux (heat) emitted from surfaces, and helps us to locate geothermal activity, classify vegetation, analyze vegetation stress, and measure soil moisture.

Band 7: 2.08 - 2.35 µm (Mid-infrared). This band is particularly helpful for discriminating among types of rock formations.

Humans can only see RED, GREEN and BLUE with various shades of gray so to visualize data in color, individual bands can be composited into the Red, Green, Blue (RGB) combination. This results to a color image with each pixel's color determined by combination of RGB of different brightness (Figure 10).

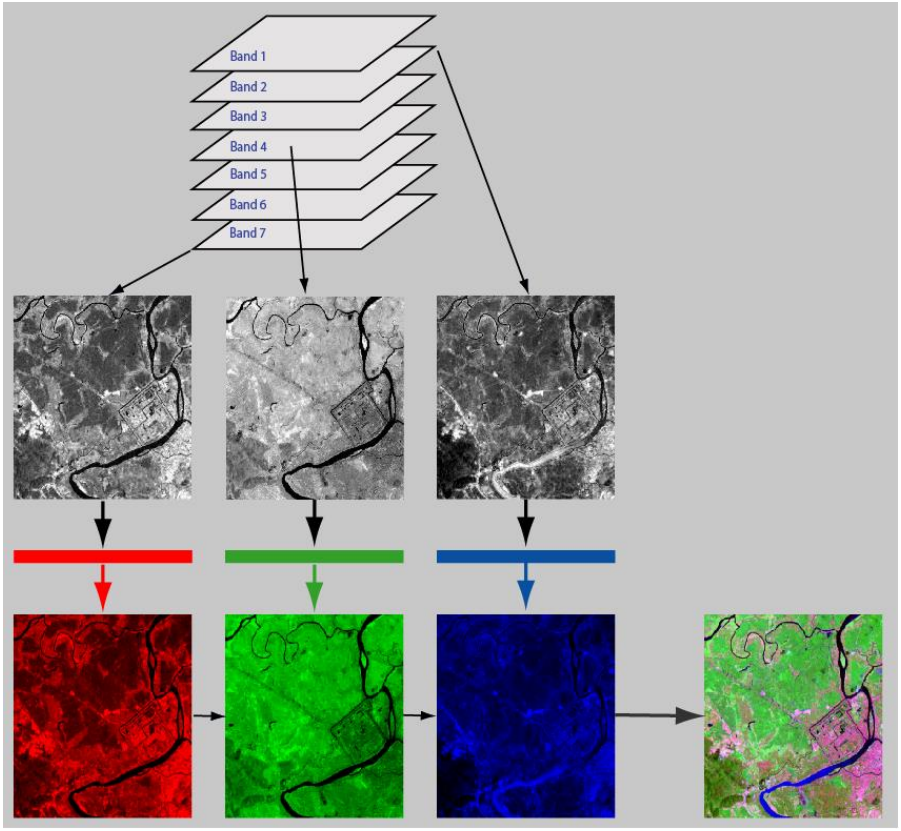

Figure 10. A band 2,4,6 color composite formation which aids visualization and interpretation of the land types.

Numerical values obtained from these images could be used with GIS software programs to quantify land cover and land use changes. Numerous aspects of our planet, from disease to forest fire, to agribusiness, flood predictions, could also be inferred using information from these image data sets. This kind of information is not attainable with conventional photographs**.**

The Landsat 7 ETM+ captures imagery in three visible light bands, one Near Infrared (NIR) band, two Shortwave Infrared (SWIR) bands, one thermal band and one broadband panchromatic band (U.S.Geological Survey, 2017a). Landsat 8 OLI captures imagery in

comparable bands to ETM+, but adds an additional thermal band, coastal aerosol and cirrus bands (U.S.Geological Survey, 2017b). The Landsat collection data is available from the U.S. Geological Survey Glovis and Earth explorer for free download. The USGS Science Processing Architecture (ESPA) ordering system provides additonal data outputproducts such as product metadata, surface reflectance, top of the atmosphere reflectance etc. The products are in the Universal Transverse Mercator (UTM) coordinate system.

3.3. Satellite altimetry

Satellite radar altimetry was initially designed to measure Sea surface height and other characteristics of oceans. It was later demonstrated to be applicable to lakes, floodplains, rivers etc. (Zwally, 1989). It is based on a simple radar principle. A short pulse of radiation with known power is transmitted from a satellite towards the ocean. After the pulse hits the sea surface, part of the incident radiation within the altimetric footprint reflects back to the radar altimeter, which records the return echo of the pulse. However, this is not the only measurement made in the process, and a lot of other information can be extracted from altimetry. The time taken for the pulse to bounce back to the satellite is used to determine the *range* which is the distance between the satellite and the surface (Figure 11).

Range can be computed as;

$$\mathrm{R} = \frac{c*t}{2} \qquad (2)$$

Where *t* is the travel time of the pulse, *c* is the speed of light. This range is converted to the instantaneous height of the sea surface h_{isl} by the Satellite Altitude (*H*) which is the distance between the

mass-center of the satellite and that of the reference ellipsoid in the normal direction.

$$h_{isl} = \mathrm{H} - \mathrm{R} \qquad (3)$$

Both the altitude and range measurements include errors like the instrumental errors ΔR_{ins} and propagation delay $\Delta R_{delay.}$ When considering radial orbit ΔH, equation (3) becomes;

$$(SSH) = H + \Delta H - \left(R + \Delta R_{ins} + \Delta R_{delay}\right) \qquad (4)$$

$\mathrm{SSH} =$ Sea Surface Height

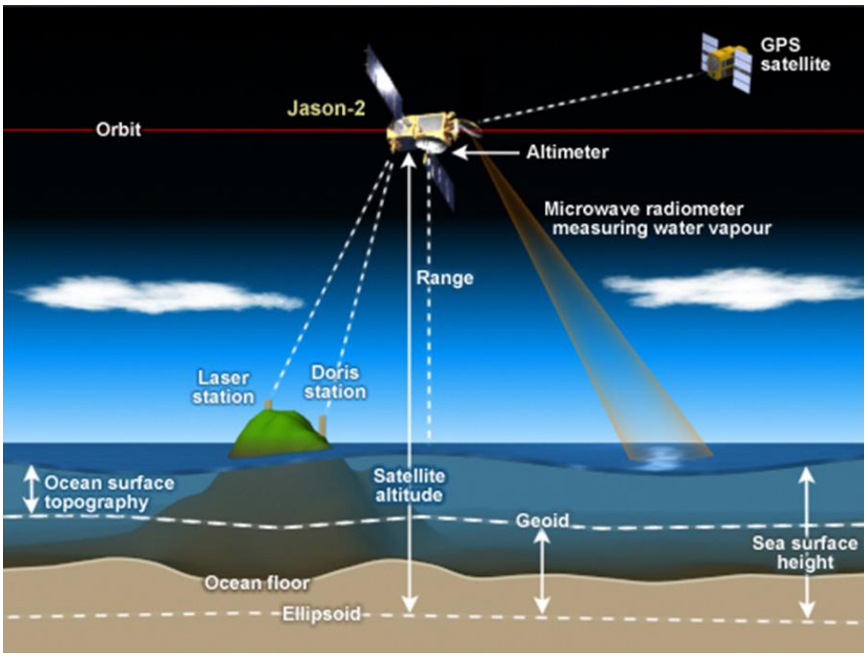

Figure 11. Functionality of Satellite altimeters. It measures sea level by measuring the time it takes a radar pulse to make a round-trip from the satellite to the sea surface and back. (NOAA, 2018)

Altimeter measurements of sea surface topography are affected by many errors; propagation effects in the troposphere and the ionosphere, electromagnetic bias, errors due to inaccurate ocean and

terrestrial tide models, residual geoid errors, inverse barometer effect. Some of these errors can be corrected with dedicated instrumentation like dual-frequency altimeter for ionospheric correction and radiometer for wet tropospheric correction. These corrections are out of the scope of this study as such, readers are refered to (Rosmorduc et al., 2011) for further details on error processing. For all the past altimetric missions, returned pulses were averaged on board before being transmitted from the satellite to reduce noise. Table 2 shows some past and current satellite radar missions.

Table 2. Satellite radar and laser altimetry missions.

Mission	Launch Period	Repeat Period (Days)
TOPEX/POSEIDON	Aug 1992 – Dec 2005	10
ERS-2	Apr 1995 – Jun 2003	35
GFO	May 1998 – Sept 2008	17
JASON-1	Nov 2001 – Present	10
ENVISAT	Mar 2002 – Present	35
ICESat-1	Jan 2003 – Present	8
Jason-2	June 2008- Present	10
CryoSat-2	Apr 2010 – Present	2
HY-2A	Aug 2011 - Present	14
Sentinel-3	2013	27
Jason-3	Apr 2014	10
ICESat	Early 2016	91

Altimetry requires a lot of information to be considered before its data could be used. This could be a complex task. However, Institutions like PECAD from the United States Department of Agriculture, Hydroweb, and European Space Agency (ESA) etc. have been making available up to date and reliable user-friendly data sets. Some altimetry data products provided by these agencies contains

information on surface water level changes in form of graphs and tables from various radar altimetry sensors. It is available via web applications Hydroweb (http://www.legos.obs-mip.fr/en/soa/hydrologie/hydroweb/), River&Lake system provided by ESA (http://tethys.eaprs.cse.dmu.ac.uk/RiverLake/shared/main) and USDA's Global Reservoir and Lake Monitor (http://www.pecad.fas.usda.gov/cropexplorer/global reservoir/). These resulting time series of height variations are expected to have an accuracy better than 20cm rms for lakes with minimal tides and limited dynamic variability

Lakes, rivers and oceans have all been monitored over the years using these data sets (Birkett, 2000; Calmant et al., 2004; Crétaux et al., 2006; Frappart et al., 2006; Calmants et al., 2008; Kropáčeket al., 2012; Mohammad et al., 2017; Yeon et al., 2018).

For the Lake Chad, satellite altimetry data has widely been used in the studies of the lake in which, in situ data sets were compared with these altimetry products. The results showed accurate water level variations for the Lake Chad between the two data sets (Birkett, 2000; Coe et al., 2004; Crétaux & Birkett, 2006; Wenbin et al, 2017). ENVISAT altimetry estimates were used in this study.

3.4. Soil moisture from GLDAS

NASA produced land data assimilation systems (LDAS) to facilitate hydrological and climatology modeling, research and forecasting. Operated by NASA and the National Oceanic and Atmospheric Administration (NOAA), The Global Land Data Assimilation System (GLDAS) is a land surface simulation system that aims to ingest satellite- and ground-based observational data products,

using advanced land surface modeling and data assimilation techniques, in order to generate optimal fields of land surface state (e.g., soil moisture and surface temperature) and flux (e.g., evaporation and sensible heat flux) products (Rodell, et al., 2004). GLDAS data sets are available in two versions online: Version 1 (GLDAS-1), drives four advanced Land Surface Models (LSMs); The Community Land Model (CLM), Mosaic, Noah, and Variable Infiltration Capacity (VIC). And a Version 2 (GLDAS-2) which drives only the Noah model. The data are available from the Goddard Earth Sciences Data and Information Services Center (GES DISC) https://disc.gsfc.nasa.gov. GLDAS provides access to global and regional environmental changes at up to 0.25° and 1.0° spatial resolution, with temporal resolutions of 3-hours and monthly products, since 1948.

GLDAS products can be accessed through several interfaces. Its dataset are regularly been used for land-surface flux simulations. When dealing with over 10 years of data, downloading the 3-hourly subset was deemed unnecessarily time consuming. I used Noah 1.0° grid data which has 4 layers of vertical soil moisture. The monthly average soil moisture is computed as the sum of all the layers (Rodell et al., 2009).

3.5. GW outputs from WaterGAP

The Water-Global Assessment and Prognosis (WaterGAP) consist of the Global Hydrological Model (WGHM), groundwater and surface water use model. It computes surface runoff, groundwater recharge and river discharge as well as storage variations of water in canopy, snow, soil, groundwater, lakes, wetlands and rivers at a spatial

resolution of 0.5^0. (Döll et al., 2003). It does this for all the continents excluding the Antarctica. Water storage changes are calculated for each grid cell through ten individual compartments. Lakes and wetlands receive runoff from the specific cells, while global surface water bodies as well as rivers receive inflow from the upstream grid cells. Human water use for irrigation, livestock, manufacturing and cooling of thermal power plants is simulated by separate sub-models. Groundwater storage is affected by diffuse groundwater recharge, which is modeled as a function of total runoff, relief, soil texture and hydrogeology.

It computes water storage in the snow pack, rooted soil zone, groundwater, on vegetation surfaces, and in surface water reservoirs (rivers, lakes and wetlands). To allow a plausible representation of the actual freshwater situation, version 2.2 of WGHM is tuned against mean annual river discharge at 1319 gauging stations by adjusting the runoff coefficient γ for all grid cells in each calibration basin. In the case that the simulated discharge deviates more than 1 % from the observed discharge, up to two additional correction factors are applied. Other climate forcing data such as temperature, cloudiness, and number of rainy days per month are taken from operational forecast or analysis data of the European Centre for Medium-Range Weather Forecasts (ECMWF) (Hunger & Döll, 2008). In Africa, most basins north of the equator do not perform well, while the inter-annual variability of the Central African Congo and the semi-arid to arid Southern African basins of the Zambezi and Orange is captured (Döll et al., 2003).

An overview of the WGHM is given in Figure 12. Water transport through the canopy, snow, soil and groundwater

compartment, as well as the partitioning of precipitation into evapotranspiration and runoff represents the vertical water balances. Runoff is partitioned into surface and subsurface runoff, which flows directly into the surface water bodies, and groundwater recharge. Precipitation over surface water is added to the lakes, wetlands, reservoirs and river compartments while evaporation reduces the amount of water. River compartments are the finale storage of the grid cells. The impact of human water use as simulated by WaterGAP water use sub-models is taken into account in WGHM. Net water use (water abstractions minus return flows) are abstracted from surface water bodies (including rivers) or groundwater (Döll et al., 2012).

WGHM is a complex model that accounts for a variety of known hydrological processes which are beyond the scope of this thesis. A detailed description can be found in (Hunger & Döll, 2008). For this study, model outputs from the (WaterGap 2.2a) forced with precipitation from the Global Precipitation Climatology Centre (GPCC) and data from the European Center for Medium-Range Weather Forecast (ECMWF) integrated forecast system were used. These output include; global-scaled groundwater storage, total water storage, baseflow, and groundwater recharge (diffuse and below surface water bodies) which are all provided by (Döll et al., 2014).

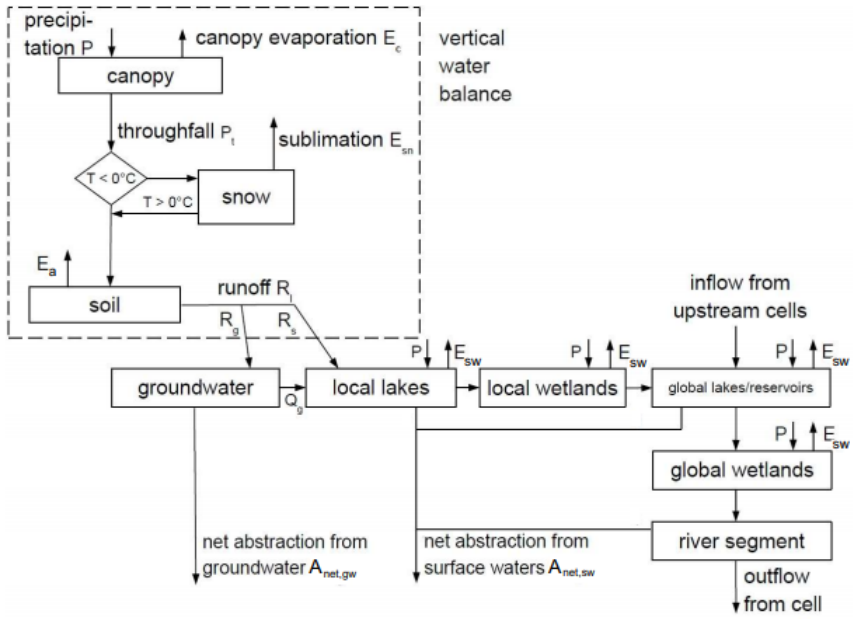

Figure 12. Schematic structure of WGHM water storage compartments and fluxes that are computed within each 0.5◦×0.5◦ grid cell (Müller Schmied et al., 2014, p. 3530). Water storage compartments are represented by boxes and water fluxes by arrows**.**

3.6. Observational data

Observed rainfall data were obtained from the Société de Développement du Lac (SODELAC), which is a Chadian state enterprise involved in the development of farmland and irrigation projects around the lake (DREM, 2014). Where the observed rainfall data were lacking, rainfall data from the Tropical Rainfall Measuring Mission (TRMM) were used as a substitute. The rainfall data were extracted from the TRMM3B43 V7 product (0.25° × 0.25° spatial resolution and 3-h temporal resolution) which is one of the several TRMM rainfall products, containing data from January 2001 to December 2015. More information about the TRMM dataset can be found and downloaded freely at https://trmm.gsfc.nasa.gov/.

Lake level data were collected from the Chadian National Meteorological and Hydrological Department (DREM) (Longuevergne et al., 2015). These control centers manage weather stations in some sub-regions around the lake, specifically around the Bol village. Our study area is characterized mainly by two seasons: a rainy season during which rainfall averages about 300 mm, spanning from May to October, and a dry season from November to March. With the absence of daily rainfall data, which would have allowed for a more precise analysis of the hydrological dynamics around the lake, I used the available monthly data sets.

Table 3. Summary of data sets used for this study

Data	Source	Resolution	Period	Use
TWS	GRACE	1^0	2003 – 2013	Water level changes
Lake level	ALT/LCBC	-	2003 – 2013	Water level changes
Rainfall	TRMM/LCBC	0.25^0	2003 – 2013	Water level changes
SM	GLDAS	1^0	2003 – 2013	Water level changes
GW	WGHM	1^0	2003 – 2009	GW levels
MR Image	Landsat	30m	2002 – 2016	Lake area estimate
HR Images	WorldView-03	0.4m	2015	Accuracy assessment

ALT: Altimetry; SM: Soil Moisture; GW: Groundwater; MR & HR: Moderate & High resolution.

3.7. Open-source and licensed software

Some software tools were used to complete this research, primarily R, RStudio, ENVI, ArcGIS, and Google Earth. R is an open-source, object-oriented statistical programming language which was used in combination with RStudio, an integrated development environment that has robust features such as code editing, debugging and various graphics and visualization tools. The open-source nature

of R makes it quite accessible as there are several packages already built in with advanced functionality and thorough documentation, and more being developed continually through various R communities such as the Comprehensive R Archive Network (CRAN).

ArcGIS is a licensed software product developed by ESRI that was initially released in 1999 and is currently in its 10th version (ArcGIS 10.3.1 was used for this research). ArcGIS is used for a variety of purposes and has many capabilities including spatial analytics, mapping and visualization, 3D modeling and visualization, real-time GIS applications, remote sensing imagery, and data collection and management. It was used to analyze "cleaned" Landsat images from ENVI.

CHAPTER IV: HYDROLOGICAL VARIABILITY

4.1. Methods

a. Cycle investigation

GRACE monthly estimates and altimetric lake height for a study period were decomposed into their respective trends and seasonal components using the Seasonal-Trend Decomposition Procedure. This Procedure is based on Loess (STL) method is a filtering procedure that decomposes a time series into additive components of variation (trend, seasonal and the remainder components) by the application of Loess smoothing models (Cleveland et al., 1990). Data analyst are usually in charge of choosing the appropriate parameter values. Usually, the degree of smoothing in the trends and seasonal components are determined by six paramters.

In detail, the steps performed during STL decomposition are:

(i) Detrending;

(ii) Cycle-subseries smoothing: series are built for each seasonal component, and smoothed separately;

(iii) Low-pass filtering of smoothed cycle-subseries: the subseries are put together again, and smoothed;

(iv) Detrending of the seasonal series;

(v) Deseasonalizing the original series, using the seasonal component calculated in the previous steps; and

(vi) Smoothing the deseasonalized series to get the trend component.

In R statistical software, the STL algorithm is available through the STL function. For this study, the default parameters were used. The

degrees for the loess fitting are d=1 in steps (iii) and (iv), and d=0 in step. Parameter values must be chosen by the data analyst.

Assuming each observation X_i in time series is the sum or the product of these components:

$T_i = Trend$ $S_i = Seasonality$ And $I_i = Irregular\ components$

Implies,

$$X_i = T_i + S_i + I_i \qquad (5)$$

Often, six parameters determine the degree of smoothing in trend and seasonal components. For detailed information on method and parameters, consult (Cleveland et al., 1990) paper on STL methods. For our study, these parameters where;

$\boldsymbol{n_{(p)}}$ *:* The number of observations in each seasonal cycle; *= 12 months (yearly periodicity with monthly data);*

$\boldsymbol{n_{(i)}}$: The number of passes through the inner loop (usually set to equal one or two) *= 1 month;*

$\boldsymbol{n_{(o)}}$ *:* The number of robustness iterations of the outer loop (Values ≥1 applies increasing robustness while a zero value has no robustness iteration) *= 5 months;*

$\boldsymbol{n_{(l)}}$ *:* The span of the loess window for the low-pass filter; *(computed as the next odd number to* $n_{(p)}$ *) = 13 months;*

$\boldsymbol{n_{(s)}}$: The smoothing parameter for the seasonal component; *= 12 months (seasonal length is same as the periodic length)*

$\boldsymbol{n_{(t)}}$ —the smoothing parameter for the trend component. *= 22 months* (Cleveland et al., 1990) Proposed this formula;

$$n_{(t)} \geq \left[\frac{1.5n_{(p)}}{1-1.5n_s^{-1}}\right] \qquad (6)$$

For this analysis, R statistical software was used (R Core Team, 2013). It is a free software environment and a programming language for statistical computing and graphics. It is widely used among statistics and data miners for developing statistical software and data analysis. MS excel was also used for subsequent data representation and analysis.

b. Subsurface water volume change

Subsurface water volume (Groundwater + soil moisture) was investigated. GRACE data provides changes in total water storage, which includes Lake's water storage (LS), Snow water equivalent storage (SWES), soil moisture storage (SMS), and groundwater storage (GWS) within the basin. With Satellite and Model based estimates of LS and SMS, subsurface water volume can be estimated. SWES is ignored for this study area since it is in a humid environment.

Estimates of the subsurface water changes (Volume) was evaluated using this disaggregation equation,

$$\Delta SSW = \Delta SM + \Delta GW = \Delta TWS - \Delta LS \qquad (7)$$

Here, ΔSSW = Subsurface Water, ΔGW = Groundwater, ΔLS = Lake water, ΔTWS = Terrestrial Water Storage, ΔSM = Soil Moisture. In an attempt to express ΔSSW and ΔLS in terms of volume, both were multiplied by the LCB area and Lake Area respectively.

4.2. Results and Discussions

a. Cycle investigation

i. TWS and altimetric lake height

Based on our study period, the STL trend of the time series of monthly GRACE TWS shows a decrease in average TWS of Lake Chad basin (Figure 13) for the periods 2003-2005 and 2009-2010 with the latter being the lowest water concentration at -0.54cm/year. There is an increase in TWS concentrations from 2006 to 2008, and 2010 through 2013 with the latter being the highest storage concentrations of 0.69cm/year.

The STL trend of the time series of altimetric lake height (Figure 14) shows a decrease in lake level from 2003 through 2005 and a steady increase up until 2008 with an average height of approximately 5.3cm/year. From where it begins to slope down towards at year 2010. From 2010 to 2012, the Lake experiences its lowest height averaging to about -2.7cm/year. Different rates are shown in Table 4.

Table 4. STL fitted trend of the time series of TWS and lake height

Period	TWS(cm)	Lake height(m)
2003-2005	0.25	0.32
2006-2009	0.84	0.62
2010-2013	0.38	-0.78

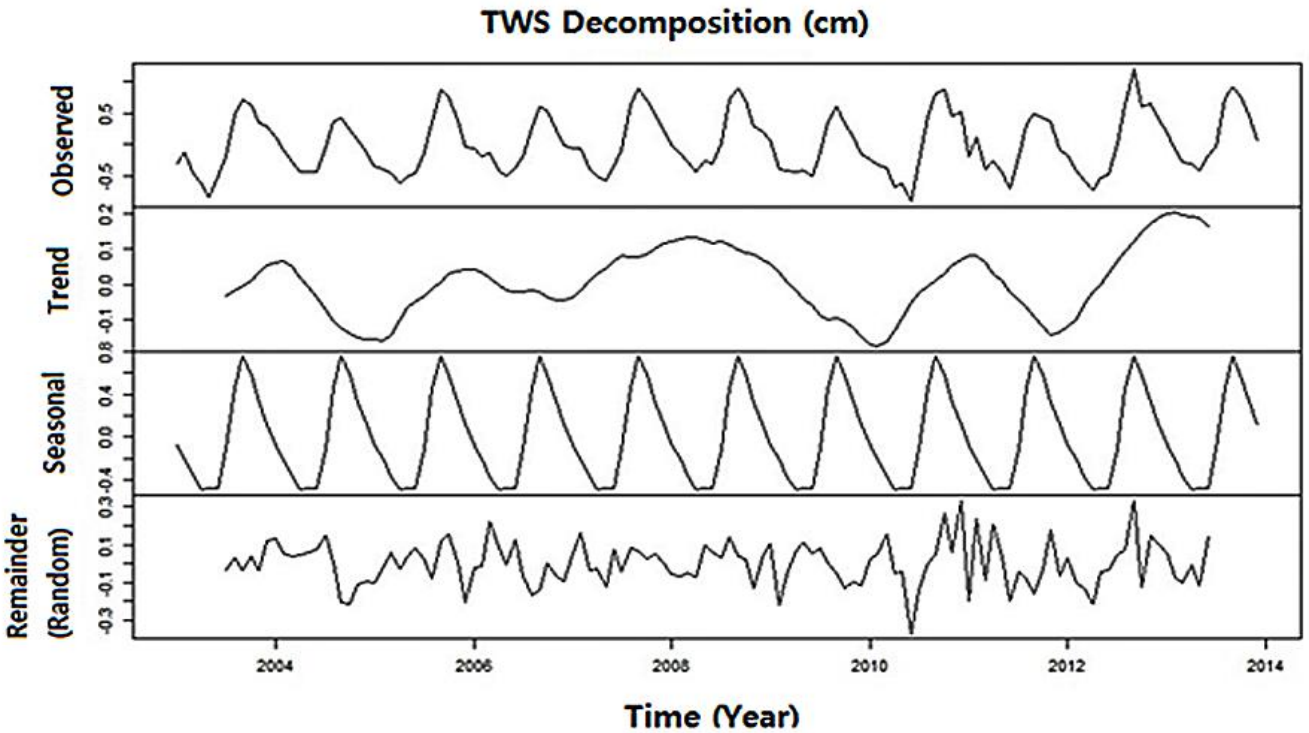

Figure 13. STL decomposition of the time series of monthly GRACE TWS.

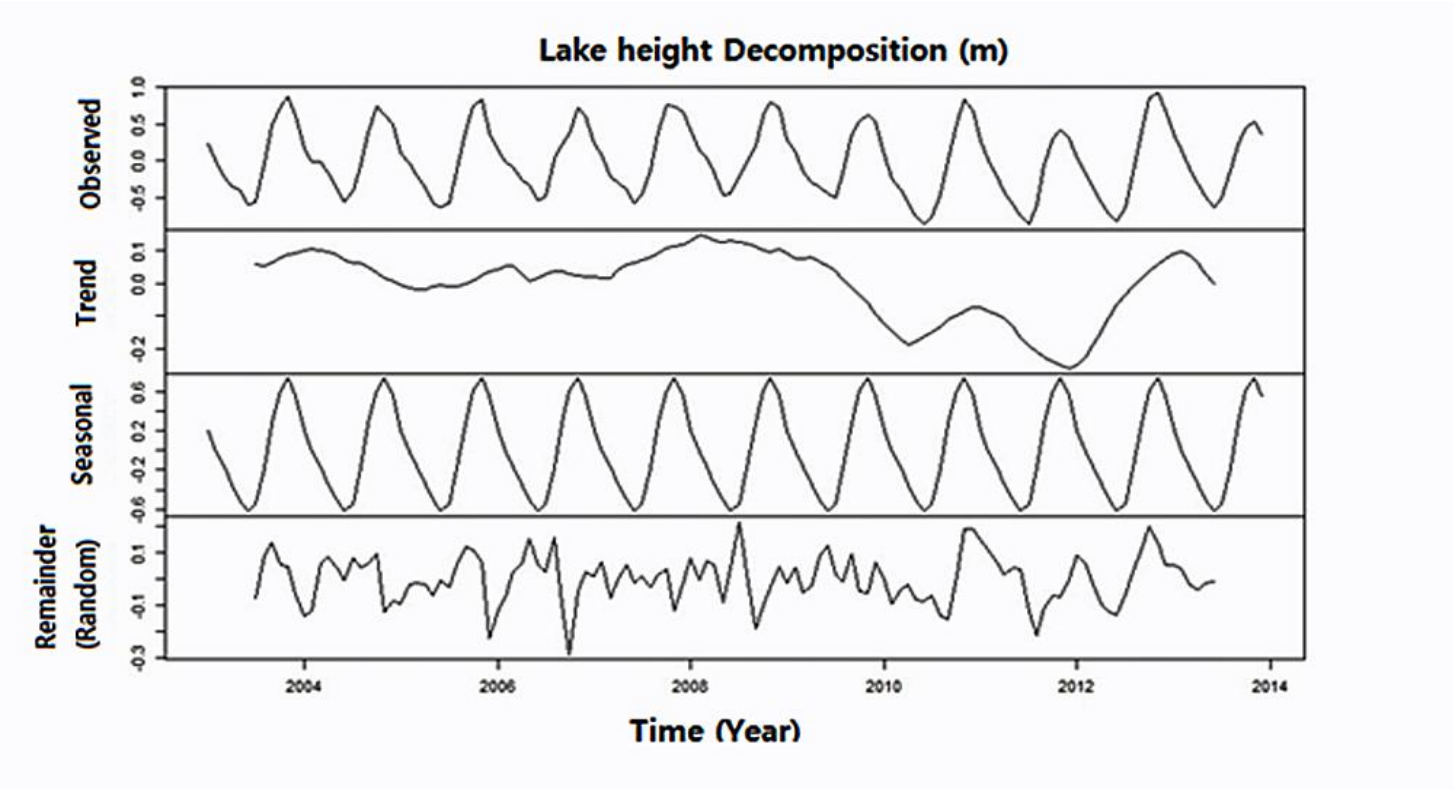

Figure 14. STL decomposition of the time series of monthly Lake altimetric height.

The STL decomposition plot of the monthly TWS estimates and Lake altimetric height shows a similar pattern with their seasonal components suggesting an annual increase from the months of Jul-Sep as well as a decrease from Oct-Jun. This implies the Lake's height follows the seasonal pattern of the rainfall cycle around this area. There is a correlation (>80%) between them which points out the similarity in their pattern (Figure 15 (a)).

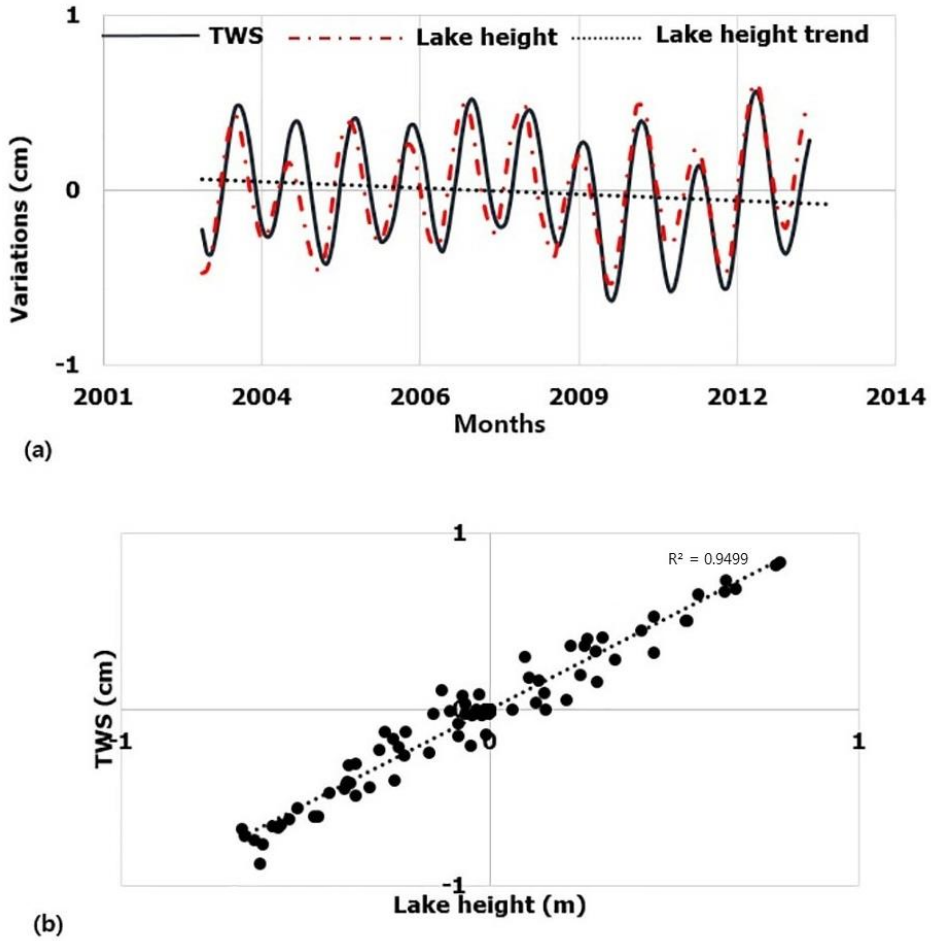

Figure 15. **(**a) Represents TWS and Lake Height after smoothing with a 6-months window. (b) Represents the autocorrelation between TWS and Lake Height.

Their seasonal component suggests an average annual increase in September and a main annual drop exists in November. This is due to the rainfall pattern over the Lake region. The largeness and uniform size of the seasonal cycle of Lake Chad means that over the years, Lake Chad has a fast water renewal process.

ii. TWS and rainfall

In this section, rainfall rates estimated from GLDAS was compared to GRACE TWS over the LCB. During the wet season (Jul - Sept), there is an increase in seasonal pattern of rainfall over the study region with 2012 having the maximum annual averages. Figure 13 shows a comparison between the time series of the monthly estimated GLDAS rainfall and the change in GRACE TWS and as expected, both curves show a good agreement during most of the study period in terms of pattern.

Based on Figure 16, an existence of a phase shift between GLDAS rainfall and GRACE TWS can be clearly pointed out. This phase shift is approximately a month and a half. Their lagged correlation was also high (>0.9). From trend analysis, rainfall which precedes TWS increases throughout the study period. Its seasonal cycle goes ahead to confirm this phase shift that exist between rainfall and TWS in this region.

Figure 17 also confirms the bimodal rainfall regime that exist within this region with most of its heavy rainfall occurring between Jul-Sep and shorter rains from Oct–Dec. Hence the bimodal rainfall regime.

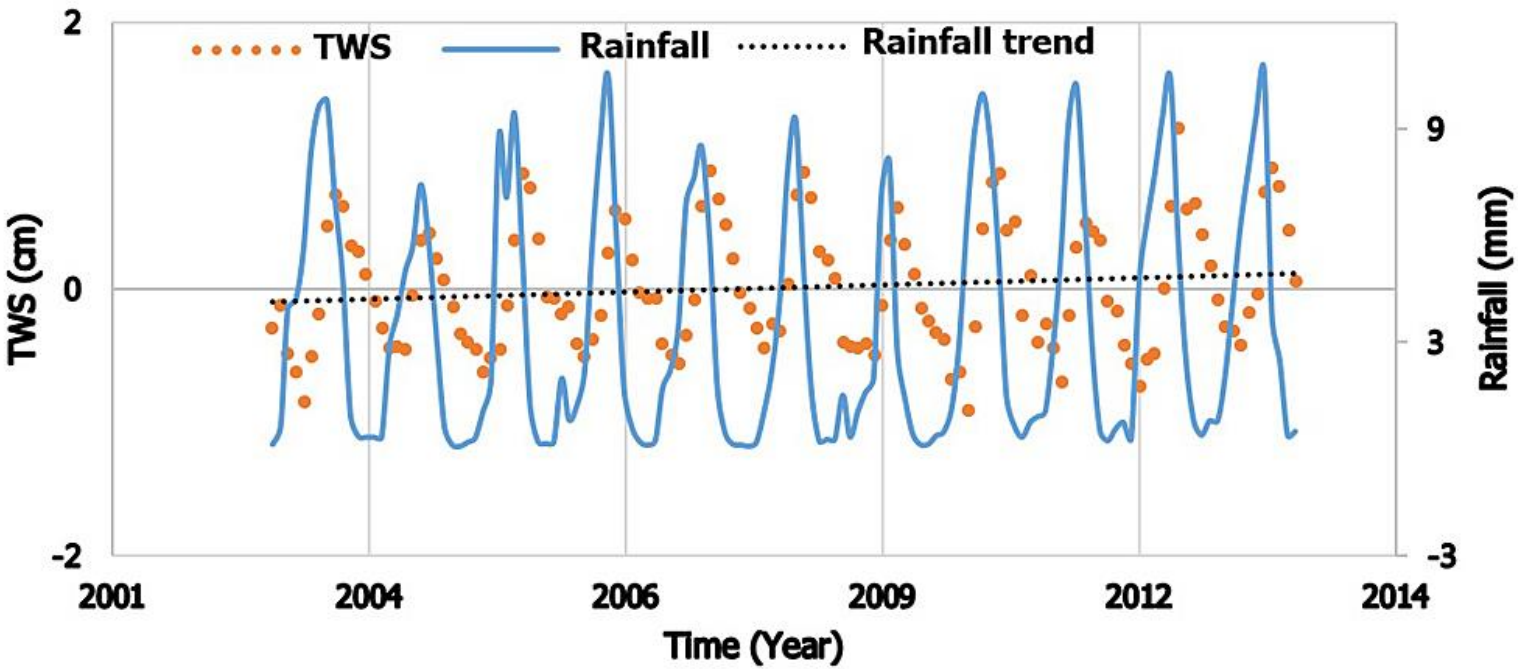

Figure 16. Comparisons between the yearly estimates of rainfall and TWS.

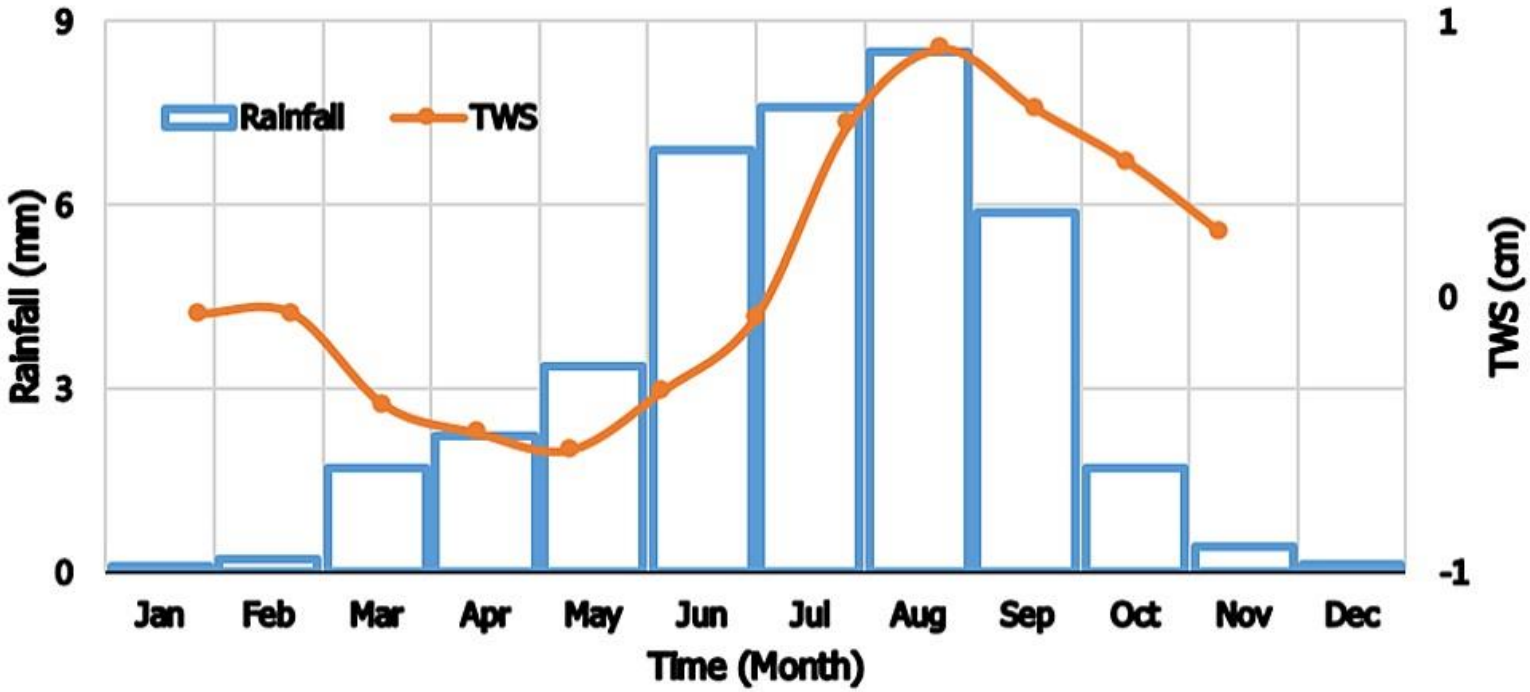

Figure 17. Comparisons between the monthly averaged of rainfall and TWS.

b. Subsurface water volume change

Total water storage (TWS) of the Lake Chad Basin and the lake's surface water volume change from altimetry are critically analyzed. Over the years, GRACE products have been improved in precision allow studies of small water basins feasible (Becker et al. 2012). GRACE can detect gravitational changes within an area of 200,000 km^2 or larger (Rodell and Famiglietti 2001). Hence, suitable for our study area which is ~$427{,}500\ km^2$.

Figure 18 shows a good agreement between altimetric lake water volumes with GRACE basin water volume with a correlation of about 73%. There is also a good agreement in their seasonal cycles (Figure 16). It is seen that surface water of the Lake Chad governs volume of water in the basin area.

GLDAS outputs of soil moisture estimates can also be seen in Figure 18. It has a weak agreement with basin water volume with a correlation of about 35%. Hence, soil moisture content plays little or no role in the variability in water volume stored in the Lake Chad Basin. It is solely governed by surface water of the Lake Chad.

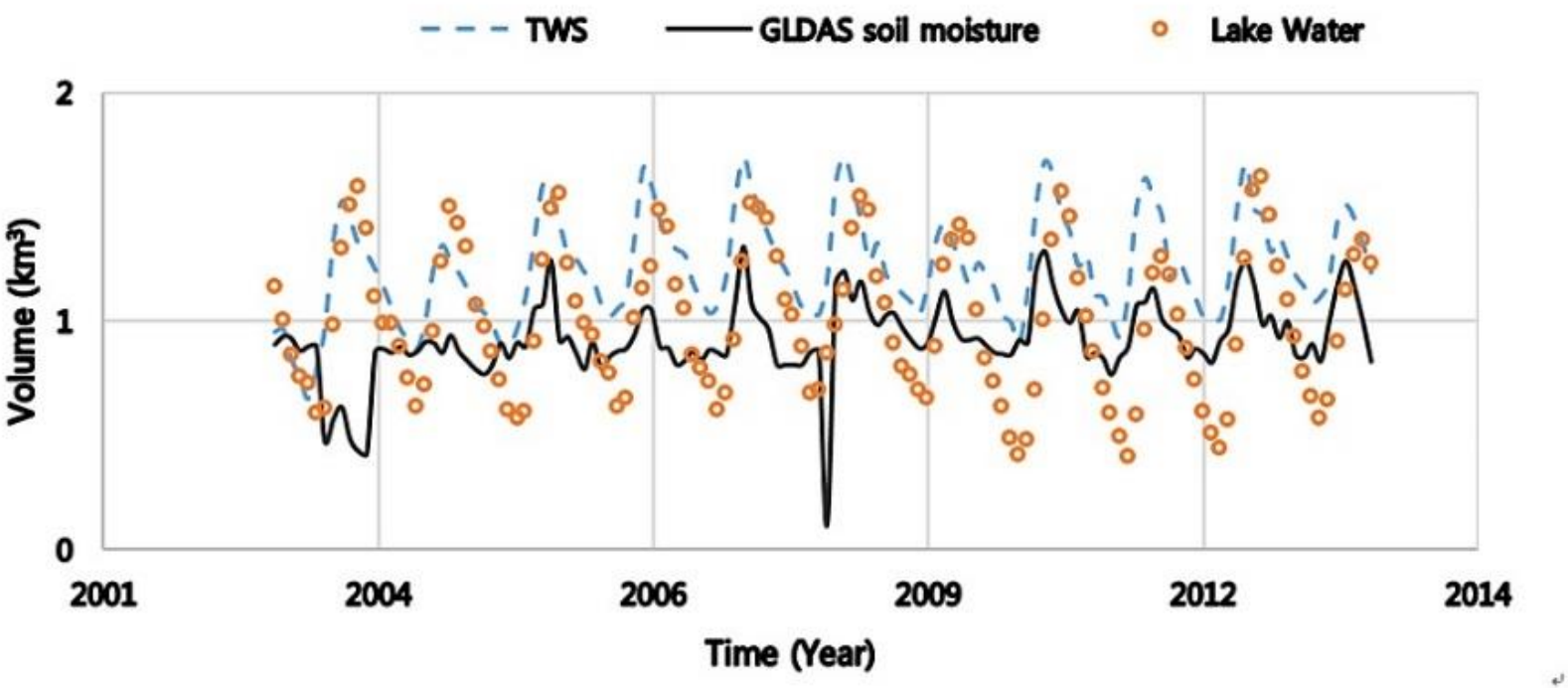

Figure 18. Effect of Altimetric Lake water and Soil moisture on TWS.

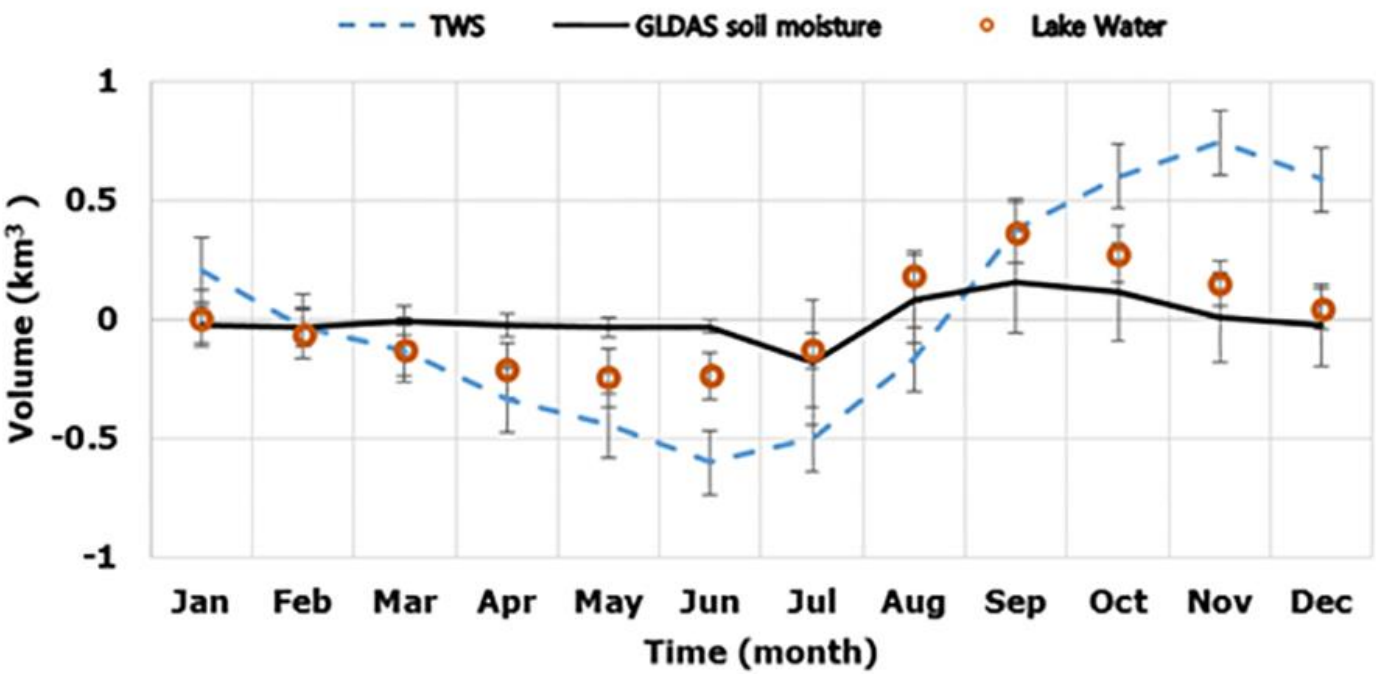

Figure 19. Monthly averaged seasonal cycle of the Lake Chad. Error bars represents the standard deviation for each month.

Also, investigated were the changes in subsurface water volume, comprising of groundwater and soil moisture (Section 4.1.1(b)). In early 2003 and 2007, there was a dissimilarity between volume estimates of WGHM groundwater and subsurface water estimates. The results obtained were compared with WGHM outputs (Figure 20). It shows two peak periods at approximately mid-2005 and 2006. Both curves have a moderately similar pattern with a correlation coefficient of approxiamtely 47% between them.

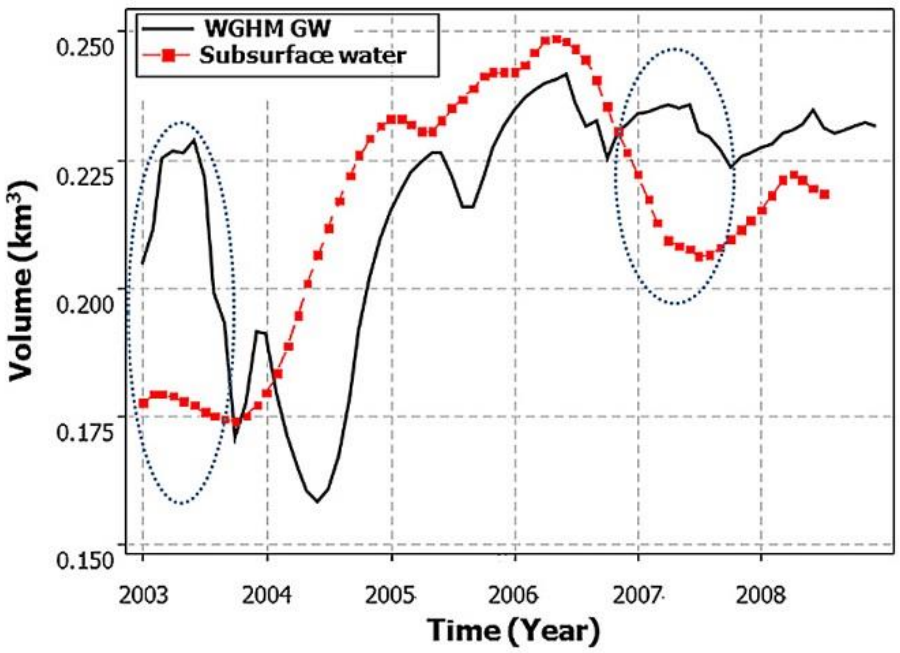

Figure 20. Changes in subsurface water (groundwater and soil moisture) and WGHM GW outputs. The annual signal is removed, and data are smoothed with a 6-month window.

4.3. Summary

GRACE TWS and altimetric lake volume showed a similar pattern for most of the study period. After comparing TWS with soil moisture content, it was determined that the discharge in this area is governed by surface water of the Lake.

For much of the study period, GRACE TWS variations within the basin shows a similar pattern as the average lake height variation from altimetry. A trend analysis showed increasing precipitation with maximum annual average increase in August, but decreasing water level in the lake from altimetry with the minimum annual average occurring in 2012 with value of ~0.2 m. Our study also showed that altimetry-based volume with TWS from GRACE provides information on soil moisture and groundwater.

Deriving this characteristic spatiotemporal analysis of surface mass anomalies across the LCB, future improvements can be made in the management of water resources in this area. The use of water volume and TWS to derive groundwater information could help in detecting subsurface water storage changes in relations to climate variability or anthropogenic activities especially in situations where in situ measurements are not available.

This characterization can help in the proposed Water Transfer Project from the Ubangi River to Lake Chad in several ways; For instance, the primary objective of this project is to halt the shrinkage of Lake Chad through an inflow of water coming from the Congo basin. The association between LC level and precipitation will enable managers to plan for the total water volume that can be released and retained based on future forecasts.

CHAPTER V: LAKE AREA ESTIMATION

5.1. Methods

a. Pre-processing

Pre-processing properly carried out could account for sensor, solar, atmospheric and topographic effects that affects the quality of Landsat images. These images are subjected to distortion because of their sensors as well as solar, atmospheric and topographic influences. Minimizing these effects using a specific order of preprocessing methods has proven to have a significant influence on results analysis (Sundaresan et al., 2007). Gains and Offsets are different between sensors and over time. Signals from sensors are calibrated to radiance values using these gains and offsets values. This is due to sensor degradation. These values are then rescaled to digital numbers as 6-bit or 7-bit (MSS), 8-bit (TM, ETM+), or 12-bit (OLI, TIRS) unsigned integers (Chander etal., 2009).

In late 2003, there was a permanent failure of the scan-line corrector for the ETM+ sensor aboard Landsat 7. This led to future generated scenes having wedge-shaped gaps and missing pixels (about 22%) within them (Chen et al., 2011). To compensate for this, a gap filling proposed by the USGS was implemented. This method, which is based on the local histogram matching technique was applied to the affected images. This method of image gap filling applies a local linear histogram matching in a moving window of each missing pixel to derive the rescaling function. This rescaling function is then used to convert the radiometric values of one input scene into equivalent radiometric values of the scene being gap-filled, and the transformed data are then used to fill the gaps of that scene. This method is very

simple to implement and can resolve many of the missing-data problems if the input scenes are of high quality (with negligible cloud and snow cover) and represent comparable seasonal conditions (USGS, 2017). To automatically run this gap filling process through our affected images, the *landsat_gapfill.sav* extension toolbox in ENVI was used. After which, radiometric correction was performed on all the images.

To comfortably distinguish between sensor defects and real ground changes, it is essential to remove sensors and atmospheric noises from downloaded Landsat images. A process known as radiometric correction.

The Landsat ETM+ sensors capture reflected solar energy and converts them to radiance. It then rescales this data to an 8-bit digital number (DN) with a range between 0 and 255 (16-bit with a range of 0 and 65536 for Landsat 8). These DNs are scaled representations of radiance and have no physical units (Chander et al.,2009; Matthew et al., 2014).

Converting the Landsat ETM+ and OLI data to Top of Atmosphere (ToA) reflectance can be done manually using a two-step process. First, DN must be converted to radiance values, then these radiance values need to be converted to reflectance values. To carry out these calculations for each scene, the distance between the sun and earth in astronomical units, the day of the year (Julian date), and solar zenith angle must be known. These parameters can be found in the metadata file (MTL.txt) provided with each downloaded scene.

- ***Converting DN to Radiance***

This was achieved using a gain and bias method using each scene's calibration data available in their respective metadata files. The Gain and Bias method can be computed using this formula:

$$L_\lambda = gain * DN + bias\ 5 \quad (8)$$

Where:

L_λ = ToA spectral reflectance

DN = Quantized and calibrated standard product piel value

Gain = Band − specific multiplicative rescaling factor from the metadata

Bias = Band − specific additive rescaling factor from the metadata

- ***Converting Radiance to ToA reflectance***

Radiance can be converted to TOA reflectance using the recalling coefficients in the header files

$$\rho_\lambda = \frac{\pi * L_\lambda * d^2}{ESUN_\lambda * \cos\theta_s}\ 6 \quad (9)$$

Where:

ρ_λ = Uniteless planetary reflectance

L_λ = Spectral radiance

d = Earth − Sun distance in astronomical units

$ESUN_\lambda$ = Mean solar exoatmospheric irradiance

θ_s = solar zenith angle

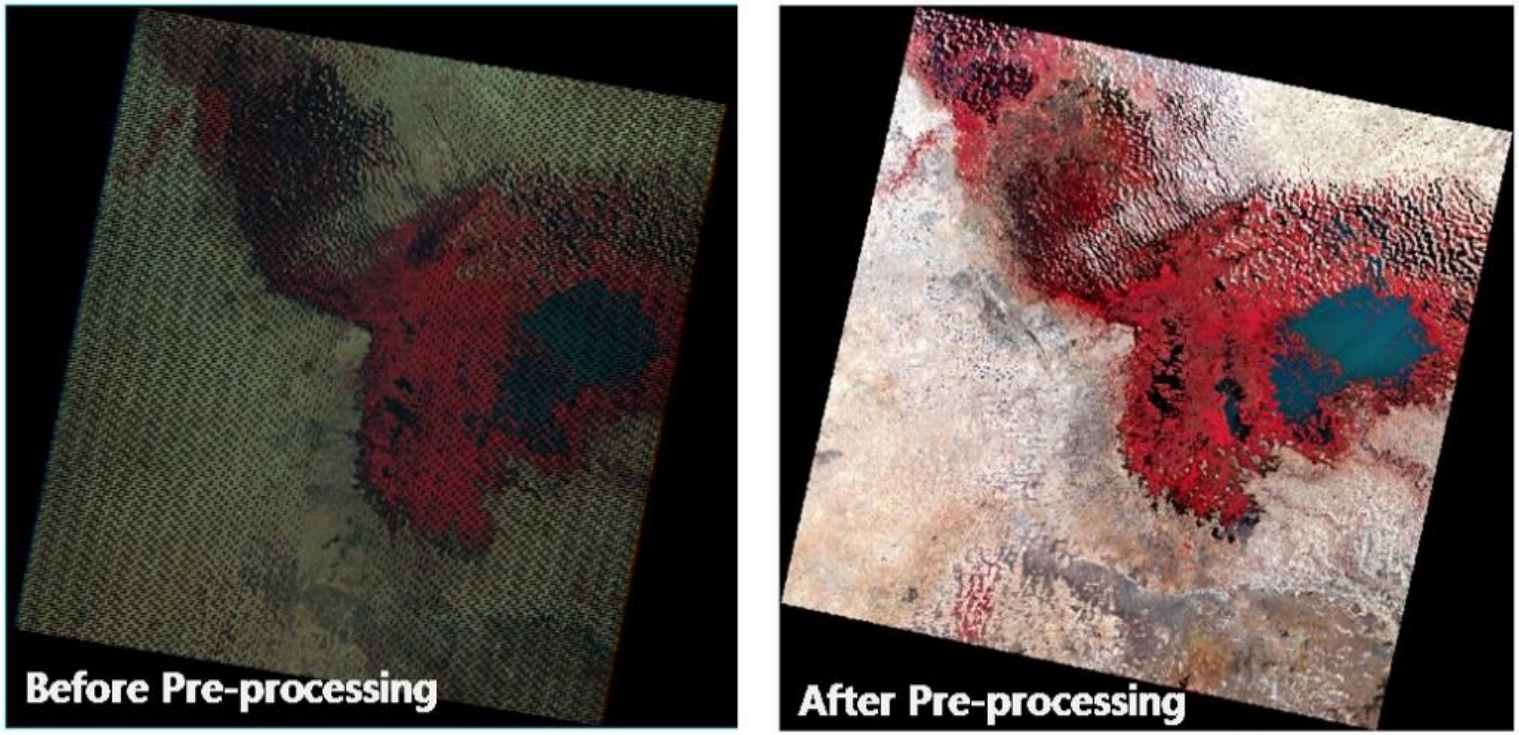

Figure 21. Result of a gap-filling procedure and radiometric correction on a downloaded Landsat image.

To automate this process, radiometric calibration was carried out for all images using ENVI v5.1 image analysis software. ENVI v5.1 can perform this calibration when supplied with metadata files of each image. Obtained values can be compared to images that have undergone the same level of correction across time or sensors. Cloud contaminated, and hazy images were not included for analyses. As such, atmospheric correction was not performed in this study. Depending on the depth of analysis or study for which downloaded Landsat images are used, proper pre-processing must be done on all the images in order to achieve "high" quality results. Failure to perform this task may lead to faulty interpretations and results in general (Feyisa et al., 2014; Willis, 2015; Estoque & Murayama, 2015). Given the size of our study area, stacking and mosaicking of adjacent images were performed for proper coverage of Lake Chad (Figure 22).

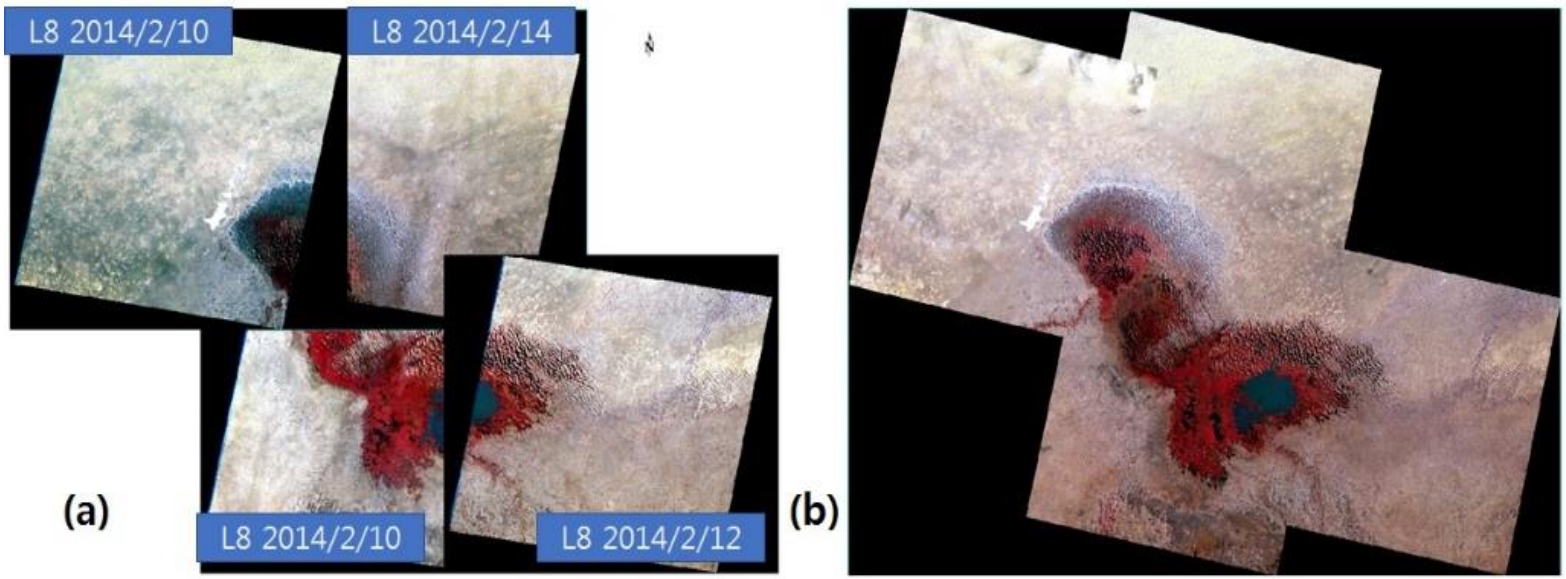

Figure 22. Seamless Mosaicking image solves the dark fields of no data in (a) resulting to a better quality image of a study area (b).

b. Processing

Materials of every kind reflects uniquely in each wavelength when exposed to EM radiations. Also, when these materials get hot, they radiate at a unique strength in each wavelength. Spectral signature plots all the variations of reflected electromagnetic radiation as a function of wavelengths. The ability to plot these unique properties allows us to distinguish between cover types based on their response values for a given wavelength. This could not have been archived when compared at a single wavelength. For example, water and vegetation may reflect somewhat similarly in the visible wavelengths but are almost always separable in the infrared. When examining a specific cover type, spectral responses can be quite variable and vary with time and location. As such, understanding the factors which influences spectral responses of the features of interest are critical to correctly interpreting this EM radiation interaction. Figure 23 represents a spectral signature plot of the three major land cover types in our study area;

Water – Typically looks blue or blue-green due to stronger reflectance at shorter wavelengths, and darker if viewed at red or near infrared wavelengths. The visible and near infrared radiation are absorbed by water. The more suspended sediment on the water surface, the brighter the reflectivity of water. Chlorophyll in algae absorbs more of the blue wavelengths and reflects the green, making the water appear greener in color when algae is present. The topography of the water surface can also lead to complications for water-related interpretation due to potential problems of specular reflection and other influences on color and brightness.

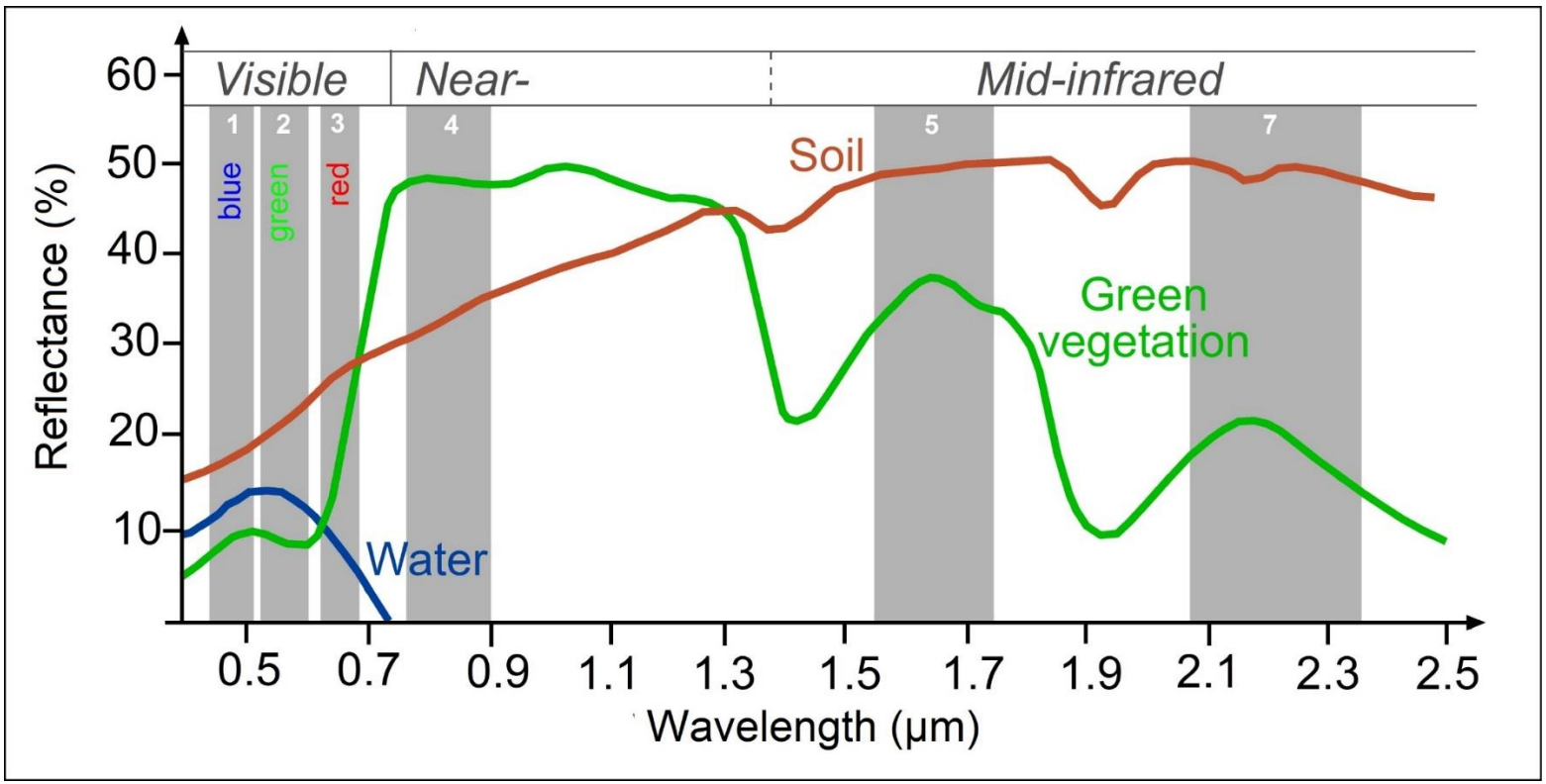

Figure 23 . A generalized spectral signature of Soil, Vegetation and Water (NASA, 2016).

Vegetation - Chlorophyll strongly absorbs radiation in the red and blue wavelengths but reflects green wavelengths. Leaves appear "greenest" to us in the summer, when chlorophyll content is at its maximum. In autumn, there is less chlorophyll in the leaves, so there is less absorption and proportionately more reflection of the red wavelengths, making the leaves appear red or yellow (yellow is a combination of red (band 3) and green (band 2) wavelengths). Measuring and monitoring the near-IR reflectance is one way that can be used to determine the state of vegetation.

Soil - Soils tend to have high reflectance in all bands which is dependent on factors such as the color, constituents and especially the moisture content. As seen earlier, water is a relatively strong absorber of all wavelengths, particularly those longer than the red part of the visible spectrum. Therefore, as a soils moisture content increases, the overall reflectance of that soil tends to decrease. Sandy soil tends to appear bright white in imagery because visible wavelengths are equally reflected, when slightly fewer blue wavelengths are reflected this results in a yellow color.

With reference from the information above, specific features in each treated image can be highlighted using spectral rationing which is an enhancement technique whereby a raster pixel from one spectral band is divided by the corresponding value in another band. Several spectral indices manipulation techniques have been designed and tested to highlight hydrological features (Yang et al., 2017) and vegetation (Athos et al., 2012) and even for assessing fire severity (Sarah et al., 2011). They have widely been used in areas where reference data do not exist to quantitatively examine ongoing changes. The Lake Chad water surface area was extracted individually from

each temporal image to detect the surface area changes during our study period. The performance of four different spectral indices was compared for the extraction of surface water (Table 5). Images from Landsat ETM+ 2007 and OLI 2015 were used for this performance analysis.

(McFeeters, 1996) calculated the NDWI using the reflectance of the green and NIR bands. This was based on the format of the normalized difference of vegetation NDVI developed by (Rouse et al., 1973) from which numerous water extraction indices have been developed simply by introducing new bands (Xu, 2005; Otukei et al., 2010; Xiao et al., 2010). The modified normalized water index (MNDWI), which is the most common water extraction index, can constrain plants and impervious areas and reveal subtle water features as well as eliminate shadow effects (Ji et al., 2009). The Automated Water Extraction Index is a multiple band index which suppresses classification noise from shadows and other non-water dark surfaces (Feyisa et al., 2014).

Table 5. Satellite-derived indexes used for water features extraction.

INDEX	EQUATION	Reference
Automated Water Extraction Index (AWEI)	$\text{AWEI} = 4 * (\text{Green} - \text{SWIR1}) - (0.25 * \text{NIR} + 2.75 * \text{SWIR2})$	Feyisa et al., 2014
Modified Normalized Difference Water Index (MNDWI)	$\text{NDWI} = \frac{\text{Green} - \text{SWIR1}}{\text{Green} + \text{SWIR1}}$	(Xu, 2005)
Normalized Difference Vegetation Index (NDVI)	$\text{NDVI} = \frac{\text{NIR} - \text{Red}}{\text{NIR} + \text{Red}}$	(Rouse et al., 1973)
Normalized Difference Water Index (NDWI)	$\text{NDWI} = \frac{\text{Green} - \text{NIR}}{\text{Green} + \text{NIR}}$	(McFeeters, 1996)

Amongst the four techniques used for our test periods, the technique with the least amount of error was used to develop the area change estimates of Lake Chad from 2003-2016.

c. Performance evaluation

The water indices in Table 5 are known to have varying performances and depends on the Landsat image conditions and study area size (Fisher et al., 2016). During the test period of 2007 and 2015, each water index was calculated from the Landsat images. To properly the water pixels with an image, an appropriate threshold is needed to differentiate between water and non-water features within that water index image. A process known as segmentation. Previous studies set the threshold values for NDWI and MNDWI to zero (Xu, 2005; McFeeters, 1996). However, adjusting these threshold values based on actual situation is necessary. This could achieve a more accurate result for water segmentation. Manually determining threshold value can also be time consuming especially when dealing with many satellite images. As such, to automate this process, some researchers have applied the Otsu's binarization algorithm for water threshold selection (Ostu, 1978; Karsli et al., 2011). The Otsu method assumes that the image contains two classes of pixels following a bimodal histogram. It then calculates an optimum threshold separating the two classes so that their inter-class variance is maximal (Sun et al., 2012). The Otsu method was used to automatically generate optimal threshold values which were later on used distinguish between water and non-water features within each water index image.

The performance of AWEI, MNDWI, NDWI and NDVI in extracting estimates of the Lake Chad's water extent was investigated

by carrying out a quantitative accuracy assessment. Since most of the lake is located within the tile (path/row 185/51), reference data was selected within this tile and its water extent was outlined as being the "true" lake extent (Table 6). Reference maps for this study were generated from a free and a commercial image source Figure 24. For the free reference image source, I made use of Google Earth aerial image. Using visual inspection, an aerial image from Google Earth was used as a visual reference to select an ETM+ image to be used as the reference image. The selected reference image was captured on 2007/02/08. Cloud influence on this image was small. There was no major rainfall or flood event during that month. Its water extent was used as reference to evaluate water area extraction for that period. The commercial image was acquired from WorldView-3 (WV-3). WorldView-3 spectral data have a spatial resolution of 0.31m. The WV-3 image was provided with 8 bands. The Red, Green, Blue and Near-Infrared bands were used in this study to generate reference maps. The closeness in acquisition dates helped in the reduction of time-dependent effects.

Table 6. Description of Landsat 7/OLI scenes and corresponding reference data**.**

Test site	**Path/Row**	**Selected Landsat data**		**Reference data**	
		Sensor	**Date**	**Source**	**Date**
Lake Chad	185/51	ETM+ (B)	2007/02/15	ETM+	2007/02/08
				Google Earth	2007/02/01
		OLI (A)	2015/12/30	WorldView-3*	2015/12/22

* The WV-3 data commercially available at www.digitalglobe.com

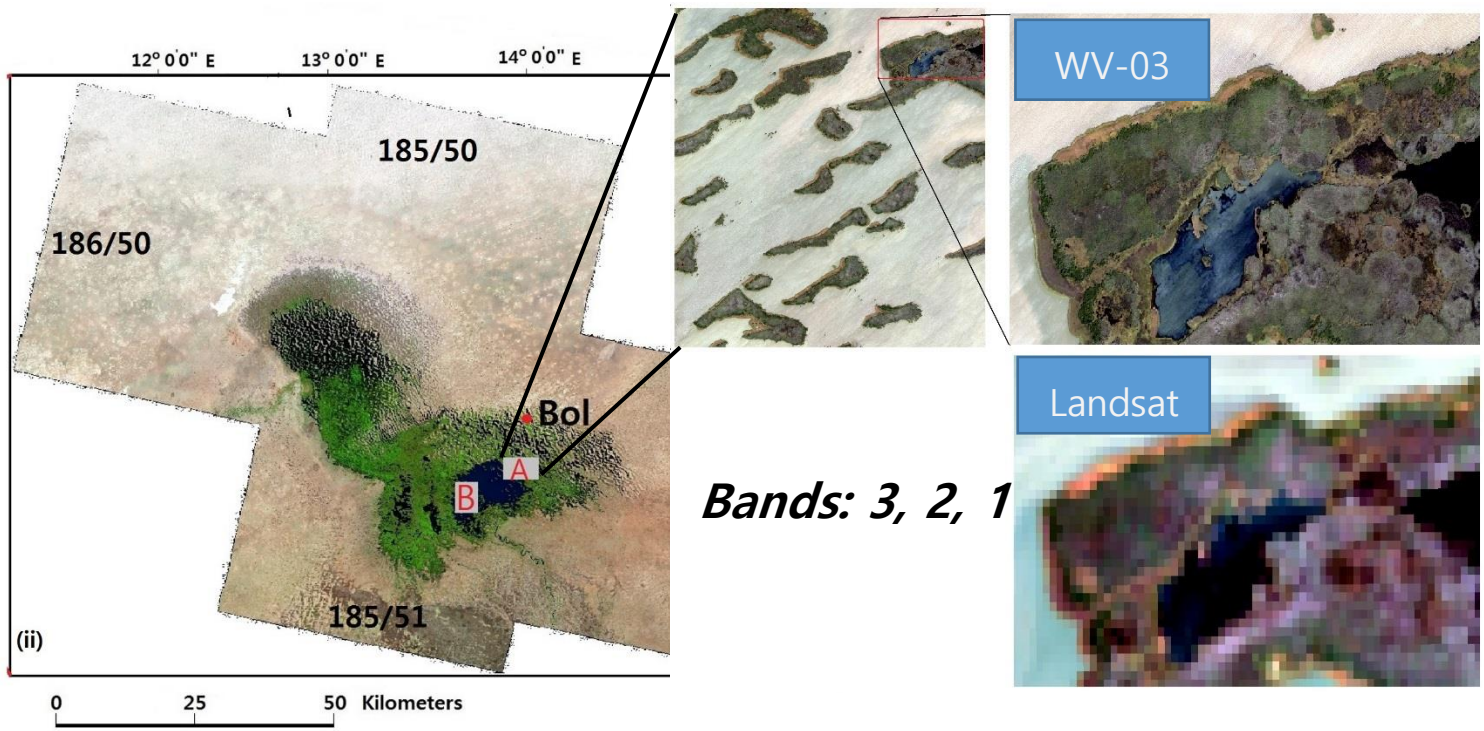

Figure 24. Point A and B represents the locations of the high-resolution reference data from WorldView-3 and Google Earth respectively

For the ETM+ sensor image, human visual inspection with the help of Google Earth aerial image was used in the delineation of the "true" reference map from the selected image. For the OLI sensor image, a multispectral image from WV-3 was used in the creation of "true" reference maps. Stratified random sampling method was used to generate 500 points within the boundaries of the high-resolution images for evaluation. I then used pixel-by-pixel comparison method to assess the accuracy of our indexes using the reference maps. Finally, an error matrix was created between the results from the water indices and the referenced water bodies. Performance evaluation was performed following recent best practices for remotely sensed data (Foody, 2002; 2009; Olofsson et al., 2014). Table 7 shows the principle of the error matrix.

Table 7. The principle of the confusion matrix.

		Predicted	
		Negative	Positive
Actual	Negative	a	b
	Positive	c	d

In Table 7, *a* is the number of correct prediction that an instance is negative, *b* is the number of incorrect predictions that an instance is positive, *c* is the number of incorrect of prediction that an instance negative, and *d* is the number of corrections that an instance is positive.

The accuracy indices include the overall accuracy, kappa coefficient, the product accuracy, and the user accuracy. The Producer accuracy represents the probability that a reference sample is correctly classified. This measures the omission error. User accuracy represents

the probability that a given point from Landsat image matches that found in the reference data (WorldView-03 image). It measures the error of commission. The overall accuracy (OA) provides the probability that a randomly selected sample on the imagery is correctly classified. OA can be calculated using equation (10)

$$\mathrm{OA} = \frac{\text{Number of true positive+Number of true negative}}{\text{Ground truth pixels}} * 100 \qquad (10)$$

The kappa coefficient (κ), which measures the percentage of agreement between the ground truth and segmented water body pixel, was determined using Equation (11).

$$\kappa = [\sum_{i=1}^{n} P_{ai} - \sum_{i-1}^{n}(P_{ic} \text{ x } P_{ri})] \div [P^2 - \sum_{i-1}^{n}(P_{ic} \text{ x } P_{ri})] \qquad (11)$$

Where:
P = total number of pixels in the reference data,
$P_{ai} =$ total number of correct pixels of the ith category,
$P_{ic} =$ total number of pixels for the ith category from the classified data
$P_{ri} =$ total number of pixels for the ith category from the reference data
n is the total number of categories.

Absolute Error (AE) which is simply the difference between the areas detected using the applied method and the reference, was determined using equation (12).

$$\mathrm{AE} = \text{Referenced area} - \text{Estimated area} \qquad (12)$$

Summarily, for this study, I first converted the digital number values of the selected Landsat TM, ETM+ and OLI images to at-sensor radiance, followed by a conversion to TOA reflectance. Next, I used the TOA reflectance to form enhanced images of our study area. After applying the equations listed in Table 5 to the processed images, I then defined their specific segmentation thresholds and used them to obtain our water extraction maps. Finally, I used the Overall Accuracy (OA),

Kappa Coefficients (κ) and Absolute Error (AE) to assess the performance of selected surface water extraction methods for Lake Chad.

5.2. Results and Discussions

a. Performance evaluation of AWEI, MNDWI, NDVI, and NDWI

After pre-processing, computed the water index using the equations listed in Table 5. After computation, each image changes to a grey image with high contrast between water and non-water pixels. The results are shown in Figure 25.

The quality of the derived grey scaled index image as well as the water index in question are two properties to monitor during threshold segmentation. As seen in Figure 25, the resulting grey scaled index images had varying degree of separability between water and non-water features. MNDWI, NDVI and NDWI could clearly delineate the patches of water in the northern section of the lake whereas AWEI was poor in this aspect (Figure 25). Vegetation is the main land cover type in this area. There is an open area of sand (Sand cap) which surrounds most of the northern section of the lake. The southern section of the lake comprises of an open water body and patches of water all surrounded by vegetation and sand

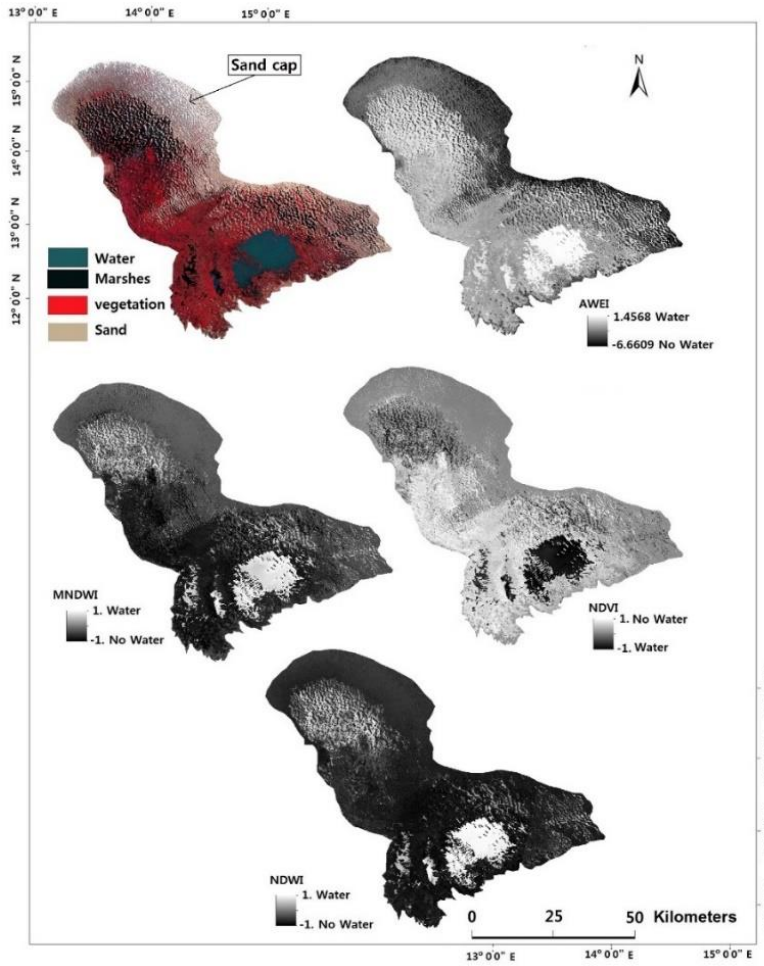

Figure 25. Lake surface water extraction from the different water index for Landsat 8, Jan-2015 image with a false colour composite (RGB 543) image.

b. Lake Surface water extraction

To evaluate the performance of the indices shown in Table 5, I compared their classification performance using images from Landsat 7 ETM+ and Landsat 8OLI sensor. Though not all indices could obtain a high degree of separability between water and non-water features, the contrast between these features was clear (Figure 25). During threshold segmentation, deviation from the optimal water threshold is a possible cause of faulty results. The Otsu method was

used to determine the optimal threshold for distinguishing between water and non-water features for our test period. Table 8 shows the lake surface area estimates of 2007 and 2015. The reference areas of 1350 km^2 and <2000 km^2 were obtained from (Gao et al., 2011), and the Lake Chad Basin Commission, respectively. We see here that the difference in estimated area sizes between 2007 and 2015 Landsat images were not that far apart between the MNDWI, NDVI and NDWI indices. The large difference between the area size of AWEI and the other indices is because AWEI was incapable of delineating much of the surface water around the northern side of the lake (Figure 25).

Table 8. Estimated area from each index and their respective threshold for the test years.

	2007		**2015**	
Reference area	1,350 km^2		<2000 km^2	
Index	**Land-Water Threshold**	**Lake Area (km^2)**	**Land-Water Threshold**	**Lake Area (km^2)**
AWEI	-0.2	1012	-0.13	1690
MNDWI	0.07	1394	0.2	2085
NDVI	0.09	1487	0.2	2175
NDWI	-0.18	1549	0.12	2137

i. Water extent extraction accuracy

Ground-truth observations are hard to come by in this area mainly because of its size and geographical location. This makes validating the accuracy of the lake area estimation methods difficult. High resolution images from other satellite collected around a similar period as the Landsat multispectral image were used for this accuracy assessment. I evaluated the performance of the different methods used to detect lake surface area changes between 2007 and 2015 by

calculating their respective absolute errors, overall accuracy and Kappa coefficient. A Google Earth aerial image was used to investigate the accuracy of the Landsat ETM+ data estimated lake area. For the Landsat OLI data, a reference data from Worldview-03 was used to assess the accuracy of the lake area estimate result (Table 6). Pixel-by-pixel comparison was used to generate error matrixes. These error matrixes were used to obtain the overall accuracy and Kappa coefficient. The Google Earth aerial image in Figure 26 shows an open water and vegetated land. As an example, we see in Figure 26 that AWEI and NDVI did not perform well in delineating water from its surrounding features as compared to MNDWI and NDWI. Some water pixels were misclassified as non-water features.

MNDWI and NDWI performed well in delineating water pixels for this area. NDWI, NDVI and MNDWI have an overall accuracy >90%. MNDWI and NDWI had kappa coefficients greater than 0.9. AWEI had an overall accuracy of 86% with the smallest kappa coefficient of 0.82. According to Table 9, the accuracy is relatively stable among the techniques, and all the water indices can achieve water extraction with an overall accuracy of greater than 80%. The kappa coefficient from the four indices is in the range of 0.8-0.9. For 2007, AWEI had the lowest kappa coefficient of 0.82. MNDWI and NDWI performed well with an averaged overall accuracy of 94.45% and a kappa coefficient of 0.89 between them.

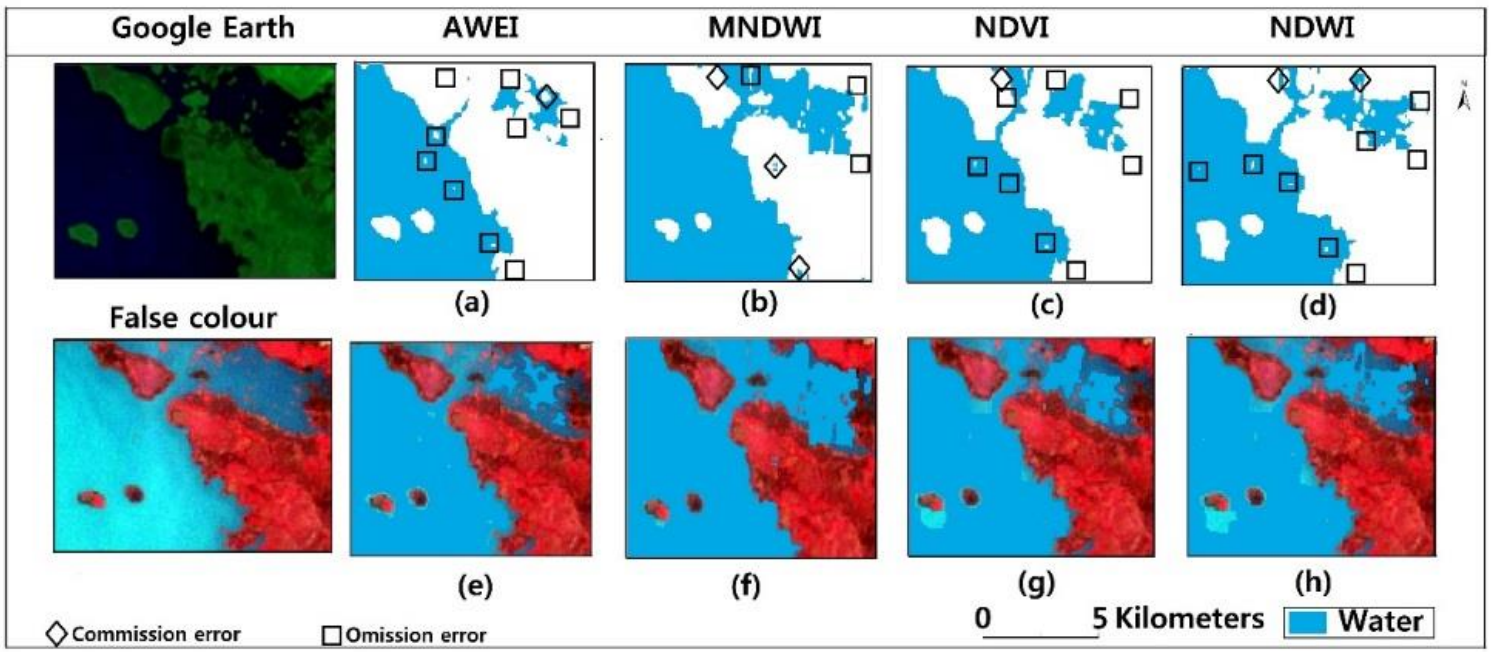

Figure 26. Performance evaluation of AWEI, MNDWI, NDVI and NDWI. (a, b, c and d) are binary images from AWEI, MNDWI, NDVI and NDWI respectively highlighting possible errors. (e, f, g, h) are water pixels overlaid on false composite of the reference image.

The performance of AWEI, MNDWI, NDVI and NDWI obtained from our OLI image was assessed using a high-resolution image from WorldView-3 (Table 6).

Table 9. Accuracy assessment analyses.

Index	2007			2015		
	AE (km^2)	**OA (%)**	**κ**	**AE (km^2)**	**OA (%)**	**κ**
AWEI	429	86	0.82	621	89	0.85
MNDWI	-44	95.7	0.9	-85	97	0.91
NDVI	-137	90	0.85	-175	92	0.89
NDWI	-194	93.2	0.88	-112	95	0.9

An area with clear and turbid water, vegetation and sandy edges was selected for this analysis (Figure 27). Looking at the first row of Figure 27, we see that the four processes did well in delineating clear water features. The producer and user accuracy are greater than 90% for all the indices. However, only MNDWI could barely delineate turbid water around the chosen area. MNDWI had an overall accuracy of 97% and a kappa coefficient of 0.91 which were both highest amongst the others (Table 9).

Based on accuracy, MNDWI for our test years had an overall accuracy of about 96.35% and a kappa coefficient of about 0.9. This was the highest when compared with the indices used in this study. MNDWI was therefore used to calculate the changes in the Lake Chad area during the period of 2003-2016 using multi-temporal Landsat images.

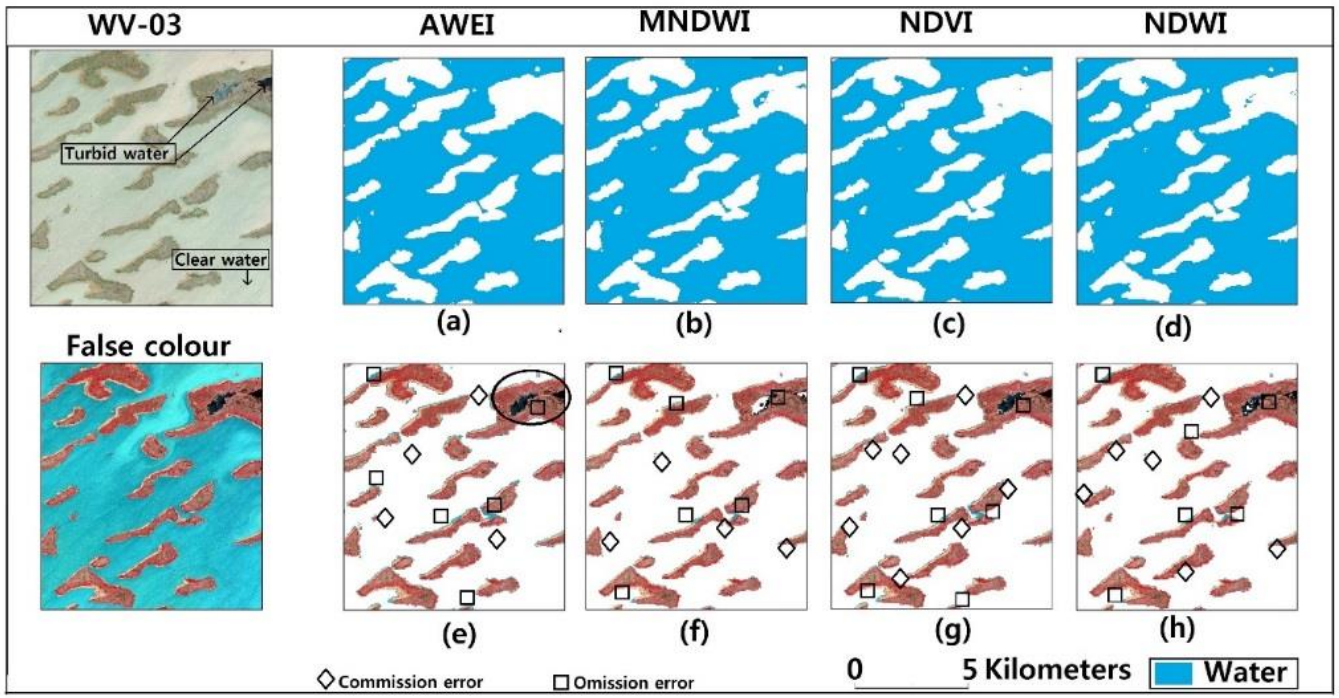

Figure 27. Comparison of the performance of AWEI, MNDWI, NDVI and NDWI on water extraction for the OLI image. (a, b, c, d) are binary images from AWEI, MNDWI, NDVI and NDWI respectively. (e, f, g, h) are water pixels overlaid on false composite image to highlight possible errors.

ii. Optimal threshold for MNDWI

The potentials of a suitable threshold method to delineate water from non-water features with high accuracy over time was tested for this study. Thresholding significantly affects the efficiency of mapping water features and it is highly influenced by the judgement of the user (Lu et al., 2011). When provided with very high quality reference data, a repeatable threshold method can be developed and its results verified. To be quite certain about our threshold segmentation method, I evaluated its dependency to MNDWI. Water features within the lake were delineated from non-water features using the Otsu method. The performance of the automated threshold values obtained using the Otsu method was tested by comparing them to threshold values generated manually through on-screen visualization with the help of the grey-scaled MNDWI image histogram for the year 2015. In doing so, I also tested the performance of the widely used 0-threshold and a 0.2-threshold in our study area (Figure 28a). From the analysis of 12 images, the deviation between the Manual and Otsu thresholds is small. Figure 28b.

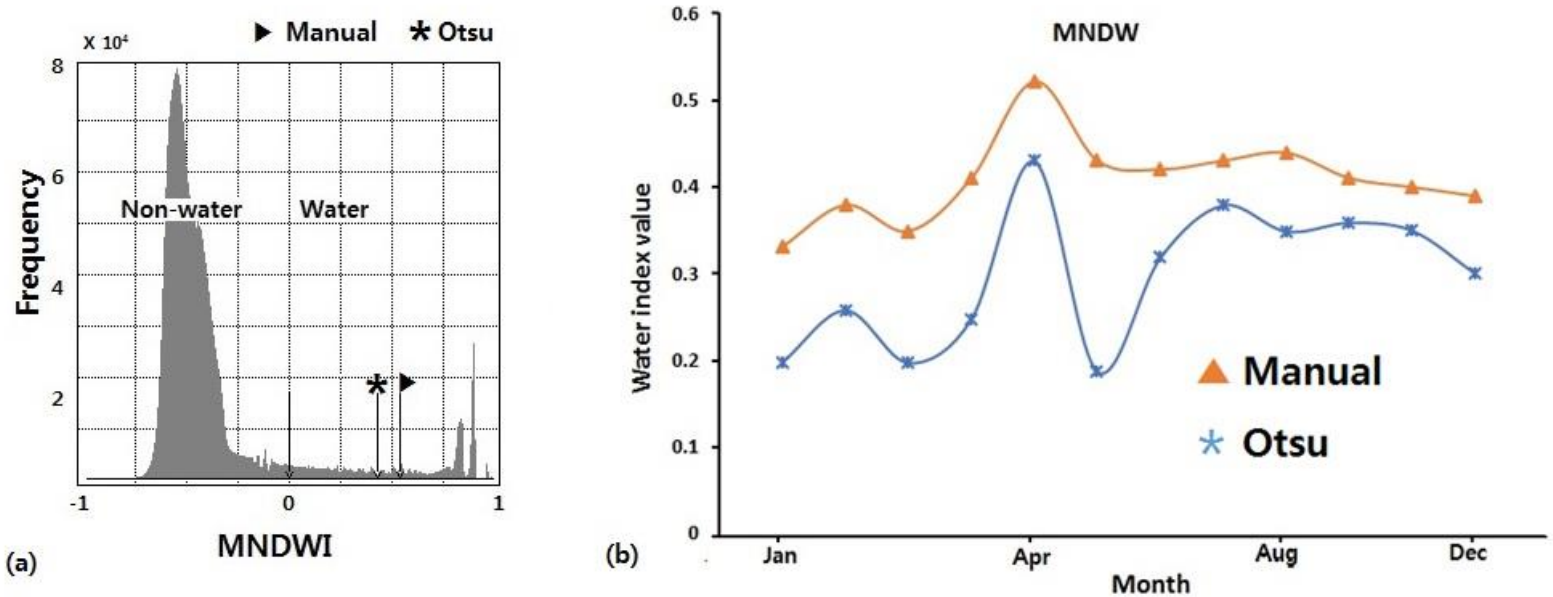

Figure 28. (a) Histogram of MNDWI image showing specific locations of water thresholds for L8 12-Jan 2015. (b) Comparison between MNDWI thresholds derived from the Otsu and Manual threshold selection methods. Landsat 8 image acquisition dates: 12-Jan, 13-Feb, 17-Mar, 17-Apr, 20-May, 21-Jun, 7-Jul, 25-Sep, 27-Oct, 28-Nov and 30-Dec 2015. Landsat 7 image acquisition date: 21-Aug-2011)

There was a high accuracy recorded between the selected thresholds for this analysis. The threshold of 0 had an overall accuracy of 80% which was the lowest (Table 10). This was due to numerous commission errors as seen in Figure 29.

The Otsu and the manual threshold values had an overall accuracy of 95.8% and 98.6% respectively. The accuracy of deviation of derived water maps by the Otsu and manual thresholds for MNDWI was less than 3%. A threshold of 0 will normally allow for rapid water feature delineation from other components. However, the classification accuracy at subpixel level based from WorldView-3 high resolution image showed that the Otsu and Manual threshold performed better than the 0 threshold in this area (Figure 29).

The threshold of 0 misclassified a significant amount of non-water features as water features (Figure 29). It had an overall accuracy of 80% and kappa coefficient of 0.82. Lowest amongst all the threshold compared (Table 10). The Otsu's threshold of 0.41 and the manual threshold of 0.52 had an overall accuracy of 96.8% and 98.6% and a kappa coefficient of 0.93 and 0.96 respectively. Judging from Figure 28b, there is a huge leap from a threshold of 0 to 0.41. I decided to test a threshold of 0.2 which lies between them to see if it had any significant changes in delineating water features. The 0.2 threshold had an accuracy of 96% and kappa coefficient of 0.91. The difference in accuracy between the manual threshold and all those used in this study was in its ability to identify some turbid water pixels as seen in (Figure 29).

Table 10. Accuracy comparison of different threshold of the lake area extracted by MNDWI.

	2015-12-12		
	Threshold	**OA (%)**	**κ**
MNDWI	0	80	0.82
	0.2	94	0.91
	0.41	95.8	0.92
	0.52	98.6	0.96

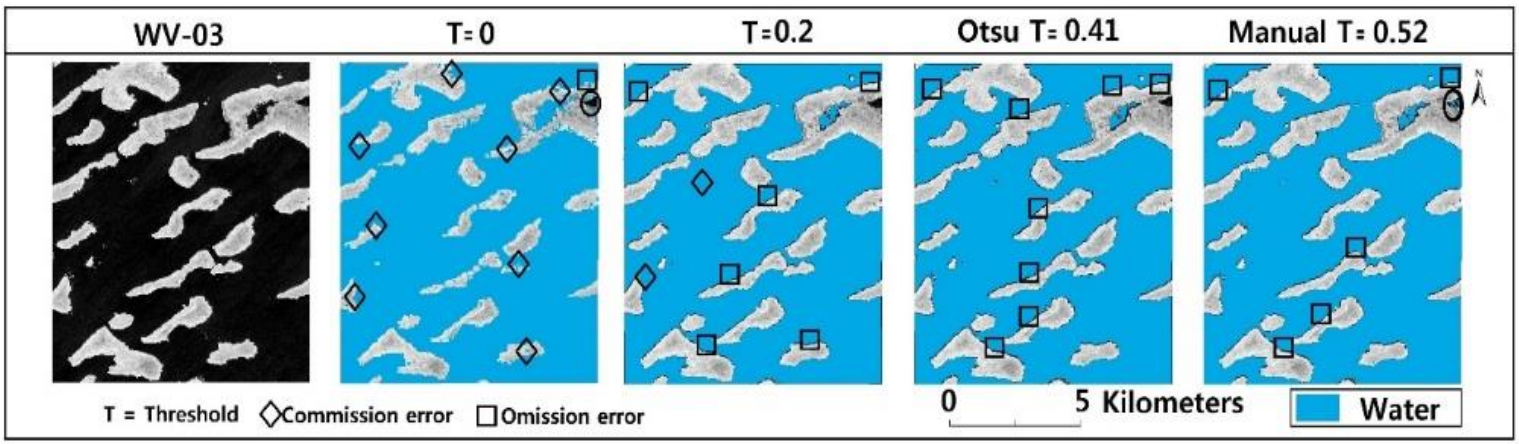

Figure 29. Water maps derived from different thresholds. Landsat date 2015-12-22. Circle represents area of turbid water.

Regardless, when using MNDWI for delineating water features for our study area, a threshold value of 0.2-0.5 will get a high degree a separability in delineating water from non-water features. The root mean square deviation between the Otsu and manual threshold was ~0.1. These experimental results show that the chosen water extraction method for this study is dependent on our threshold selection method. Also, the Otsu algorithm could be effectively used in place of manual threshold. Otsu was used for delineating water and non-water features for MNDWI for our study area.

As Figure 29 shows, MNDWI was highly accurate in delineating clear water in Lake Chad and achieved an extraction accuracy greater than 95%. However, I encountered some difficulties in extracting few turbid water pixels after applying the Otsu method of segmentation. Most of these turbid water pixels were misclassified (Figure 27 and 29). Nonetheless, this occupied less than 5% of the extracted area of the affected images.

iii. Estimated area and surface changes

To obtain appropriate area estimates for Lake Chad, optimal thresholds generated using the Otsu's method were applied to each MNDWI output. For this study, a total number of 78 monthly area covering the entire lake was generated.

Figure 30a shows estimated lake surface area maps for March, July, October and December for our test years 2007 and 2015 placed side by side. Calculated area was generated from water pixels. Area estimates showed an increase in water area for 2015 when compared to 2007. Spatially, water maps show a permanent water body in the southern

part of the lake with patches of water appearing in the northern section of the lake depending on the season (Figure 30a).

We also see in Figure 30a that water decrease mostly affects the Northern part of the lake, visually confirming that the lake recedes from North to South. Judging from the trend line, rainfall observations showed a slight increase during our study period (Figure 30b (i)). This region is primarily affected by two seasons: the rainy and dry seasons. During the rainy season which spans from May to October and peaks between July and August, averaged rainfall is usually greater than 200mm. This area also recorded occasional rains in April. Rainfall in July, August and September have the highest variations between the years. On the other hand, the dry season, which starts from November, has no rainfalls between the months of January and February. This bimodal relationship is seen in Figure 30b (iii), which presents a box plot of monthly rainfall measurements from the LCBC.

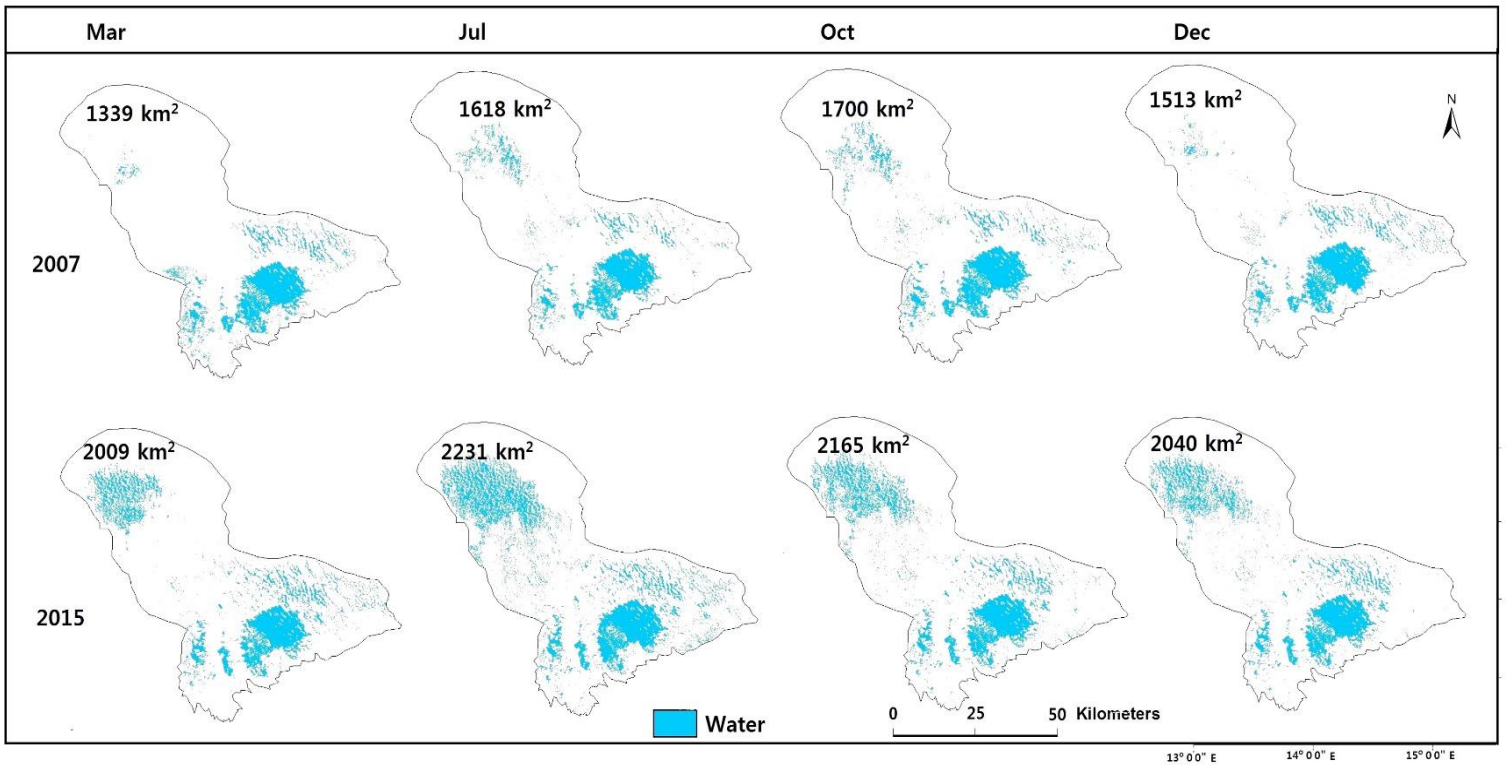

Figure 30. (a) Estimated lake surface water area changes for our test years. These years were chosen as representative examples of the 13-year period.

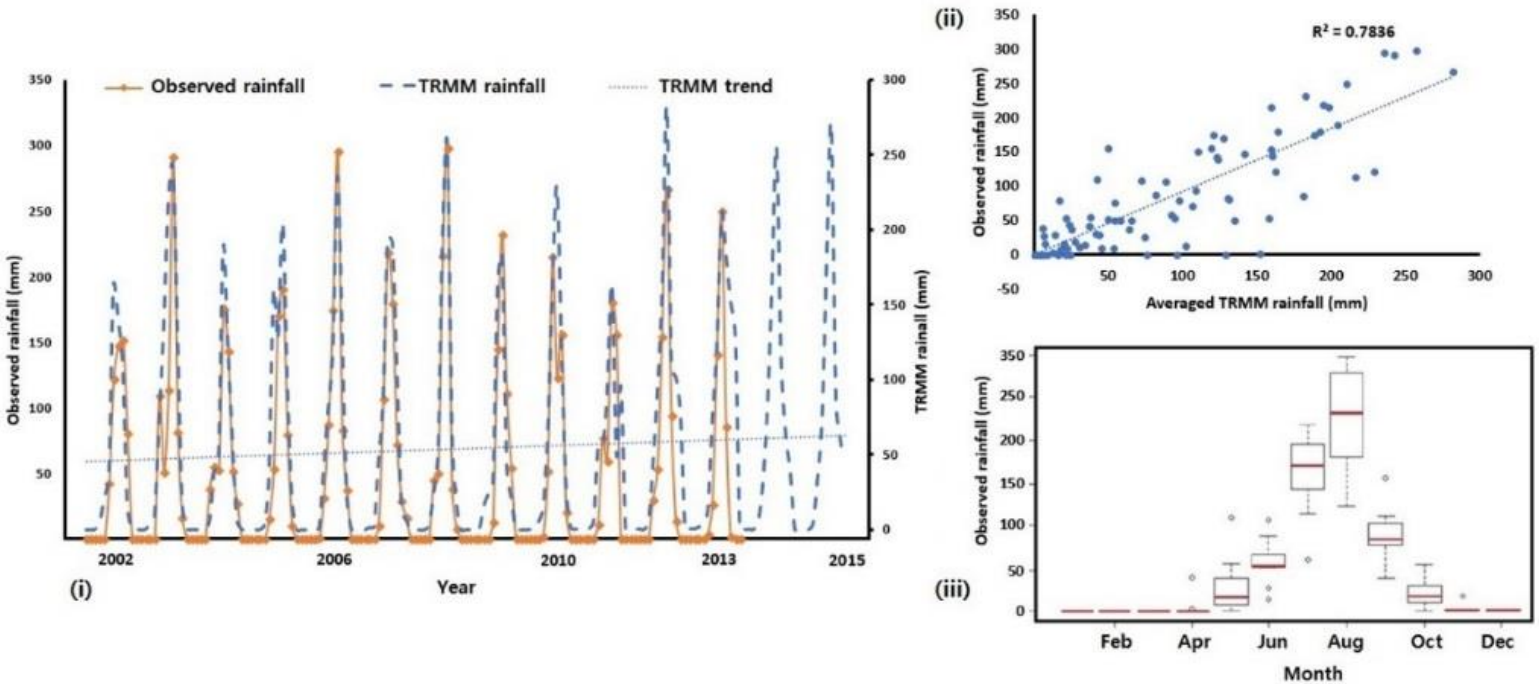

(b) (i) Monthly rainfall estimates from the LCBC and TRMM 3B42 (ii) Scatter plot comparing their monthly mean. (iii) Boxplot of the observed rainfall estimates.

iv. GRACE as an integrated indicator to Lake Chad hydrological dynamics

GRACE satellites data processing is continually evolving. Their gravitational observations have been identified as a valuable proxy of water availability over large areas, with consistent validated data free from cloud effects (Reager et al., 2014; Yang et al., 2014). GRACE, as described earlier, allows for measurements of the Earth's gravity field, producing measurements with greater magnitudes. These measurements can be used in monitoring changes in water and ice around the globe, ocean surface and deep currents, as well as provides vital information in the measurement of surface and groundwater changes (Mayer-Gürr et al., 2012; Simon et al., 2014; Longwei et al., 2016). Changes in the TWSA over the lake area has a direct influence on the hydrological and the ecological dynamics around the lake (Buma et al., 2016). TWSA was plotted as a representative metric to help illustrate the pattern of the Lake Chad's area changes during our study period. This was carried out simply to investigate if the estimated area were in line with TWSA estimates.

The estimated lake area experienced an increase with seasonal fluctuating tendencies. The R-Squared value is 0.47 which is indicative of a high variability. Besides the seasonal fluctuations, the difference in area between 2003 and 2012 are small as compared to those between 2013 and 2016 during which the lake area estimates peaked into the 2000 km^2 range with greater fluctuations (Figure 31). The TWSA trend over the Lake Chad basin slightly supports the variation in estimated lake area. The most significant decline in the TWSA occurred in late 2008 followed by its continuous increase.

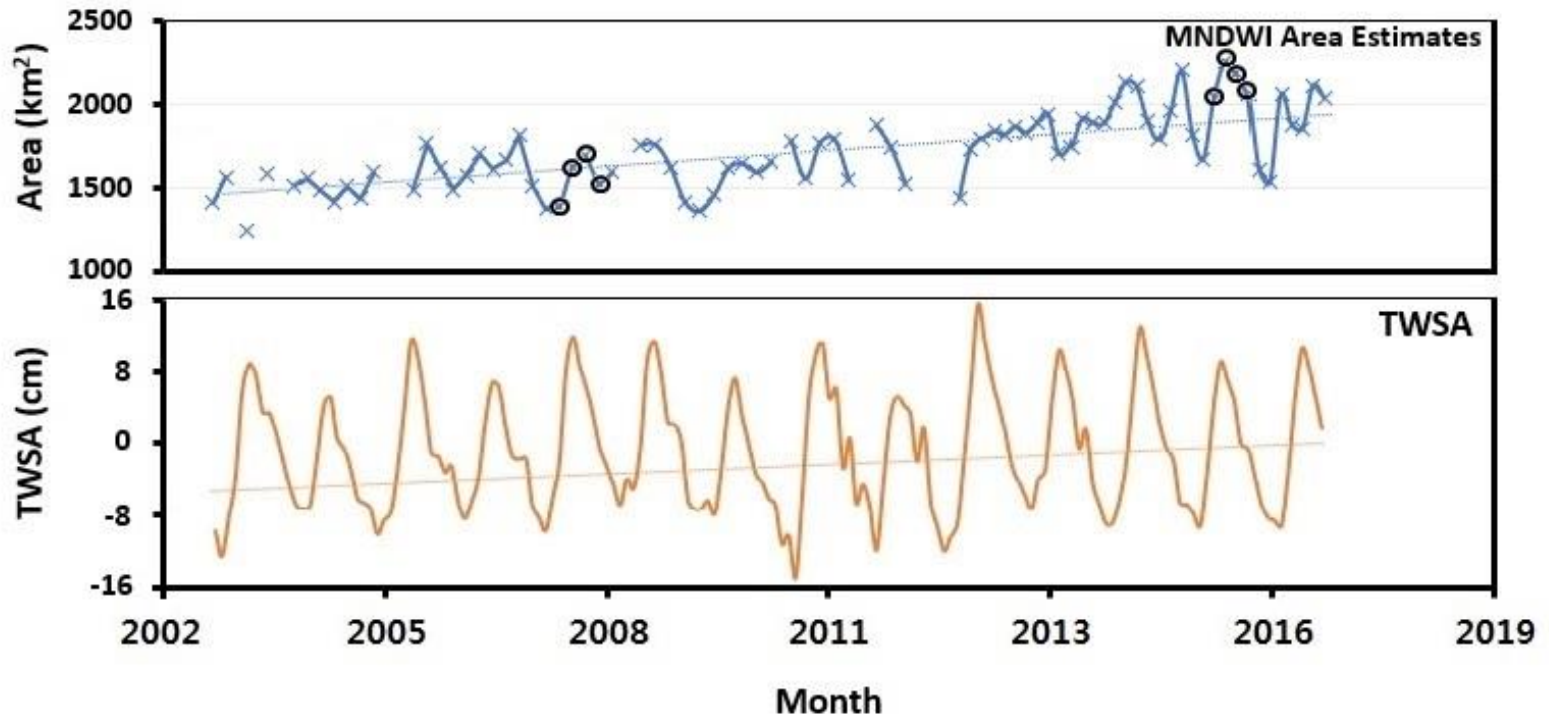

Figure 31. (a) Averaged monthly area and averaged monthly TWSA averaged over Lake Chad. The orange line represents the linear trend of the TWSA. The black circles represent selected monthly areas estimates of 2007 and 2015 illustrated in Figure 23a.

Generally, there is a slight uptrend in estimated lake area during our study period. The slight increase in lake area is in line with a study which showed improving wet conditions in the last two decades with 2002-2014 described as the wettest period. The authors attributed this to increasing rainfall in the area and the lack of any major long-term drought besides the usual seasonal fluctuations (Christopher et al., 2016). The Lake Chad average area from 2003-2016 was estimated to be 1694 km^2 with a standard deviation of about 233. The largest areas of 2087, 2182 and 2231 km^2 were recorded in October 2013, September 2014 and July 2015 respectively. This corresponds to the raining season. The smallest areas of 1242, 1325 and 1379 km^2 were recorded in March 2003, December 2006 and February 2009 respectively. Corresponding to the dry season. From Figure 31 we see that the lake area has a phase from 2003-2012 where the area changes fluctuated within the 1000 km^2 range. The average area from 2003-2012 was about 1563 km^2. From 2013-2016, area estimates entered the 2000 km^2 range with higher seasonal fluctuations. An averaged area of about 1876 km^2 was recorded for that period. Increase in lake area could be because of no major ongoing irrigation scheme going on in the Northern section of the lake as reported by the LCBC (Magrin et al., 2018). Between 2008 and 2014, there was a yearly increase of about 0.4m/year in altimetry lake levels (Christopher et al., 2016). Lake area estimates also matches with an increasing agricultural productivity. This was reported by a recent study where the authors revealed that locals have experienced an increase in maize yields from 2010 upward compared to a mild harvest during the early 2000s (Erik et al., 2016). A possible reason for such an increase in agricultural productivity is more surface water. An

increasing trend in GRACE TWSA around this area also backs the slight increase in lake area (Figure 31). Summarily, increased rainfall, lake levels and a recent halt in irrigation schemes on the lake are all consistent with the recent growth of the lake surface area from during our study period. Even though downloaded images had less than 5% cloud cover, during image processing, I noticed some images were still contaminated by clouds. As such, they were disregarded for our analysis. This explains the gaps in Figure 31.

Flooding events are limited to once a year during our 13-year study period. This is often during or after the raining season when we have patches of water forming in the northern section. Obtained water patches during the study period were included as part of the generated water maps. The Northern section of the lake is predominantly consist of dry lands during the dry season as most of it water has either evaporated or been used up. I recorded no direct link in terms of water out flow from the southern pool into the northern pool of the lake. Hence, the northern side of the lake still solely relies on direct rainfall or an inflow from the Komadugu-Yobe River. The lake bathymetry enhances water loss in this area. With water not being able to flow from the south to the north, this increases chances of evapotranspiration and seepage of the water pool in the southern part (Gao et al., 2011). Even though there was a slight increase in lake area during our study period, the large seasonal fluctuations reported to have occurred in the 80s (Leblanc et al., 2011), still happens in recent times (Figure 30a).

5.3. Summary

Lake Chad's area from Landsat 7 and 8 satellite images were estimated. MNDWI performed better than other indexes for mapping the water extent from acquired Landsat images. When used with the "proper" threshold value, MNDWI can identify open water, turbid water and small water bodies which all makes part of the larger Lake Chad. This study results demonstrated that when provided with reference data, optimized threshold values could be generated for large data set in a reproducible manner using the Otsu algorithm. Producing high accuracy lake area extraction results in this area. Due to the difficulty in delineating some turbid water in our area, when applying MNDWI for future studies in this area, a thorough investigation of the quality of image is required.

Estimated lake area generally increased from 2003-2016. From 2011-2016, the lake's area increased by a further ~314 km^2 mainly due to increasing wet conditions and less irrigation in the area. GRACE TWSA was used as a representative metric to help explain the lake area changes both seasonally and inter-annually. It could be used as a hydrological indicator for future designs of the Lake Chad's management strategies.

The FAO proposed a response strategy to water crisis in this area for the period 2017-2019. A key point they noted towards achieving this goal is to provide mapping an analysis of existing resourceful features around the Lake Chad basin and a generational analysis of land use and water utilization at cross-border levels (FAO, 2017). Using updated Landsat 8 images to generate water coverage maps and durations could in the realization of this response strategy8.

Given the advancements in the OLI sensor, a thorough study using Landsat 8 images will help determine with much accuracy the water coverage seasonal duration as well as other surface features around the lake from 2017-2019.

CHAPTER VI: CONCLUSIONS

In this study, I used various remote sensing data products mentioned in section 3 to study the hydrological dynamics within the lake Chad Basin from 2003-2016. Some of our findings are mentioned below. The two bodies of work presented in this PhD thesis illustrate that satellite data can successfully be utilized for regional scale water analysis.

Data estimates from GRACE, ENVISAT GLDAS and WGHM were used for the first part of this work where I studied the past variations in water resources in the LCB. GRACE Level 2 release 5.0 data from CSR were used to estimate the time series of the water storage changes. The data were during April 2002 to December 2013. Some months were missing for all these data sets. A temporal linear interpolation was done to make up for the missing months since they were not contiguous. A similar approach was carried out on the ENVISAT lake level estimates when missing data were recorded. GRACE data were de-striped by a non-isotropic filter and were smoothed according to Gaussian smoothing radii: 300 km. The LCB is largely characterized by highly variable surface water resources with limited hydro-geologic observations.

Rainfall is a significant driver in the observed total water storage behavior over the LCB (Figure 30b). Monthly rainfall behavior is similar to that of total water storage (with a phase shift of about a month and a half between rainfall and total water storage). At annual timescales; time series analysis shows that high rainfall events play a role in eliminating declines in total water storage from previous years, if any. Increasing variability in regional rainfall and increased

groundwater demands from growing populations and farming, groundwater sustainability is questionable. Results in this section shows patterns of hydro-climatology that has impacted changes in water storage in this data-sparse region.

The last part of the variability studies was the use of filtered data sets in the disaggregation of the groundwater component in terms of surface water volume from the GRACE total water storage estimates. Subsurface water volume estimates from GRACE were compared to those derived from the WGHM allowing for an evaluation of groundwater behaviors over the basin. Subsurface water volume estimates from GRACE and WGHM had a correlation of about 47% between.

The data for that section not only have implications for improving drought early warning lead times and drought preparation and management efforts, but they have shown the significance data from those sources and advocate for the development of future operations.

The goal of the second part of this study centered on the use water indices to identify the water extent dynamics of the LCB from Landsat 7 and 8 images. Four water indices (AWEI, NDWI, MNDWI, and NDVI) were compared to find out which performed best in delineating water features within the basin. They all performed well in delineating water features. However, accuracy results confirmed the superiority of the MNDWI out of the four widely used band ratio indices. The Otsu algorithm was used to automate the generation of threshold values for the MNDWI over the Landsat 7 and 8 images. Using a conventional fixed threshold (usually a value of 0) reduces the

performance of MNDWI due to its sensitivity to changes in thresholds (Table 10).

Errors from cloud uncertainties, shallow and turbid water, and associated mixed pixels, led to a number of outliers which can be detrimental to results. Filtering images with excessive cloud and SLC presence reduced temporal resolution to 6 images per month for our study area. This can lead to minor floods and high infiltration being overlooked by Landsat time series. Using these images with field data and modelling may overcome image availability issues and problems of incoherent hydrological dynamics.

Despite these difficulties alongside those associated with delineating shallow and turbid water, MNDWI overall accuracy rates were high for this area (Table 9). Validated against very high resolution images from WorldView-03, this study demonstrates the potential and limitations of Landsat imagery to monitor surface water extent dynamics of the LCB.

The present PhD thesis is concluded to have met the purpose for which it was conceived, according to the general aim set at the beginning of this document. For a region that is under-sampled and where policies limit data accessibility, this study has demonstrated the utility of applying remote sensing data in monitoring some aspects of water resources over the LCB. Such results can be readily applied to regional water resources modeling to interpret local-scale water resources availability. The study was limited in timeframe given short period data availability especially for small lakes. I therefore recommend that future works consider extending the analysis with inclusion of more surface lakes, to further isolate long term

anthropogenic and climate related controls on regional groundwater and associated trends.

An extension of this work would involve the use GRACE FO data and very high resolution images alongside climate model projections to estimate precipitation and resulting water storage continuously into the future given the sparse amount data management infrastructure available for the region. This information would greatly influence the planning of the current dam construction project which is aimed at replenishing the lake. It will also help in policy, mitigation strategies, and risk assessment by providing a range of the severity hydrologic extremes with associated uncertainties.

References

Adrian, R., O'Reilly, C., Zagarese, H., Baines, S., & Hessen, D. (2009). Lakes as sentinels of climate change. *Limnol. Oceanogr.*, 2283-2297.

Aladin et al, N. A. (2005). Modern hydrobiological state of the Small Aral Sea. *Environmetric 16*, 375-392.

Allen, J. K. (2011). Adaptive management for a turbulent future. *Environmental Management*, 1339-1345.

Angerbrandt, H. (2017). Nigeria and the Lake Chad Region Beyond Boko Haram. Uppsala: Nordic African Institute.

Asadullah, A. A. (2008). Evaluation of five satellite products for estimation of rainfall over Uganda. *Hydrol. Sci. J.* 53 (6) pp. 1137–1150.

Athos, A., Diofantos, G., & D.A, D. (2012). Evaluation of broadband and narrowband vegetation indices for the identification of archaeological crop marks. *Remote Sens.*, 3892-3919.

Awange, J. (2006). Lake Victoria: ecology, resources, and environment. *Springer Berlin Heidelberg*.

Ayman and Shuanggen, A. A. (2014). Lake level change and total water discharge in East Africa Rift Valley from satellite-based observations. *Global and Planetary Change*, 79-90 doi:10.1016/j.gloplacha.

B, M. (2012). Cogs in the endless machine: lakes, climate change and nutrient cycles: a review. *Sci. Total Environ*, 130-142. doi:http://dx.doi.org/10.1016/j.scitoenv.2011.07.069.

B.-L. Xue, L. W. (2013). Evaluation of evapotranspiration estimates for two river basins on the Tibetan Plateau by a water balance method. *J. Hydrol.*, 492 (2013), pp. 290–297.

Bader, J., Lemoalle, J., & Leblanc, M. (2011). Modèle hydrologique du Lac Tchad . *Hydrol. Sci. J.*, 411-425.

Bdliya, H., & Bloxom, M. (2007). Transboundary diagnostic analysis of the Lake Chad Basin. A report prepared for the Lake Chad Basin Commission as an output of the GEF project on the reversal of land and water degradation trends in the Lake Chad Basin Ecosystem. *N'djamena: Lake Chad Basin Commission.*

Becker, B. (2010). Recent hydrological behavior of the East African great lakes region inferred from GRACE, satellite altimetry and rainfall observations. *Comptes Rendus Geoscience*, 223–233.

Bettadpur, S. (2003). Level-2 gravity field product user handbook, The GRACE Project.

Bettadpur, S. (2007). Gravity Recovery and Climate Experiment. Product Specification Document,. *CSR-GR-03-02*: GRACE 327-720.

BGR, L. a. (2010). Lake Chad Sustainable Water Management. Hannover: Lake Chad Commission, Federal Institute of Geosciences and Natural Resources. Hannover Germany.

Bhuvaneswari, K., Dhamotharan, R., & Radhakrishnan, N. (2011). Remote sensing satellite data for Coastal Ecosystem and Human Interaction -A Case study in Tamilnadu, India. *International Journal of Computer Information Systems*, 77-81.

Billah, M. (2015). A methodology for evaluating evapotranspiration estimates at the watershed-scale using GRACE. *Journal Of Hydrology*, 523 574 - 586 (DOI http://dx.doi.org/10.1016/j.jhydrol.2015.01.066).

Birkett, C. (2000). Synergistic remote sensing of Lake Chad: variability of basin inundation. *Remote Sens. Environ.* 72 218–36.

Boronina, A., & Ramillien, G. (2008). Application of AVHRR imagery and GRACE measurements for calculation of actual evapotranspiration over the Quaternary aquifer (Lake Chad basin) and validation of groundwater models. *Hydrology 348 (1-2)*, 98-109 (doi:10.1016/j.jhydrol.2007.09.061).

Buma, W., Lee, S., & Seo, J. (2016). Hydrological evaluation of Lake Chad Basin using space borne and hydrological model observations. *Water*, 205.

Cai, Xiaobin, F., Lian, W., Yuxi, C., & Xiaoling. (2015). Influence of the Three Gorges Project on the Water Resource Components of Poyang Lake Watershed: Observations from TRMM and GRACE. *Advances in Meteorology*, 148913 (7 pages) - 148913 (DOI http://dx.doi.org/10.1155/2015/148913)..

CALMANT, S., SEYLER, F., & CRETAUX, J.-F. (2008). Monitoring Continental Surface Waters by Satellite Altimetry. *Survey in Geophysics*, 4-5.

Calmant, Seyler, Cazenave, & Frappart. (2004). Amazon River Stages by ENVISAT vs. Other Satellite Altimeters. Salzburg, Austria: Poster Session 4P12–02 ‘Lake Levels’, Abstract 671, ERS and ENVISAT Symposium.

Campbell, R. (2008). Lake Chad, West Africa: 1963, 1973, 1987, 1997, 2007 Earthshots:Satellite Images of Environmental. Retrieved

from Reston, VA: US Geological Survey: http://earthshots.usgs.gov

Carius, A., Dabelko, G., & Wolf, A. (2004). Water, conflict, and cooperation.www.wilsoncenter.org/sites/default/files/ecspr10_unf-caribelko.pdf.

Carvalho, L., McDonald, C., Hoyos, C., Mischke, U., & Phillips, G. (2013a). Sustaining recreational quality of European lakes: minimizing the health risks from algal blooms through phosphorus control. *J. Appl. Ecol*, 315-323.

Chander, G., Markham, B., & Helder, D. (2009). Summary of current radiometric calibration coefficients for Landsat MSS, TM, ETM+, and EO-1 ALI sensors. *Remote Sens. Environ.* , 893–903.

Charles, V., gabila, W. g., & pauline, O. t. (2005). *Millennium Ecosystem Assessment.* Washington, DC: Island Press.

Chen, J., Zhu, X., Vogelmann, J., Gao, F., & Jin, S. (2011). A simple and effective method for filling gaps in Landsat ETM plus SLC-off images. . *Remote Sens. Environ.* , 1053–1064.

Chen, L., Wilson, R., Tapley, D., & Ries, J. (2004). Low degree gravitational changes from GRACE: Validation and interpretation. *Geophys. Res. Lett.*, 359-393.

Cheng, M., & Tapley, D. (2005). ariations in the Earth's oblateness during the past 28 years. *J. Geophys. Res. Solid Earth*, 110.

Christopher, E., O.A., N., Onuwa, O., & Vagner, G. (2016). Spatio-temporal variability of droughts and terrestrial water storage over Lake Chad Basin using independent component analysis. . *J. Hydrol.*, 106-128.

Churchill Okonkwo, B. D. (2014). Characteristics of Lake Chad Level Variability and Links to. *The Scientific World Journal*, Article ID 145893, 13 pages.

Cleveland, R., Cleveland, W., McRae, J., & Thacker, E. (1990). STL: a seasonal-trend decomposition procedure based on loess. *J. Off. Stat.*, 6, 3–73.

Coe, M., & Foley, J. (2001). Human and natural impacts on the water resources of the Lake. *Geophys. Res.-Atmos.*, 3349–56.

Coe, T., & Birkett, C. (2004). Calculation of river discharge and prediction of lake height from satellite radar altimetry: Example for the Lake Chad basin. *Water Resour. Res.*, *40,*, W10205, doi:10.1029/2003WR002543.

Cole, J., Prairie, Y., Caraco, N., McDowell, W., & Tranvik, L. (2007). Plumbing the Global Carbon Cycle: Integrating Inland Waters into the Terrestrial Carbon Budget. *Ecosystems*, 172-185.

Craglia, M., de-Bie, K., Jackson , D., Pesaresi, M., & Wang, C. (2012). Digital Earth 2020: towards the vision for the next decade. *Int. J. Digit. Earth*, 4-21.

Crétaux and Birkett, J.-F. C. (2000). Synergistic remote sensing of lake Chad: variability of basin inundation. *Remote Sens. Environ*, 72 (2000) 218–236.

Crétaux, J., & Birkett, S. (2006). Lake studies from satellite radar altimetry. *Compt. Rendus Geosci.*, 1098–1112.

Crowley, J., Mitrovica, J., Bailley, R., Tamisiea, M., & Davis, J. (2006). Land water storage within the Congo Basin inferred from GRACE satellite gravimetry data. *Geophy. Res. lett*, 33.

Diplomacy, C. (2016). Insurgency, Terrorism and Organised Crime in a Warming Climate. Berlin: adelphi.

Döll, Kaspar, & Lehner. (2003). A global hydrological model for deriving water availability indicators: model tuning and validation. *J. Hydrology, 270*, 105-134.

Döll, Müller, Schuh, Portmann, & Eicker. (2014). Global-scale assessment of groundwater depletion and related groundwater abstractions: Combining hydrological modeling with information from well observations and GRACE satellites. *Water Resour. Res., 50,*, doi:10.1002/2014WR015595.

DREM. (2014). *Hauteurs Journalières du Lac à Bol. N'Djamena. .* République du Tchad. : Direction des Recherches en Eau et de la Météorologie.

Erik, N., Stefan, H.-S., Junko, M., & B.U., C. (2016). Hydro-climatic variability and agricultural production on the shores of Lake Chad. . *Env. Dev.* , 15-30.

Erik, N., Stefan, S., Junko, M., & Cintia, U. (2016). Hydro-climatic variability and agricultural production on the shores of Lake Chad. *Env. Dev*, 15-30.

Estoque, R., & Murayama, Y. (2015). Classification and change detection of built-up lands from Landsat-7 ETM+ and Landsat-8 OLI/TIRS imageries: A comparative assessment of various spectral indices. *Ecol. Indic.* , 205–217.

FAO. (2017, March 31). Food and Agricultural Organization of the United Nations. Retrieved April 1, 2018, from http://www.fao.org/emergencies/crisis/lakechadbasin/intro/fr/.

FAO. (2017, April 1). *Food and Agricultural Organization of the United Nations.* Retrieved from Food and Agricultural Organization: http://www.fao.org/emergencies/resources/documents/resources-detail/en/c/471497/.

Ferreira, F. Estimating total discharge in the Yangtze River basin using satellite-based observations. *Remote Sens*, 3415–3430.

FEWS. (2010, November 21). Chad livelihood profiles. Retrieved from Famine Early Warning Systems Network : http://pdf.usaid.gov/pdf_docs/PNADE389.pdf

Feyisa, G., Meilby, H., Fensholt, R., & Proud, S. (2014). Automated Water Extraction Index: A New Technique for Surface Water Mapping Using Landsat Imagery. *Remote Sens. Environ.*, 23-35.

Feyisa, G., Meilby, H., Fensholt, R., & Proud, S. (2014). Automated Water Extraction Index: A New Technique for Surface Water Mapping Using Landsat Imagery. *Remote Sens. Environ.*, 23-35.

Fisher, A., Flood, N., & Danaher, T. (2016). Comparing Landsat water index methods for automated water classification in eastern Australia. . *Remote Sens. Environ.*, 167–182.

Fokou, G. (2010). Tax Payments, Democracy and Rent-Seeking Administrators: Common-Pool Resource Management, Power Relations and Conflicts Among the Kotoko, Musgum, Fulbe and Arab Choa in the Waza-Logone Floodplain (Cameroon), in Disputing the Floodplains. *The Netherlands: Brill: Leiden.*

Foody, G. (2002). Status of Land Cover Classification Accuracy Assessment. *Remote Sens. Environ. ,* 185-201.

Foody, G. (2009). Classification Accuracy Comparison: Hypothesis Tests and the Use of Confidence Intervals in Evaluations of Difference, Equivalence and Non-Inferiority. *Remote Sens. Environ* , 1658–1663.

Fortnam, M., & Oguntola, J. (2009, September 18). Lake Chad Basin, GIWA Regional Assessment. Retrieved from UNEP 2004: http://www.unep.org/dewa/giwa/publications/r43.asp,retrieved

Frappart, F., calmant, S., Cauhope, M., Seyler, F., & Cazenave, A. (2006). Preliminary results of envisat ra-2-derived water levels validation over the amazon basin. *remote Sensing of Environment*, 252-264.

Fuchs, M., Bouman, J., Broerse, T., Visser, P., & Vermeersen, B. (2013). Observing coseismic gravity change from the Japan Tohoku-Oki 2011 earthquake with GOCE gravity gradiometry. *Journal of Geophysical Research: Solid Earth*, 5712-5721.

Gao, H., Bohn, T., Podset, E., McDonald, K., & Lettenmaier, D. (2011). On the causes of the shrinking of Lake Chad. *Environmental Research Letters*, vol. 6, no. 3, Article ID 034021,.

Goni. (2006.). Tracing stable isotope values from meteoric water to groundwater in the southwestern part of the Chad basin. *Hydrogeology Journal*, 742-752.

Grove. (1996). African river discharges and lake levels in the twentieth century, In The Limnology,Climatology, and Palaeoclimatology of the East African Lakes. In A. T. Grove. Newark, N.J: Gordon and Breach.

GWP. (2013). The Lake Chad Basin Aquifer System. Stockholm: Ground Water Partnership.

Haas, E., Bartholome, E., & Combal, B. (2009). Time series analysis of optical remote sensing data for the mapping of temporary surface water bodies in sub-Saharan western Africa. *J. Hydrol*, 52-63.

Haller, T., Fokou, G., Mbeyale, G., & Meroka, P. (2013). How fit turns into misfit and back: institutional transformations of pastoral commons in African floodplains. *Ecol. Soc.* , 34.

Henry, A. (2011). Groundwater storage variability and annual recharge using well-hydrograph and GRACE satellite data. *Hydrogeology Journal ,19*, 741-755.

Hunger, M., & Döll, P. (2008). Value of river discharge data for global-scale hydrological modeling. *Hydrol. Earth Syst. Sci., 12*, 841-861.

IPCC, I.-G. P. (2007). Contribution of Working Groups I, II and III to the Fourth Assessment Report of the Intergovernmental Panel on Climate Change. Geneva, Switzerland,: IPCC.

Isiorho. (1987). The interactions between Lake Chad and the phreatic aquifer in the southwest Chad Basin. Cleveland: Case Western Reserve Univ.,.

Isiorho and Matisoff, I. M. (1989). Groundwater seepage and its implication on the water resources planning and management in the Chad Basin. *Water resources.* v. 1, no. *2*, 210-215.

Isiorho and Matisoff, I. M. (1990). Groundwater recharge from Lake Chad. *Limnology and Oceanography.* v. 35, 931-938.

Jean-François, P., Andrew, C., Noel, G., & Alan, S. (2016). High-resolution mapping of global surface water and its long-term changes. *Nature*, 418-422.

JEAN-PAUL, B. (2012). Retrieval of Large-Scale Hydrological Signals in Africa from GRACE Time-Variable Gravity Fields. *Pure and Applied Geophysics. 169*, 1373–1390.

Jensen, J. (1996). Introductory Digital Image Processing: A remote sensing perspective, 2nd Edition. NJ: Prentice-Hall.

Ji, L., Zhang, L., & Bruce, W. (2009). Analysis of Dynamic Thresholds for the Normalized Difference Water Index. *Photogramm. Eng. Rem. S.*, 1307-137.

Joseph, L., Awange, Mohammad, A., Sharifi, Godfrey, O., Jens, W., Omulo. (2008). The Falling Lake Victoria Water Level: GRACE,TRIMM and CHAMP Satellite Analysisof the Lake Basin. *Water Resource Management*, 22:775–796.

Julia, B., Thomas , G., Birgit, H., Frank G, Moritz , L., & Sina, M. (2016). Satellite-derived changes in the permafrost landscape of central Yakutia, 2000–2011: Wetting, drying, and fires. . *Glob. Planet. Chang.* , 116-127.

Kadioglu and Sen, M. K. (2001). Monthly precipitation-runoff polygons and mean runoff coefficients. *Hydrol. Sci. J., 46 (1).*

Karsli, F., Guneroglu, A., & Dihkan, M. (2011). Spatio-temporal shoreline changes along the southern Black Sea coastal zone. *J. Appl. Remote Sens.*, 053545.

Kinzelbach et al, K. W. (2003). Sustainable groundwater management-problems and scientific tools. *Episodes 26(4)*, pp. 279-284.

Kropáček, J., Braun, A., Kang, S., Feng, C., Ye, Q., & Hochschild, V. (2012). Analysis of lake level changes in Nam Co in central Tibet utilizing synergistic satellite altimetry and optical imagery. *International J. of Applied Earth Observation and Geoinformation*, 3-11.

Kummerow et al, C. K. (1998). The tropical rainfall measuring mission (TRMM) sensor package. *J. Atmos. Oceanic Technol., 15*, 809-817.

L. Candela, F. E.-M. (2013). Groundwater modelling with limited data sets: the Chari– Logone area (Lake Chad Basin, Chad). *HYDROLOGICAL PROCESSES*.

LACBO. (2013). Observatoire du Bassin du Lac Tchad. D'Njamena: Bulletin du 2ème trimestre 2013.

Lauwaet, D., Van-Lipzig, N., Van-Weverberg, K., & de-Ridder, K. (2012). The precipitation response to the desiccation of Lake

Chad. *Quarterly Journal of the Royal Meteorological Society.* , 707-719.

LCBC. (2014). Hauteurs Journalières du Lac à Bol. N'Djamena, République du Tchad.: Direction des Recherches en Eau et de la Météorologie.

LCBC and BGR, L. C. (2009). Lake Chad Sustainable Water Management. Hannover, Germany: Lake Chad Commission, Federal Institute of Geosciences and Natural Resources. Hannover Germany.

LCBC, L. C. (1992). Master Plan for the development and environmentally sound management of the natural resources of the Lake Chad conventional basin. N'Djamena , Chad; 70: Lake Chad Basin Commission, United Nations Environment Program and UNSO,.

Leblanc, M., Favraux, G., Tweed, S., Leduc, C., Razack, M., & Mofor, L. (2007). Remote sensing for ground water modelling in large semiarid areas: Lake Chad basin, Africa,. *hydrology journal*, 15:97-100. DOI: 10.10007/s10040-006-0126-0.

Leblanc, M., Favreau, G., Maley, J., Nazoumou, Y., Leduc, C., Stagnitti, F., & van Oevelen, P. (2006). Reconstruction of Megalake Chad using Shuttle Radar Topographic Mission data. *Palaeogeogr. Palaeoclimatol. Palaeoecol*, 16-27.

Leblanc, M., Lemoalle, J., Bader, J., Tweed, S., & Mofor, L. (2011). Thermal remote sensing of water under flooded vegetation: new observations of inundation patterns for the 'Small' Lake Chad. *Hydrology*, 87-98.

Leblanc, M., Razack, M., Dagorne, D., Mofor, L., & Jones, C. (2003). Application of Meteosat thermal data to map soil infiltrability in the central part of the Lake Chad basin, Africa. *Geophys. Res. Lett.*

Le-Coz, M., Declaux, F., Genthon, P., & Favreau, G. (2009). Assessment of Digital Elevation Model (Dem) Aggregation methods for hydrological modeling: Lake Chad Basin. *Comp. Geosci*, 1661-1670.

Lee, S.-I., Kim, J., S., and Lee, S., K. (2010). Estimation of average terrestrial water storage changes in the Korean Peninsula using GRACE satellite gravity data. *Korean Water Resour. Asso*, 805-814.

Lee, S.-I., Seo, J.Y., and Lee, S., K. (2014). Validation of terrestrial water storage change estimates using hydrologic simulation . *Journal of Water Resources and Ocean Science*, 5-9.

Lemoalle. (1991). The hydrology of Lake Chad during the drought period (1973–1989). Rome: UN Food and Agricultural Organization, FAO Fisheries Report.

Lemoalle, L., Bader, J., Leblanc, M., & Sedick, A. (2012). Recent changes in Lake Chad: Observations, simulations and management options (1973-2011). *Glob. Planet. Change*, 247-254.

Li, K., Coe, M., & Ramankutty, N. (2007). Modeling the Hydrological Impact of Land-Use Change in West Africa. *Journal of Hydrology*, 258-268.

Lillesand, T. M., Kiefer, W. R., & Jonathan, W. C. (2008). Remote Sensing and Image Interpretation. 6 ed. River Street, Hoboken: Wiley and Sons.

Longuevergne, L., Laurent, S., & Bridget, R. (2015). Global analysis of approaches for deriving total water storage changes from GRACE satellites. *Water Resources Research* , 2574-2594 (DOI http://dx.doi.org/10.1002/2014WR016853).

Longuevergne, L., Wilson, C., Scanlon, B., & Crétaux, J. (2013). GRACE water storage estimates for the Middle East and other regions with significant reservoir and lake storage. *Hydrol. Earth Syst. Sci.*, 17, 4817–4830.

Lu, S., Wu, B., Yan, N., & Wang, H. (2011). Water body mapping method with HJ-1A/B satellite imagery. *Int. J. Appl. Earth Obs. Geoinf.*, 428–433.

Luxereau, A., Genthon, P., & karimou, A. (2011). Fluctuations in the size of Lake Chad: consequences on the livelihoods of the riverain peoples in eastern Niger. *Reg. Environ. Change*, 507-521.

Magrin, G. D., Lemoalle, J., & Lajaunie, M.-L. (2018, March 1). The Lake Chad development and climate resilience action plan (Vol. 2): Main report (English). Retrieved from World Bank Group.: http://documents.worldbank.org/curated/en/489801468186879029/Main-report.

Maria, V. M., Ralph, A. K., & Mika, G. T. (2018). A Global Analysis of Wildfire Smoke Injection Heights Derived from Space-Based Multi-Angle Imaging. *Remote Sensing*, 1609.

Massuel. (2001). Modélisation hydrodynamique de la nappe phréatique quaternaire du bassin du lac Tchad. In *Sciences de l'eau dans l'environnement continental.* Montpellier: Université de Montpellier II, France.

Matthew, M., Allen, L., Zelalem, T., Brian, W., & Dennis, R. (2014). Radiometric calibration methodology of the Landsat 8 thermal infrared sensor. *Remote Sens.*, 8803-8821.

Mayer-Gürr, T., Savcenko, R., Boschb, W., Daras, I., Flechtner, F., & Dahlec, C. (2012). Ocean tides from satellite altimetry and GRACE. *J. Geody.*, 28–38.

McFeeters, S. (1996). The Use of the Normalized Difference Water Index (NDWI) in the Delineation of Open Water Features. *Int. J. Remote Sens*, 1425–1432.

Milzow et al, M. K. (2011). Combining satellite radar altimetry, SAR surface soil moisture and GRACE total storage changes for hydrological model calibration in a large poorly gauged catchment. *Hydrol. Earth Syst. Sci., 15,* , 1729–1743.

Mohamed, A., & Karem, A. (2018). Quantifying Modern Recharge and Depletion Rates of the Nubian Aquifer in Egypt. *Survey in Geophysics*, 729-751.

Mohammad, T., E, O., Abolfazl, M., & Nico, S. (2017). Estimating River Depth from SWOT-Type Observables Obtained by Satellite Altimetry and Imagery. *Water*, 753.

NASA. (2016). Applied Remote Sensing training program. U.S: https://arset.gsfc.nasa.gov/sites/default/files/airquality/Health 16/week1_final.pdf.

Ngatcha, B. (2009). Water Resources Protection in the Lake Chad Basin in the Changing Environment. *European Water*, 3-12.

Ngounou Ngatcha et al, N. N. (2007). Groundwater Recharge from Rainfall in the Southern Border of Lake Chad in Cameroon. *Worl Applied Sciences Jornal 2*, 125-131.

NOAA. (2018). National Oceanic and Atmospheric Administration. U.S: https://www.nesdis.noaa.gov/content/noaa-enter-third-decade-monitoring-sea-level-jason-3.

Novoa, S., Chust, G., Sagarminaga, Y., & Revilla, M. (2012). Water quality assessment using satellite-derived chlorophyll-a within the European directives, in the southeastern Bay of Biscay. *Mar. Pollut. Bull.*, 739-750.

Odada, E., Oyebande, L., & Oguntola, J. (2009). Lake Chad experience and lessons learned. Retrieved from http://www.iwlearn.net/publications/ll/lakechad_2005.pdf.

Okonkwo, C., & Demoz, B. (2014). Identifying anthropogenic 'hotspots' and management of water resources in Lake Chad Basin using GIS. *J. Nat. Resour. Policy Res.*, 135-149.

Okpara, U., Stringer, L., Dougill, A., & Bila, M. (2015). Conflicts About Water in Lake Chad: Are Environmental, Vulnerability and Security Issues Linked? *Progress in Development Studies*, 308-25.

Olofsson, P., Foody, G., Herold, M., Stehman, S., Woodcock, C., & Wulder, M. (2014). Good practices for estimating area and assessing accuract of land change. *Remote Sens. Environ*, 42-57.

Ostu, N. (1978). Discriminant and Least Squares Threshold Selection. . *4IJCPR.*, 592–596.

Otukei, J., & Blaschke, T. (2010). Land cover change assessment using decision trees, support vector machines and maximum likelihood classification algorithms. . *Int. J. Appl. Earth Obs. Geoinf.*, 27-31.

Pete, B., Ake, R., Richard, M. L., Lisa-Maria, R., Lammert, H., Nathan, T., Max, F. (2018). The Global Mangrove Watch—A New 2010 Global Baseline of Mangrove Extent. *Remote Sensing*, 1669.

Purcell, A., Dehecq, A., Tregoning, P., Potter, E., McClusky, S., & Lambeck, K. (2011). Relationship between glacial isostatic adjustment and gravity perturbations observed by GRACE. *Geophysical Research Letters*, 18.

R Core Team. (2013). *R:* a language and environment for statistical computing. R Foundation for Statistical Computing. Retrieved from Vienna, Austria3-900051-07-0: http://www.Rproject.org/

Ramillien et al, R. F.-D. (2006). Time variations of the regional evapotranspiration rate from Gravity Recovery and Climate Experiment (GRACE) satellite gravimetry. *Water Resour. Res., 42*, W10403 http://dx.doi.org/10.1029/2005WR004331.

Ramillien, G., Famiglietti, J., & Wahr, J. (2008). Detection of Continental Hydrology and Glaciology Signals from GRACE: A Review. . *Surveys in Geophysics* , 361-374.

Rani, M., Kumar, P., Yadav, M., & Hooda, R. S. (2011). Wetland Assessment and Monitoring Using Image Processing Techniques: A Case Study of Ranchi, India. . *Journal of Geographic Information System*, 345-350.

Reager, J., Thomas, B., & Famiglietti. (2014). River basin flood potential inferred using GRACE gravity observations at several months lead time. *Nat. Geosci.*, 588–592.

Rodell, Chen, Kato, Famiglietti, Nigro, Wilson. (2007). Estimating groundwater storage changes in the Mississippi river basin (USA) using GRACE. *Hydrogeology*, 15 (1), 159-166.

Rodell M., C. J. (2007). Estimating groundwater storage changes in the Mississippi river basin (USA) using GRACE. . *Hydrogeology*, 15 (1), 159-166.

Rodell, M., & Famiglietti, J. (1999). Detectability of variations in continental water storage from satellite observations of the dependent gravity field. *Water Resour. Res*, 2705-2723.

Rodell, M., Houser, R., Jambor, U., Gottschalck, J., Mitchell, K., Meng, C., Toll. (2004). The global land data assimilation system. *American Meteorological Society*, 85, 381-394.

Rodell, M., Velicogna, I., & Famiglietti, J. (2009). Satellite-based estimates of groundwater depletion in India. *Nature*, 460, 999-1002.

Rosmorduc, V., Benveniste, J., Bronner, E., Dinardo, S., Lauret, O., Milagro, M., & Picot, N. (2011, Jan 1). *Radar Altimetry Tutorial,*. Retrieved from http://www.altimetry.info.

Rouse, J., Haas, R., Schell, J., & Deering, D. (1973). Monitoring Vegetation Systems in the Great Plains with ERTS (Earth Resources Technology Satellite). *In Proceedings of Third Earth Resources Technology Satellite Symposium*, (pp. 309-317). Greenbelt, ON, Canada.

Rummel, R. (2005). Geoid and Gravity in Earth Sciences - An Overview. *Earth, Moon, and Planets*, 3-11. doi:10.1007/s11038-005-3755-8.

Rummel, R., Balmino, G., Johannessen, J., Visser, P., & Woodworth, P. (2002). Dedicated gravity field missions - principles and aims. *Journal of Geodynamic*, 3-20.

Sabins, & Floyd, F. (2007). Remote Sensing, Principles and Interpretation. New York: W.H. Freeman and Company.

Sakumura, C., Bettadpur, S., & Bruinsma, S. (2014). Ensemble prediction and intercomparison analysis of GRACE time-variable gravity field models. *Geophysical Research Letters*, 1389-1397.

Sarah, H., Sander, V., & Simon, H. (2011). Evaluating Spectral Indices for Assessing Fire Severity in Chaparral Ecosystems (Southern California) Using MODIS/ASTER (MASTER) Airborne Simulator Data. . *Remote Sens.*, 2403-2419.

Sarch, M., & Birkett, C. (2000). Fishing and farming at Lake Chad: responses to lake-level fluctuations. *Geograph. J*, 156-72.

Schneider. (1989). Géologie et hydrogéologie de la République du Tchad. These deDoctorat d'état, Universite d' Avignon, Avignon; 738: Unpublished.

Schnitzer, S., Seitz, F., Eicker, A., Guntner, A., Wattenbach, M., & Menzel, A. (2013). Estimation of soil loss by water erosion in the Chinese Loess Plateau using Universal Soil Loss Equation and GRACE. *Geophysical Journal International*, 1283-1290.

Sensing, C. C. (2015). Fundamentals of remote Sensing. Canada: https://www.nrcan.gc.ca/node/14641.

Shengnan, N., Jianli, C., Clark, R., & Xiaogong, H. (2017). Long-Term Water Storage Changes of Lake Volta from GRACE and Satellite Altimetry and Connections with Regional Climate. *Remote sensing*, 842.

Simon, P., Williams, b., Matt, A., Pippa, L., & Whitehouse, d. (2014). Revisiting GRACE Antarctic ice mass trends and accelerations considering autocorrelation. . *Earth Planet. Sci. Lett.*, 12–21.

Singh, A. (2006). *Africa's Lakes: Atlas of Our Changing Environment* . Nairobi: UNEP.

Sita, K., Mohamed, S., Racha, E., & Tamer, E. (2018). Mapping and Forecasting Onsets of Harmful Algal Blooms Using MODIS Data over Coastal Waters Surrounding Charlotte County, Florida. *Remote Sensing*, 1656.

Song, C., Huang, B., & Ke, L. (2013). Modeling and analysis of lake water storage changes on the Tibetan Plateau using multi-mission satellite data. *Remote Sens Environ*, 135:25–35.

Stendera, S., Adrian, R., Bonada, N., Cañedo, M., Argüelles, Hugueny, B., Hering, D. (2012). Drivers and stressors of freshwater biodiversity patterns across different ecosystems and scales: a review. *Hydrobiologia*, 696.

Sun, F., Sun, W., Chen, J., & Gong, P. (2012). Comparison and improvement of methods for identifying waterbodies in remotely sensed imagery. *Int. J. Remote Sens.*, 6854–6875.

Sundaresan, A., Varshney, P., & Arora, M. (2007). Robustness of change detection algorithms in the presence of registration errors. *Photogramm. Eng. Rem. S.*, 375–383.

Swenson, S., & Wahr. (2009). Monitoring the water balance of Lake Victoria, East Africa, from space. *J. Hydrology*, 370 (1).

Swenson, S., & Wahr, J. (2006). Post-processing removal of correlated errors in GRACE data. *Geophy, Res. Lett*, 33.

Tapley, B., Bettadpur, S., Watkins, M., & Reigber, C. (2004). The gravity recovery and climate experiment: Mission overview

and early results. *GEOPHYSICAL RESEARCH LETTERS*, 31, L09607, doi:10.1029/2004GL019920.

Tilho. (1928). Variations et disparition possible du Tchad. *Geographie*, 239-260.

U.S., G. S. (2017a). Product guide: Landsat 4-7 Surface Reflectance (LEDAPS) product. Version 7.9. Washington: USGS.

U.S., G. S. (2017b). Product guide: Landsat 8 Surface Reflectance Code (LaSRC) product. Version 4.0. Washington: USGS.

UN. (2012, April 1). AfricaRenewal. Retrieved from UN Website: https://www.un.org/africarenewal/magazine/april-2012/africa%E2%80%99s-vanishing-lake-chad

USGS. (2017, January 1). U.G. Geological Survey. Retrieved from SCL Gap-Filled Products Phase One Methodology: http: //landsat.usgs.gov/documents/SLC_Gap_Fill_Methology

Wahr, G., & Zhong, J. (2012). Computations of the viscoelastic response of a 3-D compressible Earth to surface loading: an application to Glacial Isostatic Adjustment in Antarctica and Canada. *Geophysical Journal International*, 557-572.

Wahr, J., Molenaar, M., & Bryan, F. (1998). Time variability of the Earth's gravity field: Hydrological and oceanic effects and their possible detection using GRACE. *J. geophys. Res.*, 30205-30229.

Wahr, J., Swenson, S., & Velicogna, I. (2006). Accuracy of GRACE mass estimates. *Geophysical Research Letters*, 6.

Wahr, J., Swenson, S., Zlotnicki, V., & Velicogna, I. (2004). Time-variable gravity from GRACE: First results. *GEOPHYSICAL RESEARCH LETTERS*, 31, L11501, doi:10.1029/2004GL019779.

Warh, J. (2006). Time-variable gravity from GRACE:. *Geophys. Res. Lett., 31*.

Wenbin, Z., Jiabao, Y., & Shaofeng, J. (2017). Monitoring Recent Fluctuations of the Southern Pool of Lake Chad Using Multiple Remote Sensing Data: Implications for Water Balance Analysis. *Remote sensing*, 1032.

Willis, K. (2015). Remote sensing change detection for ecological monitoring in United States protected areas. *Bio. Conserv.* , 233-242.

Xiao, Y., Zhao, W., & Zhu, L. (2010). A study on information extraction of water body using bandl and band7 of TM imagery. *Science of Surveying and Mapping*, 226– 227, 216.

Xu, C., Weigelt, M., Sideris, M., & Sneeuw, N. (2007). Spaceborne gravimetry and gravity field recovery. *Canadian Aeronautics and Space Journal*, 65-75.

Xu, H. (2005). Study on Information Extraction of Water Body with the Modified Normalized Difference Water Index (MNDWI). *J. Remote Sens.*, 589–595.

Yang, J., & Du, X. (2017). An enhanced water index in extracting water bodies from Landsat TM imagery. *Annals of GIS* , 141-148.

Yang, P., Xia, J., Zhan, C., Qiao, Y., & Wang, Y. (2017). Monitoring the spatio-temporal changes of terrestrial water storage using GRACE data in the Tarim River basin between 2002 and 2015. *Sci Total Environ*, 218-228.

Yang, Y., Di, L., Huade, G., Bridget, R., Craig, T., Lei, J., & Xiang, X. (2014). GRACE satellite observed hydrological controls on interannual and seasonal variability in surface greenness over mainland Australia. *J. Geophys. Res. Biogeosci.*, 224.

Yeh, P., Swenson, S., Famigleitti, J., & Rodell, M. (2006b). Remote sensing of groundwater storage changes in Illinois using GRACE. *Water Resou. Res*, 7.

Yeon, Y., Jurng-Jae, Y., Hong, S.-Y., & K, K. (2018). Evaluation of the Accuracy of Bathymetry on the Nearshore Coastlines of Western Korea from Satellite Altimetry, Multi-Beam, and Airborne Bathymetric LiDAR. *Sensor*, 2926.

Zwally, H. (1989). Mass changes of the Greenland and Antarctic ice sheets and shelves and contributions to sea-level rise: 1992-2002.